Peninsula Technikon

Faculty of Engineering

Center for Research in Applied Technology

Distributed Piezoelectric Actuator with complex shape

Yan Qiu

B.Sc. Eng. (P. R. China)

Submitted towards the Degree of
Master of Technology in Mechanical Engineering

Under Supervision of

Prof. Bohua Sun

CAPE TOWN, 2002

Acknowledgments

There are a number of people who sincerely deserve my thanks for their effort in the support of my master's thesis. Special thanks goes to my supervisor Prof. Dr. Bohua Sun who gave me the perfect balance of technical direction and freedom in the pursuit of my research interests. I would like to thank Mr. Keith Jacobs (HOD of Mechanical Engineering) for the earmarked-funding programmes assistance and other help. I would like to thank Mr Helmut Bowles for his financial assistance. Thanks also go to Mr Paul Wayne Alexander (exchange student from the University of Michigan) and Mr Frumence E. Utou for many important discussions and support. I would also like to thank all the members of Center for Research in Applied Technology (CRATech) and staff members at the Department of Mechanical Engineering for the fantastic environment for learning, friendly atmosphere, and technical support.

Specially, I would also to like thank my father and my mother for their endearing encouragement, patience, and love. I would like to thank all my friends and classmates for two years of support and motivation to partake in social activities: Oscar Philander, Mornay Riddles, Philemon Simelane. I would also like to thank Ms. Bernedette Gonzalves (Secretary of CRATech) for the help during the two years and Mrs. Elvina Moosa (Secretary of Dept. Mechanical Engineering) for her help.

Finally, I would like to thank the National Research Foundation (NRF) of South Africa for supporting this work under the project: Smart Structures and Devices. The Peninsula Technikon scholarship is also gratefully acknowledged.

Abstract

Title of Thesis: Distributed Piezoelectric Actuator with complex shapes

Degree Candidate: Yan Qiu

Degree and Year: Master of Technology, 2002

Thesis directed by: Prof. Dr. Bohua Sun
Department of Mechanical Engineering and
Center for Research in Applied Technology

Distributed Piezoelectric Actuator (DPA) is one kind of actuator in the smart technology field. Firstly, DPA is one kind of solid-state actuator, and can be embedded in the structure. Secondly, it can be controlled by the electrical signal with high bandwidth and high precision. So it can be applied in the many different fields, such as high-resolution positioning, noise and vibration detection and shape control.

Up to now, all of the DPA theory investigations and the product designs are based on applying the approximate electrical field. And only the rectangular shape DPA has been studied. The accurate distribution and intensity of electrical and mechanics field, and the numerical imitation for the DPA products with rectangular and other shapes have never been discussed and studied. Therefore, the development of DPA to be used in the micro application, such as in the Micro Electro-Mechanical System (MEMS), has been limited.

This thesis has developed the analytical analysis models for two types of DPA elements and the part circular shape DPA element. The MathCAD and MATLAB program have been used to develop the analytical models. The ABAQUS program has also been used to compare the results between the analytical models and Finite Element Method (FEM). Finally, the accuracy and reliability of analytical models have been proved by results comparison between the analytical models, FEM and the product testing data from the industry.

This thesis consists of five chapters. Chapter 1 is the introduction of smart structure. The characterizations of constituent materials, including the piezoelectric material and matrix epoxy material have been discussed in Chapter 2. In Chapter 3, the analytical models for two type of DPA element have been developed and the comparisons have also been completed. The analytical models for part circular shape DPA element have been developed in Chapter 4. The conclusions and recommendations are included in Chapter 5.

Table of Contents

List of Figures

List of Tables

Chapter 1

Introduction

1.1 Motivation

The demand for new generations of industrial, military, commercial, medical, automotive and aerospace products has been a strong driving force behind the research and development of advanced materials and smart structures. This situation has been further stimulated by the intellectual curiosity of humankind. Global competition among the principal industrial nations has also been a parameter in the equation governing the rate of technological progress.

Thus, by integrating the knowledge-bases associated with advanced materials, information technology and biotechnology, these three mega-technologies are facilitating the creation of a new generation of bio-mimetic materials and structures with inherent brains, nervous systems and actuation systems, which are currently a mere skeleton compared with the anatomy perceived in the not-too-distant future. This quantum jump in materials technology will revolutionize the future in ways far more dramatic than the way in which the electronic chip has impacted on our lifestyles. These new materials are termed 'Smart Materials', and they will typically feature fibrous polymeric composite materials, embedded powerful computer chips that will be interfaced with both embedded sensors and actuators by networks of optical-fibre wave-guides, through which large volumes of data will be transmitted at high speeds.

In the smart technology field, Distributed Piezoelectric Actuator (DPA) is one kind of the most useful actuator. Firstly, DPA is one kind of solid-state actuator, and can be embedded in the structure. Secondly, it can be controlled by the electrical signal with high bandwidth and high precision. So it can be applied in many different fields, such as high-resolution positioning, noise and vibration detection and shape control.

During the last decade, lots of investigations have been done on the DPA development. For instance, Crawley and Anderson (1990) developed two analytical models of beams with extension piezoelectric actuators. Chandrashekhara and Varadarajan (1997) presented a numerical model of a composite beam using a higher-order shear deformation theory. Aldraihem et al (1997) developed a laminated beam model using two theories, namely the Euler-Bernoulli beam theory and the Timoshenko beam theory. Abramovich (1998) presented analytical formulation and closed form solutions of composite beams with extension piezoelectric actuators. Classical plate and shell theories have been widely used for the analysis of piezoelectric laminated plates (1991) and shells (1994) respectively. Lee (1990), Huang and Wu (1996), Mitchell and Reddy (1995) and others have developed plate theories for rectangular hybrid laminates. Recently, Vel and Batra (2000) have derived three-dimensional analytical solutions for thick piezoelectric plates

subjected to various mechanical and electrical boundary conditions at the edges. Sun and Huang (2001) have developed the theory of composite beams with piezoelectric damping layer. Ray et al (1997) Rongong and Tomlinson (1997) had developed the shell and ring structure models. Ray et al (1993) and Heyliger and Brooks (1996) have obtained exact three-dimensional solutions for the cylindrical bending of simply supported piezoelectric laminates. Exact solutions for simply supported rectangular laminates were given by Heyliger (1994) and Lee and Jiang (1996). Due to commercial requirement some of the high-tech companies have been set up to manufacture DPA for industrial applications. ACX (2002) and Piezo System (2002) are the leader companies in this field.

Up to now, unfortunately, all of the DPA theoretical investigations and the product designs are based on applying the approximate electrical field, and only the rectangular shape DPA has been studied for the applications in the published papers. The accurate distribution and intensity of electrical and mechanical field, and the numerical imitation for the DPA products with rectangular and other shapes have never been discussed and studied. Therefore, the development of DPA applications in the complex situation and micro volume field, such as in the micro electro-mechanical systems (MEMS), has been limited by insufficient research.

This work deals with the development of distributed piezoelectric actuator technology. In particular, this thesis focuses on piezoelectric materials as distributed actuators for control of structures. The accurate distribution and intensity of electrical and mechanics strain and stress fields in the rectangular and quarter circular shapes DPA have been studied. The mathematical models on the two kinds of shapes DPA have been built, and the reliability and correctness of rectangular shape DPA model has been proved by the FEM and experiment data. Those results have proved that the mathematical models can be used in the DPA product numerical imitation and improvement and advice design in future.

1.2 Objectives

The major goal of this work is to develop the analytical analysis models for two type of distributed piezoelectric actuators (DPA) with the rectangular and part circular shapes, which meet the demands of active control applications in complex technology field, such as aerospace structures and micro electro-mechanical system (MEMS). Supporting tasks, which highlight the major contributions of this thesis, are the following:

- Develop the analytical analysis models for two types of distributed piezoelectric actuator (DPA) elements
- Develop the analytical analysis models for distributed piezoelectric actuator (DPA) with rectangular and part circular shapes
- Identify the key issues and tradeoffs in the design of distributed piezoelectric actuators (DPA).

The ultimate objective is to enable highly distributed actuation for active structural control applications. For industrial field, the major objective is to develop the design program of distributed piezoelectric actuators for the product manufacture process and applications.

1.3 Background

1.3.1 Smart Materials

The technological field of "smart materials" is not transparent or clearly structured. It has evolved over the past decades with increasing pace during the 1990s to become what it is today, at the transition to the next millennium. Generally speaking these materials respond with change in shape upon application of externally applied driving forces. Typically this shape change is reflected in an elongation of the sample, thus allowing the use as for example. a small linear motor. The term "smart materials", sometimes also called intelligent materials or active materials, describes a group of material systems with unique properties. At this stage, the following materials are the active ones:

- Piezoelectric materials
- Shape memory alloys
- Magnetostrictive materials
- Electrorheological materials
- Magnetorheological fluids

Lots of available smart materials have been investigated for complex applications. And perhaps the most widely used of these are piezoelectric materials, due to their relative ease of implementation and use. Actuation and sensing is applied through electrical signals, and their low field linear behavior has aided in modeling for transducer applications. Their high stiffness gives adequate energy densities, and their fast response times provide high bandwidth. In comparison (Table 1.1), other smart materials are less well suited for the desired applications.

	PZT 5H	PVDF	PMN	Terfenol D	Nitionl
Actuation Mechanism	Piezoceramic (31)	Piezo film	Electro-strictive	Magneto-strictive	Shape memory alloy
Max Strain	0.13%	0.07%	0.1%	0.2%	2%-8%
Modulus (GPa)	60.6	2	64.5	29.7	28m, 90a
Density (kg/m^3)	7500	1780	7800	9250	7100
Actuation Energy Density (J/kg)	6.83	0.28	4.13	6.42	252-4032

Hysteresis	10%	>10%	<1%	2%	High
Temp Range (°C)	-20 to 200C	low	0 to 40C	high	---
Bandwidth	100 kHz	100 kHz	100 kHz	<10 kHz	<5Hz

Table 1.1: Comparisons of Available Smart Materials (Commercial and Potential)

Piezo-polymer films (PVDF) are robust to damage, but lack the high stiffness to provide significant actuation authority. Electrositrictive materials (PMN) have low hysteresis losses and high stiffness, but have poor temperature stability, and require high currents to cooperate due to their high material dielectric. Shape memory alloys (Nitinol) are capable of very high strains, but are limited to ultra-low bandwidth applications (<5 Hz) due to the time needed for thermal dissipation/heating. Finally, magnetostrictive actuators (Terfenol) have similar actuation energy density and bandwidth as piezoceramics, but are much less effective when the coils and flux path materials are accounted for. Although piezoceramics at first seem ideally suited for planar structural actuation applications, they suffer from distinct disadvantages associated with reliability, performance, strength, and large scale distributed control.

In addition some material systems that do not exhibit a shape change, but rather have other significant properties are sometimes also called smart materials (while other, for some strange reason are not). Examples of "other" smart materials include electro- and magneto-rheological fluids (ER and MR fluids). These fluids can change viscosity over many orders of magnitude upon application of an external magnetic or electric field. Consequently, the term "smart materials" is not very well defined and frequently used to describe different systems and systems' behaviors. Although there have been approaches to quantify and classify different levels of smartness or intelligence in systems, from a practical standpoint it is most important to understand that none of the classifications is established and used as a standard in the academic, scientific, or industrial community. Furthermore one should note that the terms

- Smart materials
- Intelligent Materials
- Active Materials
- Adaptive Materials
- and to some extent "actuators" and "sensors"

are almost always used interchangeably. This can sometimes lead to confusion as different terms can really describe the same effect or property of a material.

To add to the confusion the terms "smart devices", "smart systems" or "smart structure" are often carelessly used. Here one should note that in general the system complexity increases from the unit "material" to "device" to "systems" to "structures". Any

permutation of the adjective (smart, active,) with the subject (material, device,) is more or less meaningful and seems to have been used already in one way or the other in published reports and papers. Much more important than the actual word definition is the general understanding of the field.

1.3.2 Smart Structure

Smart structures are the structures made of smart materials, in other words, are those which incorporate actuators and sensors that are integrated into the structure and have structural functionality, as well as integrated control logic, signal conditioning and power amplification electronics. Such actuating, sensing and signal processing elements are incorporated into a structure for the purpose of influencing its states or characteristics, be they mechanical, thermal, optical, chemical, electrical or magnetic. For example, a mechanically intelligent structure is capable of altering both mechanical states, i.e. its position or velocity, or its mechanical characteristic, i.e. its stiffness or damping. However there are a wide variety of less sophisticated smart materials and structures that exploit the basic sub-disciplines, which defines three classes of smart materials. These include materials with only sensing capabilities, those with only actuation capabilities and those with both sensing and actuation capabilities, at primitive level relative to motions of intelligence.

The input or stimulus can be for example a change in temperature or in magnetic field. The material then intrinsically responds with an output, which in turn can be for example a change in length of the material, change in viscosity or change in electrical conductivity. Active materials can be divided into two groups. One group comprises the "classical" active materials as viewed by the academic community and is characterized by the type of response these materials generate. Upon application of a stimulus the materials respond with a change in shape and/or in length of the material. Thus input is always transformed into strain, which can be used to introduce motion or dynamics into a system. These materials are the most widely used group for design of smart structures, where active materials are integrated into a mechanical host structure (for example a building or a helicopter rotor blade) with the goal to change the geometrical dimensions of the structures.

The desired change in geometrical dimensions is mostly time dependant and often the steady state of the structure is a dynamic system where integrated active materials or devices are constantly agitated to change in real time the characteristics of the host. Devices based on materials that respond with a change in length are often referred to as actuators or solid-state actuators to be more specific. Conversely active materials can be also used as sensors where a strain applied on the material is transformed into a signal that allows computation of the strain levels in the system. The figure below (Figure 1.1) illustrates the basic principles of an actuator/sensor smart material system. Depending on the stimulus-response-direction an active materials device can be used as both actuator and sensor.

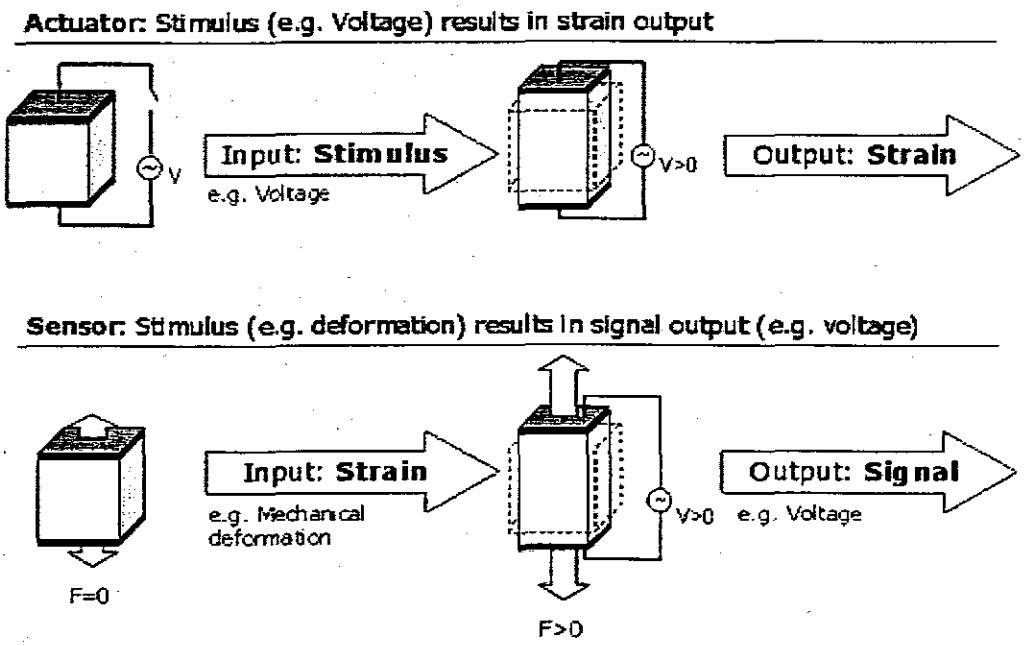

Figure 1.1: Active material devices used as actuator (top) and sensor (bottom)

The second group consists of materials that respond to stimuli with a change in a key material property, for example electrical conductivity or viscosity. While they are equally important from a scientific point of view, they are less frequently integrated into mechanical structures but rather used to design complex modules, for example clutches, fasteners, valves or various switches. Frequently these materials are used as sensors. Although materials in this group do not produce strain upon application of an external stimulus they are sometimes also referred to as actuator systems. Examples include the electro- and magneto-rheological fluids, which respond with an increase in viscosity upon application of an external electrical or magnetic field.

1.3.3 Piezoelectric Actuator

Research and development of different kinds of actuators for the applications that have different situation are a major part in the 'Smart' technology. At present, some kinds of actuators have been researched and developed, which include different materials, such as PZT, SMA, ERF or Magentostrictive materials, and different structure, such as line, layer, stack, block, and so on. The 'Piezoelectric Actuator' is the most important actuator of all.

Piezoelectric actuator elements allow the construction of all electric actuators of compact design with few parts and minimum number of moving parts that offer high bandwidth and high precision. So, in the last years, piezoelectric actuators have been researched and developed to be used successfully in many applications in the field of high-resolution positioning, noise and vibration detection and cancellation, shape control and many others (Crawley, 1994; Tzou and Anderson, 1992; Newnham and Gregory, 1991). The examples range from video type head positioner, modulated automotive suspension

systems, rotor vibration control for helicopters (Strub, 1996), vibration control and vertical tail buffeting alleviation for aircraft structures (Suleman and Goncalves, 1997; Hopleins et al., 1998), sound radiation control for noise suppression or acoustic camouflage (Shields, Ro and Baz, 1997), to underwater smart skins for submarines (Gentilman et al., 1998).

1.3.4 Inter-digital Electrode Monolithic Ceramics

The interdigital electrode (IDE) concept was introduced as a 'performance enhancement technology' for monolithic ceramic actuators (Hagood et al., 1993). Although interdigital electrodes have been used extensively in the past for surface acoustic wave (SAW) transducers (Feuillard et al., 1993), the idea was never applied to ceramics for the purpose of actuating structures until recently (Yoshikawa and Shrout, 1993). Figure 1.2 shows the concept of IDEs. Electrode fingers of alternating polarity are arranged on the top surface of a monolithic ceramic wafer, with an exact mirror image on the bottom. This arrangement of electrodes causes a portion of the electric field to be aligned within the plane of ceramic, as it travels between the electrode fingers. The percentage of field oriented in this direction depends upon the various geometry parameters: electrode finger width, wafer thickness, and electrode finger spacing. In general, for a large electrode spacing, and small electrode width and wafer thickness, the majority of the field is aligned in the plane, with little field in homogeneity under the electrodes.

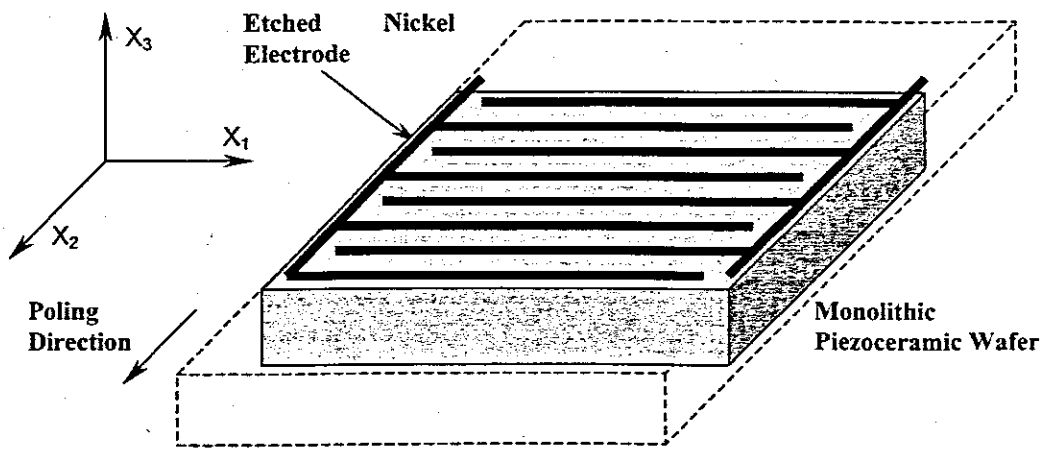

Figure 1.2: Concept of the interdigital electrodes on monolithic ceramic (IDE)

Such an electrode arrangement offers several advantages. First, the poling direction is now in the plane, allowing use of the much larger primary piezoelectric effect (d_{33}). Second, the actuation is anisotropic: the planar actuation is out of phase in the two directions, as illustrated in the figure. Such directionality is advantageous for tailoring actuation and sensing to particular modes of a structure. Models developed for prediction of the device response verified for these benefits. An energy technique (Rayleigh-Ritz) using assumed modes for the displacement and voltage degrees of freedom was developed to provide a closed form solution of the effective constitutive properties. This model showed that an increase of almost two times in actuation strain was possible for

geometry ratios b/h of 6 and a/h of 1. More importantly, an increase in induced stress capability (i.e. actuation authority) of three times was possible in the primary direction. The IDE device was also modeled using a commercially available finite element code. This model revealed the details of the internal electric fields, and validated the assumed modes used in the Ritz model in regimes of high electrode spacing, where field distortions near the electrodes had been ignored.

For the experimental work, the electrodes of a number of monolithic wafers were etched into the interdigital pattern using photolithography techniques. Measurements did show an increase in free strain similar to that predicted in the models. However, it was also found that many of the ceramics failed due to catastrophic cracking during poling. Furthermore, unpublished results later found that it was difficult to obtain significant induced stress in samples laminated to passive materials. The difficulty originates in electric field gradients near the electrodes, causing stress concentrations in the so-called 'dead areas' of the actuator. A second difficulty may be due to local areas of high electric field near the electrode edges and terminations where charge can collect.

A similar problem occurs in multiple layer ceramic (stack) actuators, where micro cracks are preferentially initiated near the electrodes, leading to crack propagation under stress and eventual actuator failure (Pan and Yoshikawa, 1996). Researchers have visually detected these cracks using microscope CCDs in a number of active materials, including electrostrictors, switching ceramics, and piezoceramics (Aburatani et al., 1994). Several alternative electrode schemes have been investigated to reduce the stress concentrations in multiple layer actuators, including floating electrodes, slits in the ceramic, and insulator materials (Yoshikawa and Shrout, 1993). However, these methods increase cost and do not directly solve the problem. An ideal solution is to remove the electrode material from the ceramic, thus desensitizing the actuator performance from damage caused at the electrodes by field concentrations in these areas. Electrodes on separate materials, such as an inter laminar electrode in the PFC design would accomplish this.

1.4 Scope of Thesis

The organization of this M-tech work is based on the philosophy of vertical technology integration, the development of the design for distributed piezoelectric actuators and the application to the problems of active control.

Chapter 2 details the characterization of the piezoelectric materials and epoxy-matrix used in the distributed piezoelectric actuator (DPA). The purpose of the characterization is two fold: to provide model inputs of the material properties, and to allow for design of optimal actuators based on a combination of processing and performance. The characterization is divided into the two materials, piezoceramic and epoxy-matrix. Chosen bulk materials are characterized in a series of poling, aging, and actuation free strain studies. The epoxy-matrix material, although passive, plays an important role in the electrical, mechanical, and actuation properties of the composite. Studies are undertaken

to understand the tradeoffs existing between processing ease and composite performance by adding fillers to the pure epoxy starting material.

Chapter 3 assumes knowledge of the material constitutive properties and applies the electromagnetic principle to determine the analytical analysis models for the two types of distributed piezoelectric actuator elements. Two analytical electro-mechanically coupled models are developed to predict the properties. The accurate mathematical model for the distribution and intensity of electrical and mechanics field in the rectangular shapes DPA elements have been developed. A commercially available Finite Element program (ABAQUS) has been used to model the DPA, and compare the results with the analytical models. The objective of this work is to develop accurate model for the DPA elements, which can be applied in further work.

Chapter 4 applies the models developed in the previous chapter to develop the analytical analysis models for the part circular shape DPA. The Finite Element Methods (FEM) also has been used to model the part circular shape DPA. And the mechanical properties have been determined and discussed during the results comparison.

Chapter 5 closes the thesis with principal conclusions from each chapter, and recommendations for future work in distributed piezoelectric actuators.

Chapter 2

Characterization of Piezoelectric Materials

2.1 Introduction

One way to improve the distributed piezoelectric actuator (DPA) performance is approached at the structural level, through the use of interdigitated electrodes that will be discussed in chapter 3. A second way is to approach at the material level, by auspicious selection of the bulk properties. This chapter deals with fundamental issues of the bulk materials, and understanding how the choice of these materials can affect the behavior and ease of manufacturing.

This chapter is divided into the characterization of piezoelectric materials (PZT). Different PZT ceramic materials will be characterized for performance and according to specific to needs of structural actuation. A single PZT type is then selected and characterized in bulk form for the application to DPA product, including a study in poling and aging.

The effects of epoxy-matrix material on DPA can be reduced or ignored by improving the structural design of DPA, which will be discussed in chapter 3. In this chapter, the characterization of epoxy-matrix material will not be discussed.

2.2 Piezoceramic Characterization

2.2.1 Piezoelectric Effect

Piezoelectricity, discovered in Rochelle salt in 1880 by the brothers Jaques and Pierre Curie is defined as a change in electric polarization; with change in applied stress, which is usually referred to as the direct piezoelectric effect. The converse piezoelectric effect is in analogy the change in strain for a free crystal (or stress for a clamped system) with change in applied field. Thus the converse piezoelectric effect is typically used when a material system is to be used an actuator: Input is a voltage gradient, output is a strain. For low fields, there is a linear relationship between strain and electrical field. Reversing the field also reverses the direction of the strain.

Historically, Rochelle salt and quartz are the most frequently used piezoelectric materials. However only a relatively new materials system like PZT offers properties that enable the development of active structural devices. The microscopic origin of the piezoelectric effect is the displacement of ionic charges within a crystal structure. In the absence of external strain, the charge distribution within the crystal is symmetric and the net electric dipole moment is zero. However when an external stress is applied, the charges are

displaced and the charge distribution is no longer symmetric. A net polarization develops and results in an internal electric field. A material can be only piezoelectric if the unit cell has no center of inversion. Virtually all piezoelectric materials crystallize in the perovskite structure (Figure 2.1.).

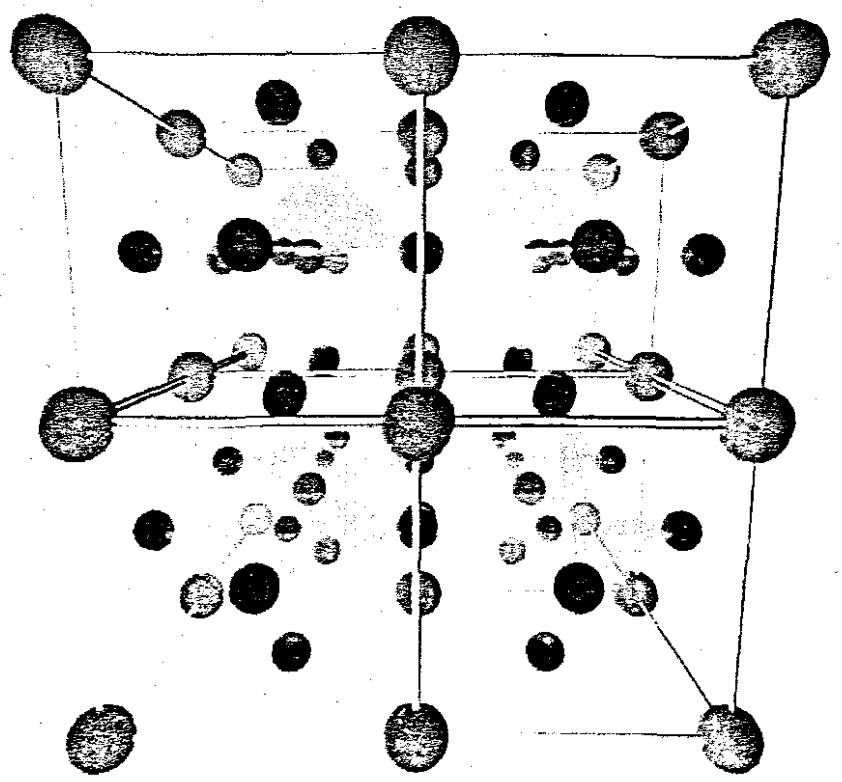

Figure 2.1: A representation of eight perovskite unit cells, on which most commercially available piezoceramics are based on. The generic formula is ABO3. Oxygen sits in the octahedral sites (red dots), an A^{++} material (e.g. Pb) in the cube corners (green dots) and a small B^{++++} action (e.g. Zr, Ti) in the center (small black dots). The unit cell is electrically neutral.

Ideally polarization vectors of all unit cells would add up and results in the total polarization, forming one large domain within the crystal. However commercially available piezoceramics are always polycrystalline. The sum of all polarization vectors of all unit cells (and of all polarization vectors of all domains) results in an electrically neutral sample as vectors cancel each other out due to a random statistical distribution of directions. The trick is then to pole the ceramic at high electric fields to force the domains to rotate and switch into the desired direction. This is represented in Figure 2.2. The result is never a full orientation off all domains; nevertheless the polycrystalline ceramic exhibits significant net polarization that can be used for actuation or sensing purposes. The simple reason that singly crystal piezoceramics are not used is that so far nobody was able to grow crystals of sufficient size at reasonable costs (Single crystal piezoceramics as well as lead-free systems – for environmental reasons – are currently an area of significant research activities).

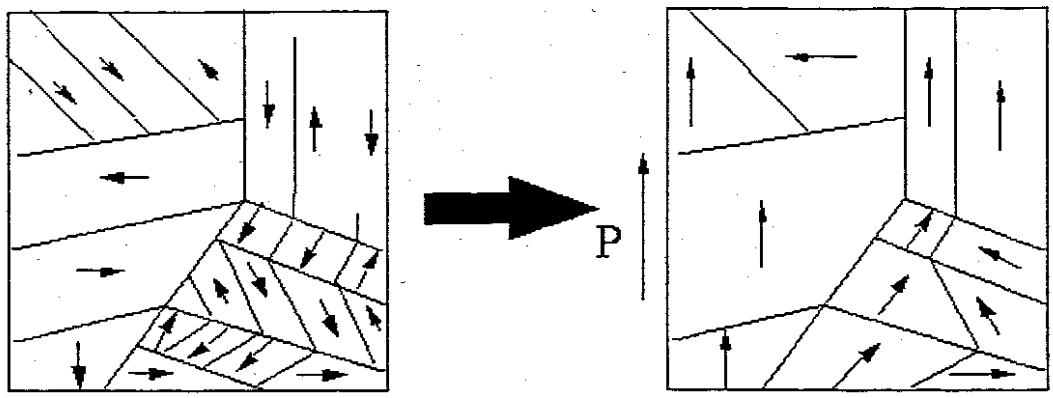

Figure 2.2: Representation of domain rotation and switching during poling of a polycrystalline ceramic.

As previously discussed, piezoelectric materials were base lined for a number of reasons. However, even within the piezoelectric ceramic families there are a number of types, which range from 'soft' to 'hard' piezoceramics. These differences are caused by slight variations in oxide compositional ratios, or additional dopant materials. These compositions affect the mobility of the domains to spontaneously polarize with a given electric field. This, in turn, affects the degree of 'hardness' of the ceramic. A soft piezoceramic has higher domain mobility, and thus is easier to pole, often has a lower coercive field, and has higher electrical-mechanical coupling factors (a measure of energy conversion efficiency). By the same token, however, easier domain mobility also results in easier ceramic depolarization from stress or electric field, higher hysteresis and non-linearity, and higher rates of piezoelectric 'creep'. Transducer applications that are subject to mechanical shock and high stresses are often designed with hard piezoceramics to avoid depolarization in service, and hysteretic heating. Structural actuation has typically utilized the softer ceramics for high levels of actuation. Heating is generally not an issue for low frequency dynamic problems such as structural vibration suppression.

2.2.2 Piezoelectric Material

Piezoceramics are identified by Navy designations (Navy types I, II, IV, etc.), or more commonly by the Morgan-Matroc trademark names. Four of these are shown in Table 2.1 (PZT 5H, 5A, 4S, 8M), which represent a range of piezoceramics from soft (5H) to very hard (8M). Applications design has usually been done using the low field linear properties. These properties are conveniently described in the linear constitutive relationships, which demonstrate the electrical and mechanical coupling through the piezoelectric properties. One form used for structural control applications is (IEEE, 1986),

$$\begin{Bmatrix} \mathbf{D} \\ \mathbf{S} \end{Bmatrix} = \begin{bmatrix} \varepsilon^{\mathbf{T}} & \mathbf{d} \\ \mathbf{d}_t & \mathbf{s}^{\mathbf{E}} \end{bmatrix} \begin{Bmatrix} \mathbf{E} \\ \mathbf{T} \end{Bmatrix} \tag{2.1}$$

where **D** is the electrical displacement (Coulombs/m^2), **S** the strain, **E** the electric field (kV/cm), and **T** the stress (MPa). These complementary electrical and mechanical fields are related through the material properties: the constant stress (unclamped) dielectric ($\varepsilon^{\mathbf{T}}$), the induced strain constant (**d**), and the constant field (shorted leads) compliance ($\mathbf{s}^{\mathbf{E}}$). Subscript 't' denotes matrix transpose. Another common form is expressed in terms of the stress as the dependent variable, which is convenient for describing the induced piezoelectric stress possible,

$$\begin{Bmatrix} \mathbf{D} \\ \mathbf{T} \end{Bmatrix} = \begin{bmatrix} \varepsilon^{\mathbf{S}} & \mathbf{e} \\ -\mathbf{e}_t & \mathbf{c}^{\mathbf{E}} \end{bmatrix} \begin{Bmatrix} \mathbf{E} \\ \mathbf{S} \end{Bmatrix} \tag{2.2}$$

where $\varepsilon^{\mathbf{S}}$ is the clamped dielectric, $\mathbf{c}^{\mathbf{E}}$ is the constant field stiffness, and **e** is the induced stress. A more complete description of the constitutive equations and relationships between the various constants are contained in Appendix A.

These properties will be important in the design of DPA, as they dictate the actuation capability when combined with the epoxy-matrix properties. However, it is unclear from the linear material properties alone which piezoceramic is best suited for the DPA application. For true structural actuation applications, it is also important to know how the material performs in the high field nonlinear regime. Quantities such as the coercive field (field to polarize and depolarize the ceramic), remnant polarization, and maximum induced strain levels are of great interest, as they describe the maximum performance limitations of the piezoceramics. These quantities are less well defined and need to be determined experimentally, and in the framework of the current problem.

A summary of low field material properties and high field properties is given in Table 2.1. Comparisons are made considering a one-dimensional mode of operation (along the 33 direction). The low field properties are typically measured using well-established resonance techniques (IRE, 1976), taken using very low voltages. The piezoelectric constants can also be determined using quasistatic methods, which give values that are within 1.5% of the values measured using resonance techniques. PZT 5H has very high induced strain constants (strain per unit voltage) due to the domain mobility of the ceramic. More importantly, PZT 5H has the highest induced stress constant (blocked stress per unit electric field), indicating high actuation authority. Since the induced stress is a combination of both induced strain and ceramic stiffness, the hard ceramics have comparable performance using this quantity. This is even more evident in the coupling coefficient, which is a measure of the fraction of electrical energy converted to mechanical energy and vice versa, which also takes into account the dielectric constant. For PZT based electro ceramics, this value is quite high (as opposed to 0.1 for Quartz, and 0.4 for Barium Titanate), and similar among the different PZT compositions.

	PZT 5H	PZT 5A	PZT 4S	PZT 8M
Dielectric K_{33}^T	3350	1770	1500	800
Induced Strain d_{33} (m/V)	555	392	360	215
Induced Stress e_{33} (N/C)	23.2	15.8	14.6	17.3
Coupling Coefficient k_{33}	0.790	0.774	0.861	0.767
Young's Modulus[3] (GPa)	48	53	60	77
Coercive Field E_c (kV/cm)	7.2	11.2	8	8.4
Remnant Polarization (mC/m^2)	300	375	110	80
Saturation Strain (ppm)	3200	4100	2100	1400
Rep Cycle Strain (ppm)	2350	2800	1875	1070
Rep Cycle Hysteresis (%)	24	24	7	4
Rep Cycle Energy Density (J/kg)	17.7	27.7	14.1	5.9
Depole Stress T_{33}^{max} (MPa)	444	72	>150	>150

Table 2.1: Comparison of longitudinal properties for four PZT ceramics.
Low field data provided by Morgan Matroc, Bedford, Ohio.

The effect of ceramic composition is also apparent in the high field constants. The quantities come from the results shown in Figures 2.3 and 2.4. In Figure 2.3, the left column contains plots of the strain versus electric field, also known as the butterfly curves. The softer ceramics have sharp, well defined coercive fields where repolarization occurs, whereas the hard ceramics (4S, 8M) appear to have a greater distribution of domain coercive fields, spreading the net ceramic repolarization over a range of voltages. The soft ceramics also have high saturation strains, as expected, taken as the total strain in the butterfly curve. The right column of Figure 2.3 shows the electrical displacement versus electric field, which is the well known hysteresis curve. It describes the nonlinear polarization switching behavior as a function of applied field. The hysteresis comes from the energy needed to reverse the metastable dipoles during each cycle (Jaffe et al., 1971). These curves demonstrate the maximum remnant polarization for each bulk ceramic.

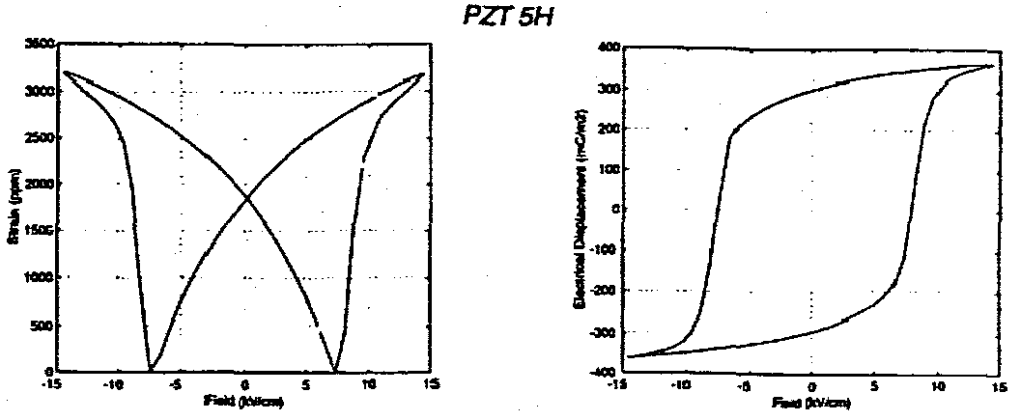

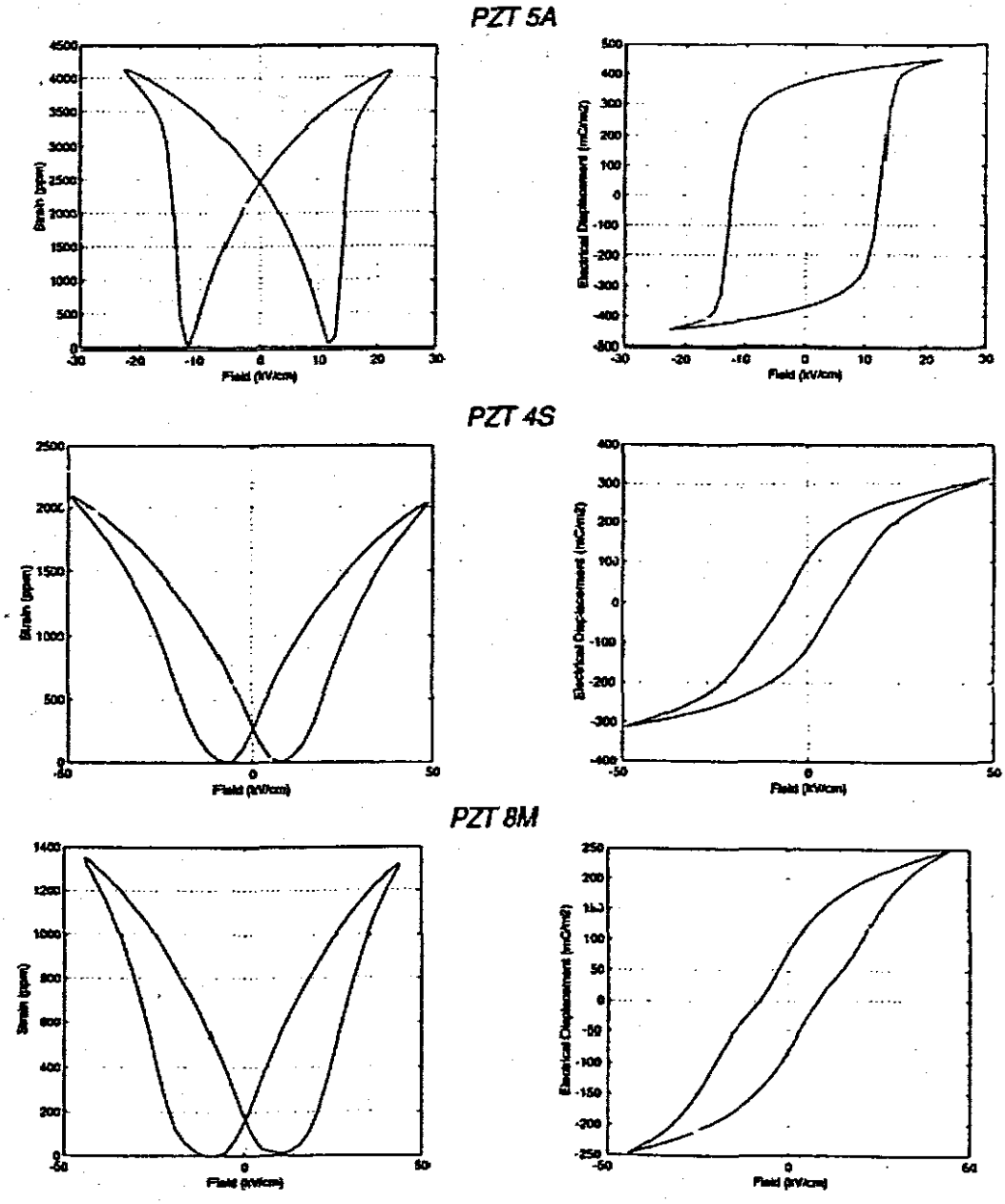

Figure 2.3: Nonlinear strain versus electric field and electrical displacement versus electric field, illustrating full polarization reversal

The representative work cycle strains are shown in Figure 2.4. These curves can be considered a portion of the butterfly curve, but are somewhat lower in value due to the more limited voltage drive range used to avoid repolarization. Note the high level of hysteresis and nonlinearity accompanying the higher strains of the soft ceramics. Since the energy density is proportional to the square of the strain, and only linear with stiffness, PZT 5A has substantially higher Rep Cycle actuation energy than others.

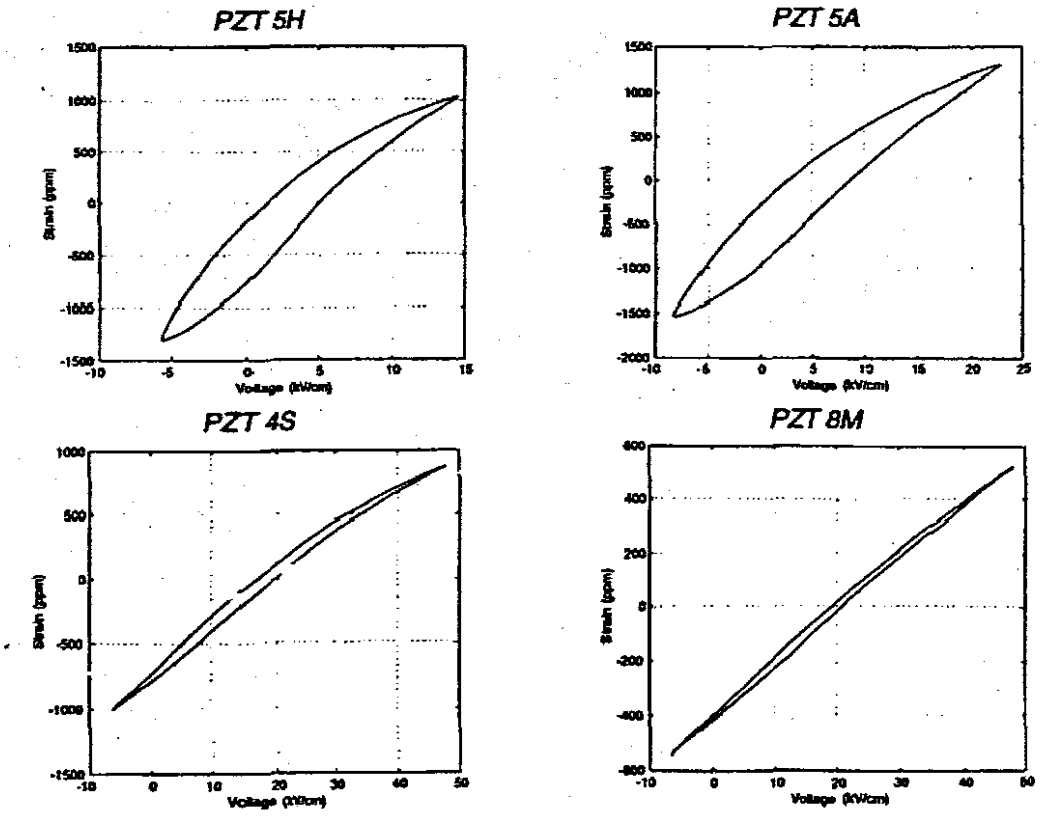

Figure 2.4: Maximum Representative Work Cycle Strains for four PZT types

A final property of the ceramic comparison is the compressive stress depolarization level. A compressive stress aligned with the direction of poling will tend to reorient the diploes 90° to the original poling axis, causing a loss of piezoelectric properties. The highest depolarization stresses are found in the hard ceramics, making them suitable for high stress environments. At this point, PZT 5H was chosen as the ceramic for use in the initial composite design and manufacture. This choice was made based on the high actuation strains (and stresses), ease of polarization, and the commercial availability of fine PZT 5H.

2.2.3 Ceramic Polarization Study

Polarizability is a property inherent in all dielectrics. One type is electronic polarization, caused by shifts in electron clods of the material away from their equilibrium positions for an applied field. Polar materials have additional contributions to the material Polarizability from orientation polarization of the dipoles for and applied electric field. In all cases, application of the electric field to the dielectric material induces a volume polarization. The field created in the material is offset by additional charges that collect on the electrodes (for a parallel plate capacitor analogy). Thus, the dielectric constant is used as a measure of the charge storage capability of the material.

One way to describe the polarization state of the material is the volume charge density. Alternatively, it can be described in terms of the surface charge on the material that exactly cancels the net volume charge. The polarization (**P**) of a material is related to the electrical displacement (**D**) and applied electric field (**E**) through the following:

$$\mathbf{D} = \varepsilon_0 \mathbf{E} + \mathbf{P} \tag{2.3}$$

where ε_0 is the dielectric of vacuum. Note that these parameters are vector quantities. Since the electrical displacement and electric field are related through the material dielectric constant (ε) in linear dielectrics by

$$\mathbf{D} = \varepsilon \mathbf{E} \tag{2.4}$$

it is possible to write the polarization in terms of the applied field as

$$\mathbf{P} = (\varepsilon - 1)\mathbf{E} \tag{2.5}$$

Generally, ε is much larger that one in most dielectrics, so that the polarization can be approximated by the electrical displacement, as written in Equation 2.4. In most cases, it is easier to measure the electrical displacement directly, and the terms are often used interchangeably.

Note that the polarization vanishes with zero electric field. That is, that removal of the field causes the material to return to its original unpolarized state, and the internal field no longer needs to be canceled by additional charges on the electrodes. In contrast to pure dielectrics, is the phenomenon of piezoelectricity, described as electric polarization produced by a mechanical stress or strain. In these cases, the polarization of piezoelectric materials is non-vanishing even after the field is removed

The piezoelectric phenomena were originally studied in single crystals of Rochelle salt. The lack of center symmetry of these single crystals causes a net movement of the positive and negative ions with respect to each other upon application of a stress. This results in an electric dipole, and charges appear on the surface of the crystal. This external surface charge (polarization) is a quantity with the units of charge per area. Many crystals make up a polycrystalline ceramic, whose individual dipoles are initially randomly aligned, showing no net polarization. That is, unpoled polycrystalline piezoceramics show no piezoelectric effects because the individual dipole moments within the ceramic cancel. Ferro electricity is defined as the existence of 'reversibility in a polar crystal of the direction of the electric dipole by means of an applied electric field' (Jaffe et al., 1971). With the application of a high electric field, these dipoles align preferentially, giving rise to the piezoelectric effect and a net polarization. Thus, polycrystalline piezoceramics owe their usefulness to the existence of Ferro electricity.

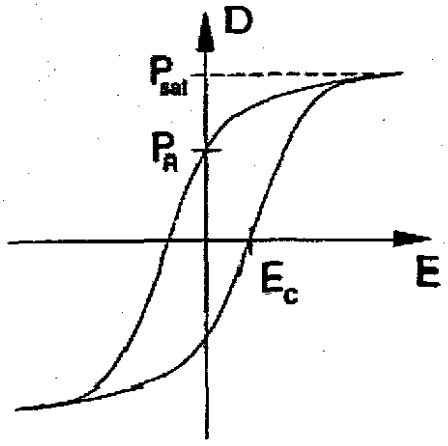

Figure 2.5: Hysteresis plot, illustrating saturation polarization (P_{sat}) and remnant polarization (P_R)

The magnitude of the piezoelectric coupling coefficients have been shown to depend on the degree of polarization (Belincourt, 1964). In other words, full polarization is necessary to realize the maximum benefits of the material. Evidence of polarization in a piezoelectric is usually described by the hysteresis plot of the **D** versus **E** curve, shown in Figure 2.5. For a non-ferroelectric, this curve would be a straight line (ideal capacitor), with its slope equal to the dielectric of the material. For a ferroelectric material, the flow of charges from dipole alignment causes a hysteretic path. The value for electrical displacement depends on the time history of the ceramic. The curve is shown for one complete cycle of dipole reorientation. The maximum level of instantaneous polarization is the saturation polarization (Psat), and the polarization remaining after the electric field has been removed is the remnant polarization (Pr). It is the remnant polarization that indicates the degree of poling in the ceramic. For a non-ferroelectric material, this value would always be zero. Finally, the point at which the electrical displacement vanishes is the coercive field (Ec), corresponding to the coercive field found in the butterfly curve.

The degree of remnant polarization has been show to be dependent on the magnitude of the electric field, the temperature of the ceramic during poling, and the length of time the poling field is applied. The best technique is to apply the poling field while the ceramic cools through its Curie temperature (Jaffe et al., 1971), where the dipoles align as they appear spontaneously. This is difficult to do for all but the softest ceramics, such as Barium Titanate that has a Curie temperature around 130°C. Other ceramics (even PZT 5H with a Curie temperature of 193°C) would require temperatures damaging to the composite structure. However, some level of increased temperature may improve the degree of polarization. The need for higher temperatures may also be offset by applying the field longer or at higher levels (at some percentage of the coercive field).

Although the level of remnant polarization is easy to measure for a sinusoidally varying electric field, it is difficult to accurately measure the charges associated with dipole switching in a long duration poling process (on the order of minutes), due to leakage currents and other difficulties. Since the remnant polarization is likely a function of time, it is important to be able to assess other than the AC value. Instead, this experimental

study will use the change in dielectric constant of the piezoceramic as an indicator of the degree of remnant polarization. This is a natural choice, considering the dielectric is the low field polarization. This section determines the degree of polarization of PZT 5H as a function of the three above mentioned variables, by monitoring the increase in dielectric constant.

In the previous section, several piezoceramics were compared on the basis of their material constants, particularly for the magnitude of the piezoelectric effect in both low field and high field regimes. These quantities were based on the assumption that the materials were already fully poled. Polarizing of ceramics is not a well documented phenomenon, and the conditions used to accomplish poling are often proprietary to the manufacturer. Since the piezoceramic will not be poled prior to composite manufacture, it is necessary to pole the ceramic in-situ. Once surrounded by matrix, it is difficult to establish whether the measured composite piezoelectric constants represent fully poled ceramic. However, the coercive field is a quantity that is easily measured for both the bulk ceramic and composite, and can be used to represent the level of electric field in the ceramic, regardless of configuration. This section established the necessary poling conditions in bulk ceramic using the coercive field as a metric. Then, the necessary poling conditions are easily identified for the composite form, once the composite coercive field is measured. It is important to accurately determine the poling field, not only to achieve full poling, but to avoid using fields that are unnecessarily high that may damage the composite.

Directly related to the phenomenon of poling is ceramic aging, or the post-poling change in properties with time. Aging has been observed for a variety of ceramics, with different aging rates dependent on the hardness of the ceramic. Change in material constants, and the coupling factor, and an increase in the stiffness and mechanical quality factor. This aging is likely caused by the relief of various internal stresses that arise from the spontaneous polarization (Jaffe et al., 1971). Following poling, domains are slowly reoriented into positions of lower energy. For Barium Titanate, the trend of aging has been shown to be linear when plotted against the log of time:

ε_{33}^{T} 4% per time decade

k_{33} 2.5% per time decade

A similar trend might be expected for PZT 5H, although the per-decade changes will be different. Such a change in material properties implies that a potentially large discrepancy in measurements are possible if taken at different periods in the aging process. Thus, the aging process of PZT 5H is characterized here by following the material constants as a function of time after poling. Again, the capacitance will be used as an indication of the remnant polarization, and hence, the trends in all piezoelectric constants. Piezoelectric constants are not measured, as the application of electric field to the sample at levels high enough to get significant strains may affect the aging rate (Jaffe et al., 1971).

2.2.4 Ceramic Characterization Summary

Four PZT ceramic types, ranging from soft (5H) to very hard (8M) were compared for their capabilities in low field and high field regimes. PZT 5H was found to have the largest low field response, and was easiest to polarize. Other ceramics, such as PZT 5A showed better high field capabilities, while hard ceramics like PZT 4S and 8M were better suited for high stress applications. The best ceramic choice for DPA product was not clear at this point in time, although PZT 5H was chosen for further characterization and the majority of the experimental work. Poling and aging studies were performed to better prepare for the use of PZT 5H in composites. The poling conditions necessary to maximize piezoelectric properties was determined as a function of the electric field strength and application time, and ceramic temperature. These can be related to the composite conditions through the easily measured coercive field. The aging study verified the aging trend of linear property reduction with the time decade.

Remnant polarization, dielectric and coercive field data all indicated a one third reduction in piezoelectric and electrical performance. All of this information, coupled with the matrix data and the models of the next chapter will provide design capability for current and future actuators.

Chapter 3

The Analytical Models of DPA Elements

3.1 Introduction

The most important effort of this work that has developed the Distributed Piezoelectric Actuator (DPA) is directed at the modeling of effective analytical properties. Models generate an understanding of the issues involved, particularly the limitations and tradeoffs of a given design. The desired outcome of analytical modeling is to obtain predictions of the properties response of the DPA products. These effective properties then become a way to describe the averaged response of the DPA for use in applications.

Models developed in this chapter are combined with the material characterization of the previous chapter and the analytical electrical characterization for property prediction of DPA. Due to the electrical field models that have been developed in this chapter, and the accurate distribution and intensity models, the analytical analysis models that have been developed in this chapter have been used in further analysis of different shape DPA in Chapter 4. In the subsequent chapters, the analytical models are verified by the result of FEM and products testing data. To support this goal, the objectives for this chapter are

- Develop the analytical electrical field models for two types of DPA elements
- Develop the mechanical performances analysis for the prediction of DPA
- Comparison of the models results between the analytical model and FEM
- Comparison of the results between the analytical model and the product testing data

In this chapter, firstly, based on the theory of electromagnetics, the two types of DPA elements have been considered as two kinds of capacitors. The charge distributed density on the interdigitated electrode (IDE) and the capacitance of DPA elements have been analysed and concluded. The distribution and intensity of electrical field in DPA elements have also been concluded and discussed. Secondly, applying the piezoelectric constitutive relations, the models for strain and stress field of DPA elements have been developed, and the mechanical performances of rectangular DPA have been concluded and analysed. In the models of strain and stress field, the affects of epoxy-matrix material have also been considered in the models.

Due to the minimum hypotheses have been applied during the processes of conclusion, the characteristics of this chapter are that the accurate distribution and intensity of

electrical field in DPA have been concluded, and then the models can be used in the DPA design and manufacture in order to reduce the cost of DPA products in future.

3.2 The Electrical Field Analytical analysis of DPA Elements

The most important difference and benefits between the normal materials and piezoelectric material is the piezoelectric phenomenon, which has been discussed in Chapter 2. The properties of electrical field in the piezoelectric actuators are the key points that affect the mechanical performances of piezoelectric actuator. Due to the special polarization phenomenon in DPA elements, which applied the IDE technology, these effects between the electrical and mechanical performances are more evident than other kind of piezoelectric actuator.

As the first step for building the analytical analysis models of DPA elements, the accurate distribution and intensity analysis of electrical field in DPA elements has been completed in this section, which have been ignored by the previous works.

3.2.1 Two Types of Polarization of DPA Elements

Depending the Interdigital Electrode that are used in the DPA, the DPA products can be delimited to some different types of element. Figure 3.1 and Figure 3.2 show the two principal types of DPA elements.

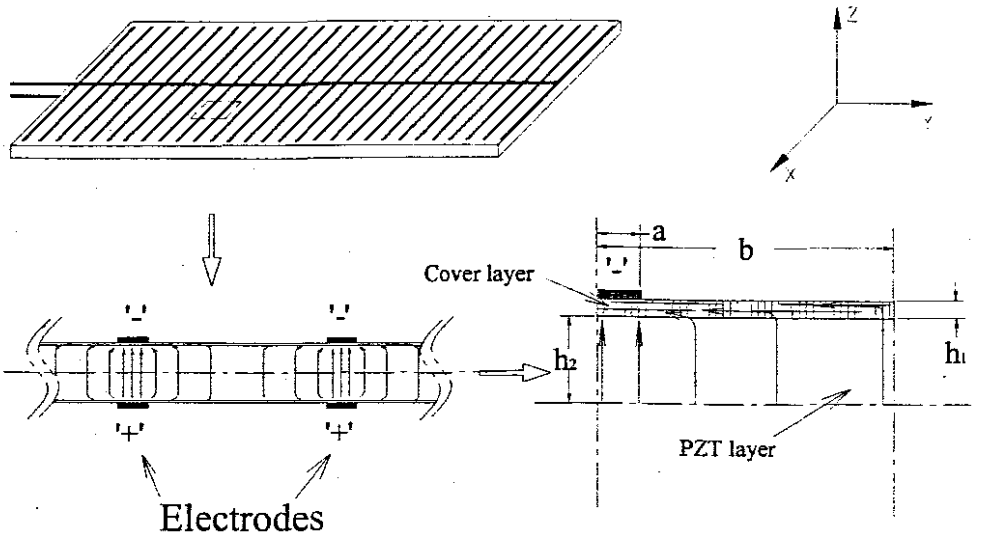

Figure 3.1: The first type of DPA element

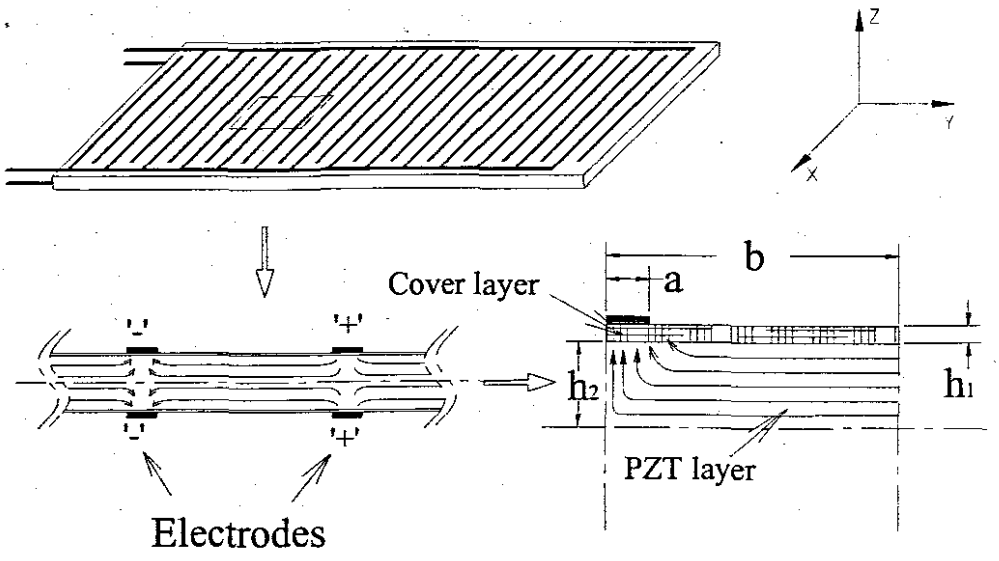

Figure 3.2: The second type of DPA element

In the Figure 3.1, the IDE was applied for keeping the same poles on one side of the DPA, and keeping the opposite poles on the other side. The electrical field and polarization tensor in this type of elements follows the thickness direction – 'Z' direction and runs through the piezoelectric material and the epoxy-matrix material. However, for the second type of DPA element, which has been shown in the Figure 3.2, the poles of actuator have been superseded between the close IDE branches. The electrical field and polarization tensor follows the material length direction – 'Y' direction. The differences of analytical analysis models between the two types of DPA elements will be shown in the following sections.

For the one element of DPA, considering the structures that DPA elements have, some hypotheses have been raised:

- The materials properties of piezoelectric material and epoxy-matrix material in the actuator are uniform.

- Due to the general dimension of actuator in the 'X' direction always much bigger than the IDE branch center distance '2b', the electrical and mechanical effect on the 'X' direction have been ignore.

- The following analysis processes have supposed that the dimension of actuator in the 'Y' direction is much bigger than the IDE branch center distance '2b'. The electrical edge effects for the each element have been ignored.

The above hypotheses are necessary for building the analytical analysis models, and the accuracy and reliability of models that have applied these hypotheses will be proved.

3.2.2 Charge density analysis

For the analytical analysis of electrical field in the DPA elements, the charge density on each pole have to be understood and described at the beginning, which has always been ignored during previous work.

According to the theory of electromagnetic, the every point on the poles will have the same electric potential, and the inter electrical field tensor $\mathbf{E}_{int}$ equal to zero.

$$\mathbf{E}_{int} = 0 \tag{3.1}$$

Considering the structure of IDE branch and the distribution of poles, the $\mathbf{E}_{int}$ for the one point on the pole in one elements (showing in the Figure 3.1 and Figure 3.2) can be obtained by the following formula.

$$\mathbf{E}_{int} = \sum_{i} \iint_{S_{pole}} \frac{\rho(s)}{4\pi\varepsilon R^2} \mathbf{r} ds \tag{3.2}$$

where $\rho(s)$ is the surface charge density on the electrode in the DPA elements. It can be resolved by the product of two line charge densities;

$$\rho(s) = \rho_X(l) \cdot \rho_Y(l) \tag{3.3}$$

where $\rho_X(l)$ is the line charge density on the 'X' axis, and $\rho_Y(l)$ is the line charge density on the 'Y' axis. Considering the electromagnetic knowledge, the function $\rho_X(l)$ is equal to one constant that will depend on applying voltage on the actuator. The function $\rho_Y(l)$ has been constrained with three boundary conditions.

$$\left.\frac{d\rho_Y(l)}{dy}\right|_{y=0} = 0, \qquad \rho_Y(l)\big|_{y=\pm a} = \infty, \qquad \left.\frac{d\rho_Y(l)}{dy}\right|_{y=\pm a} = \infty \tag{3.4}$$

The $\rho_Y(l)$ have been obtained following the integration and the matrix vector analysis. Due to the nature of charge density function $\rho_Y(l)$, it can be resolved with three sub-functions – $f(y)$, $g(y)$ and $h(y)$. Applying the formula (3.1) and the boundary conditions (3.4),

$$\rho_Y(l) = f(y) \cdot g(y) \cdot h(y) \tag{3.5}$$

and

$$f(y)=\frac{1}{-|y|+1}$$
$$g(y)=\left[A\left(-|D\cdot y|+D\cdot C\right)^{-B}\right]^{-1} \qquad (3.6)$$
$$h(y)=\sum_{i=1}^{n}A_i\left(-|y|+C\right)^{i}+C_1$$

where, $n=4$ – for the first type of DPA element
$n=2$ – for the second type of DPA element

In the formula (3.6), $f(y)$ and $g(y)$ can be considered as the shape functions in formula (3.5), and $h(y)$ is the correct function for formula (3.5). C and D are the constants of analysis that depended on the matrix vector analysis during the solving for the function $\rho_Y(l)$. A, A_i, B and C_1 are the constants of structure that depended on what type of elements structure have been considered during the solution process. Unfortunately, the exact relationships between these constants and IDE structure have not been completed in this chapter. But the charge density functions $\rho_Y(l)$ has been affected evidently by the ratios between 'h' – the piezoelectric material thickness, 'a' – the width of the IDE branch electrode and 'b' – the electrodes center distance.

The following tables and figures show the $\rho_Y(l)$ trend with the different 'h/a' and 'b/a' for the structure of IDE in the first and second types of DPA elements. Due to the similar distribution of the intensity of charge density, the sub-function $g(y)$ in the charge density function $\rho_Y(l)$ is more important than other sub-functions. The constant of structure – 'A' and 'B' are the most important constants of all constants in formula (3.6). The general effect of the relationships between the constants 'A', 'B' and the IDE structure ratios 'h/a' and 'b/a' have not been completed. The constants in the function $\rho_Y(l)$ with the different IDE structure ratio are shown in the Table-1 and Table-2. Further work on the relationship between the constants and the IDE structure ratios will be done in future.

		A	B	C	D	A4	A3	A2	A1	C1
h=0.25a	b=2a	44.818	-0.8054	1.005	100	6.00E-08	-1.00E-05	0.0012	-0.0362	1.248
	b=4a	45.705	-0.8079	1.005	100	6.00E-08	-1.00E-05	0.0012	-0.0367	1.2567
	b=6a	45.824	-0.808	1.005	100	6.00E-08	-1.00E-05	0.0012	-0.0369	1.2596
	b=limitless	44.11	-0.8015	1.005	100	6.00E-08	-1.00E-05	0.0012	-0.036	1.2644
h=a	b=2a	19.549	-0.6511	1.005	100	3.00E-08	-6.00E-06	0.0006	-0.0184	1.1564
	b=4a	21.793	-0.6533	1.005	100	3.00E-08	-6.00E-06	0.0006	-0.0198	1.1576
	b=6a	21.868	-0.6528	1.005	100	3.00E-08	-7.00E-06	0.0006	-0.0199	1.1584
	b=limitless	23.013	-0.6579	1.005	100	3.00E-08	-7.00E-06	0.0006	-0.0213	1.1689
h=2a	b=2a	15.651	-0.5761	1.005	100	9.00E-09	-2.00E-06	0.0002	-0.0094	1.0892
	b=4a	18.657	-0.6148	1.005	100	2.00E-08	-4.00E-06	0.0004	-0.0147	1.1237

	b=6a	18.215	-0.614	1.005	100	2.00E-08	-4.00E-06	0.0004	-0.0141	1.119
	b=limitless	19.401	-0.6217	1.005	100	2.00E-08	-5.00E-06	0.0004	-0.0158	1.1316

Table-1: the constants in the charge density with different 'h/a' and 'b/a'(first type)

		A	B	C	D	A2	A1	C1
h=0.25a	b=2a	7.113	-0.4081	1.005	100	5*10^-5	-0.0047	1.0767
	b=3a	8.762	-0.4517	1.005	100	5*10^-5	-0.0051	1.0777
	b=4a	9.3559	-0.4655	1.005	100	6*10^-5	-0.0053	1.078
	b=5a	9.6334	-0.4716	1.005	100	6*10^-5	-0.0053	1.0783
	b=6a	9.7847	-0.4749	1.005	100	6*10^-5	-0.0054	1.0783
	b=limitless	10.603	-0.4861	1.005	100	6*10^-5	-0.0059	1.0837
h=0.5a	b=2a	6.9766	-0.4149	1.005	100	1*10^-5	-0.0016	1.0347
	b=3a	8.6943	-0.4595	1.005	100	2*10^-5	-0.0023	1.0394
	b=4a	9.3637	-0.4647	1.005	100	3*10^-5	-0.0026	1.041
	b=5a	9.6862	-0.4815	1.005	100	3*10^-5	-0.0027	1.0417
	b=6a	9.8649	-0.4852	1.005	100	3*10^-5	-0.0027	1.0422
	b=limitless	11.799	-0.561	1.005	100	6*10^-5	-0.0075	1.0298
h=a	b=2a	10.0125	-0.4981	1.005	100	3*10^-5	-0.0019	1.0292
	b=3a	10.831	-0.5117	1.005	100	3*10^-5	-0.0024	1.0342
	b=4a	11.862	-0.5267	1.005	100	3*10^-5	-0.0028	1.0391
	b=5a	12.33	-0.5337	1.005	100	3*10^-5	-0.003	1.0407
	b=6a	12.589	-0.5376	1.005	100	3*10^-5	-0.0031	1.0415
	b=limitless	13.888	-0.5516	1.005	100	4*10^-5	-0.0037	1.0491
h=1.5a	b=2a	12.362	-0.5269	1.005	100	4*10^-5	-0.0036	1.0489
	b=3a	14.041	-0.5534	1.005	100	4*10^-5	-0.004	1.0526
	b=4a	16.142	-0.5816	1.005	100	5*10^-5	-0.0047	1.0599
	b=5a	10.388	-0.5393	1.005	100	9*10^-6	-0.0007	1.0085
	b=6a	13.332	-0.557	1.005	100	3*10^-5	-0.0029	1.0369
	b=limitless	15.615	-0.576	1.005	100	5*10^-5	-0.0041	1.052
h=2a	b=2a	13.427	-0.5439	1.005	100	4*10^-5	-0.0038	1.0506
	b=3a	14.85	-0.5653	1.005	100	5*10^-5	-0.0041	1.0521
	b=4a	15.462	-0.574	1.005	100	5*10^-5	-0.0042	1.0534
	b=5a	10.388	-0.5393	1.005	100	5*10^-6	-0.00043	1.0547
	b=6a	16.318	-0.5858	1.005	100	3*10^-5	-0.0029	1.0573
	b=limitless	16.472	-0.5871	1.005	100	5*10^-5	-0.0043	1.0533

Table-2: the constants in the charge density with different 'h/a' and 'b/a'(second type)

In the following figures, the intensity and distribution of charge density on the IDE have been clearly shown. The intensity of charge density shows the evident difference between the center and the edge of the electrode. In the first type of DPA element, the range of the intensity ratios between the edge and the center of electrode is 6 to 13. And in the second type of element, the range of ratios increases to around 13 to 30. In Figure 3.11 and 3.12, the trend of charge density with different structure ratios – 'h/a' and 'b/a' have also been shown clearly. For the first type of element, the non-uniform phenomenon of charge

density with the small ratios of 'h/a' and 'b/a' is more evident than that with the big ratios. Oppositely, in the second type of element, the non-uniform phenomenon is more evident when the ratios of 'h/a' and 'b/a' are big.

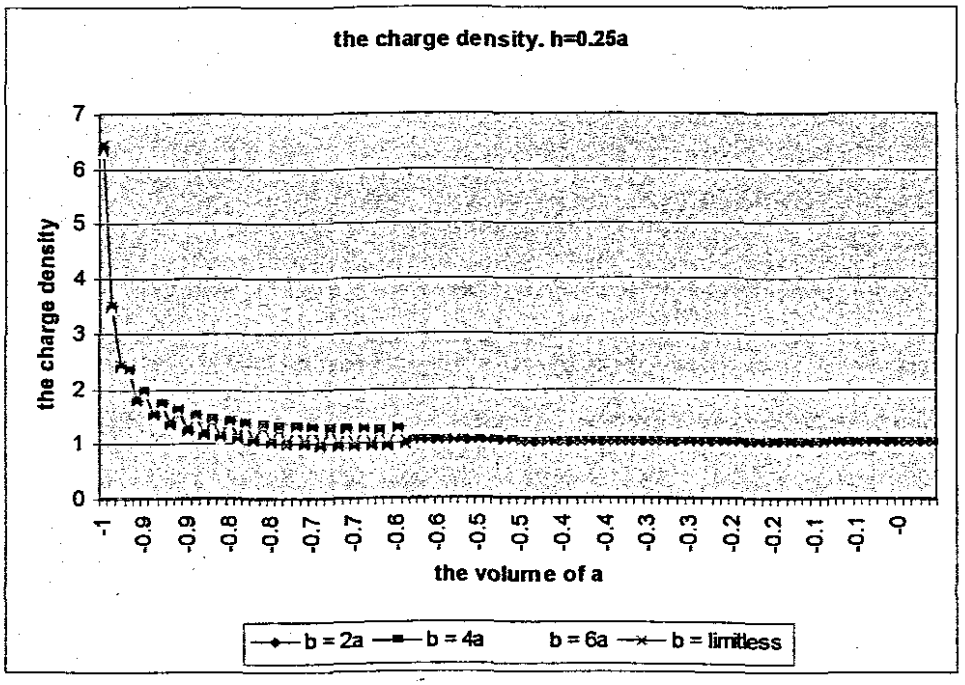

Figure 3.3: the charge density with different b/a at h=0.25a in the first type DPA element

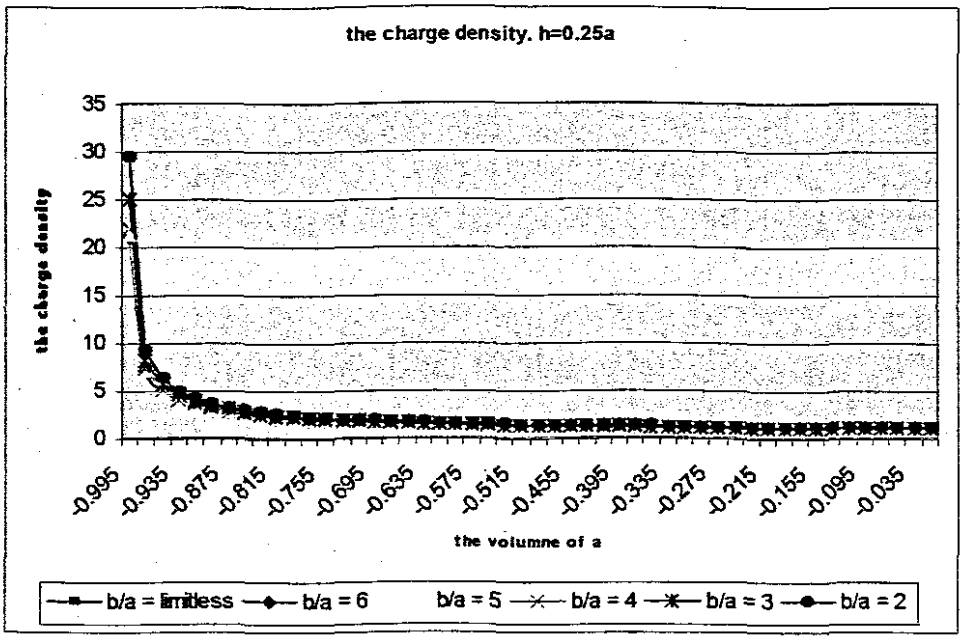

Figure 3.4: the charge density with different b/a at h=0.25a in the second type DPA element

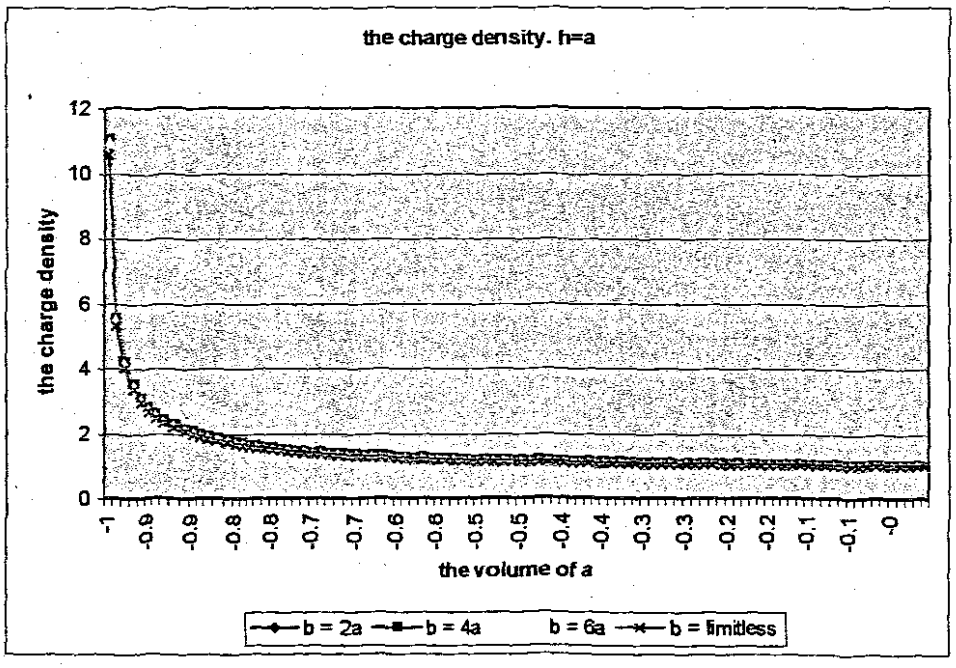

Figure 3.5: the charge density with different b/a at h=a in the first type DPA element

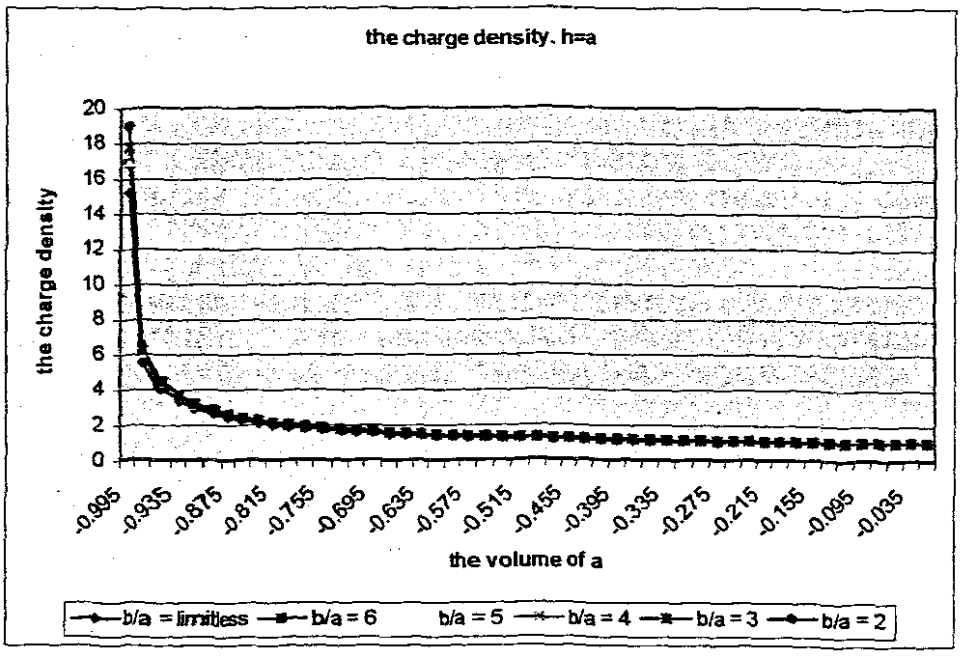

Figure 3.6: the charge density with different b/a at h=a in the second type DPA element

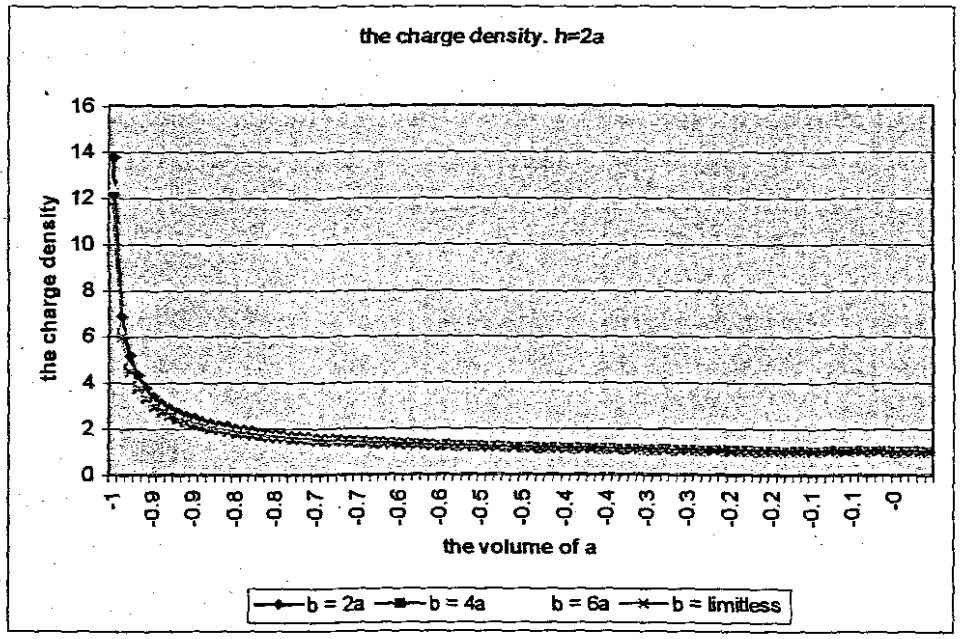

Figure 3.7: the charge density with different b/a at h=2a in the first type DPA element

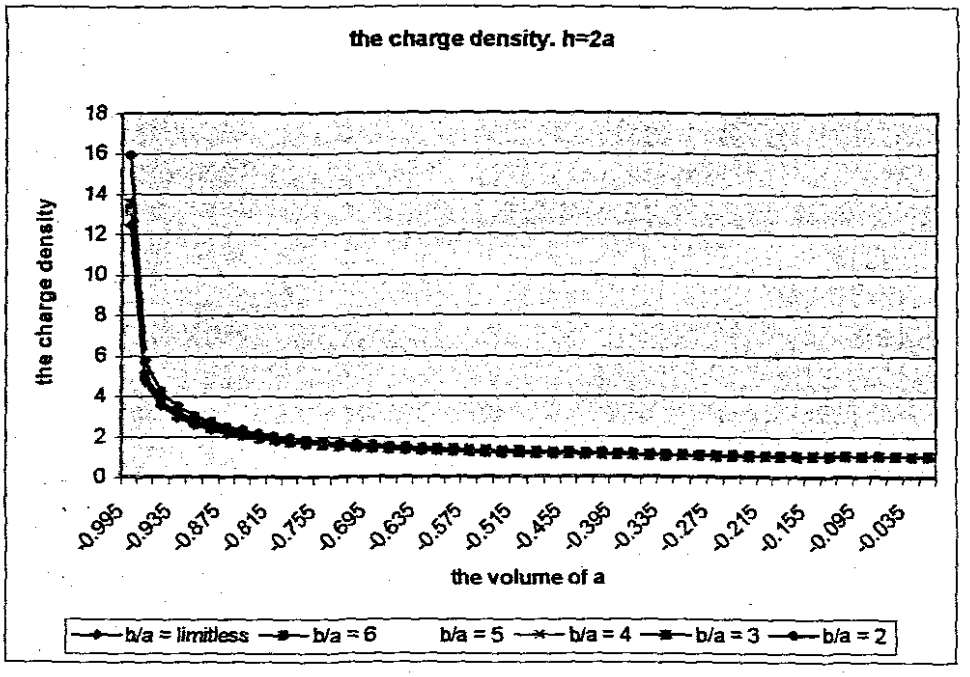

Figure 3.8: the charge density with different b/a at h=2a in the second type DPA element

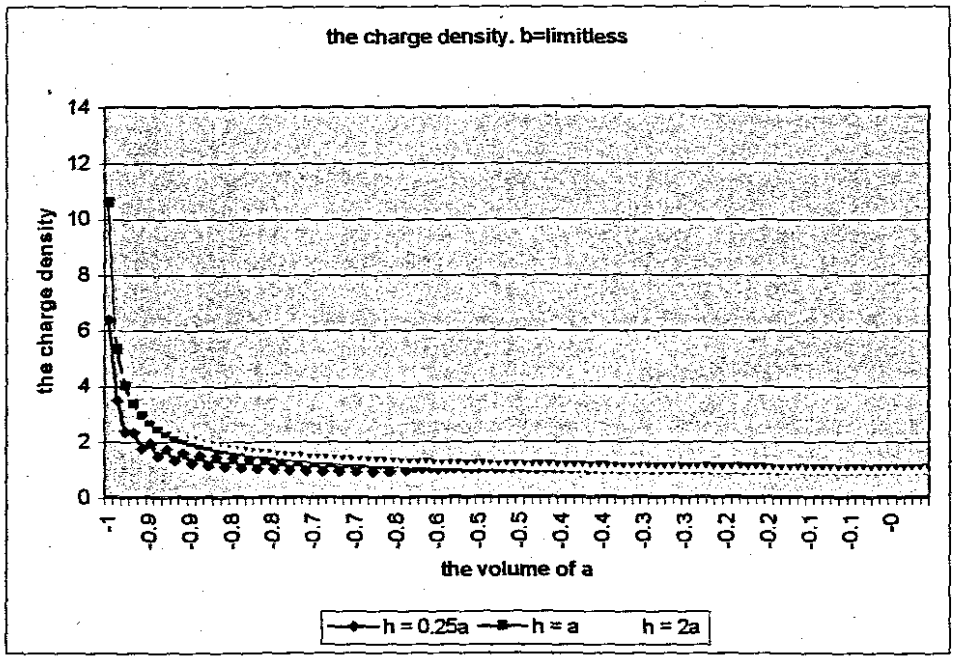

Figure 3.9: the charge density with different h/a at b=limitless in the second type DPA element

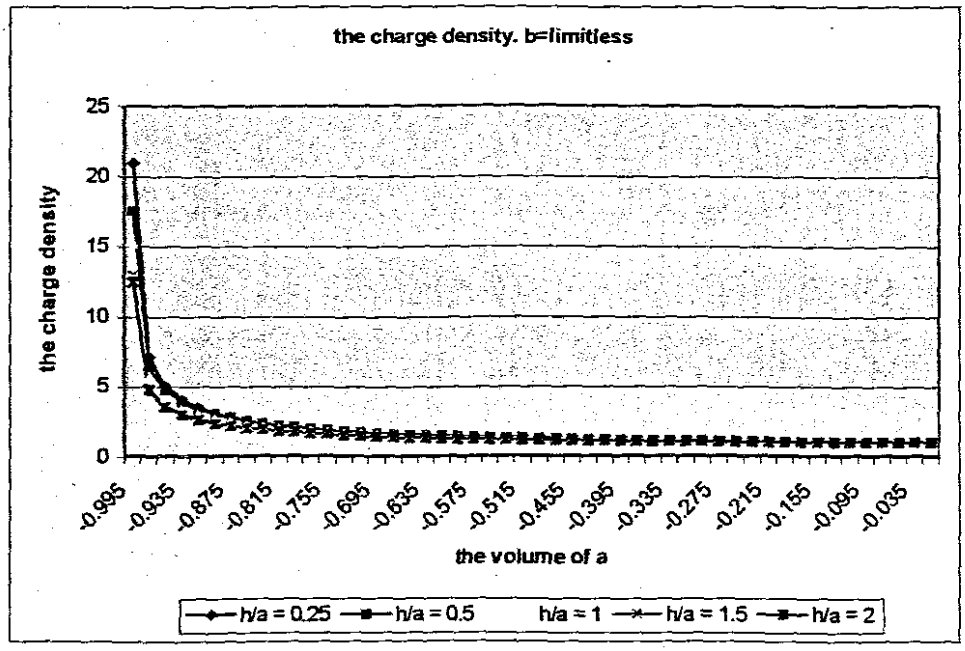

Figure 3.10: the charge density with different h/a at b=limitless in the second type DPA element

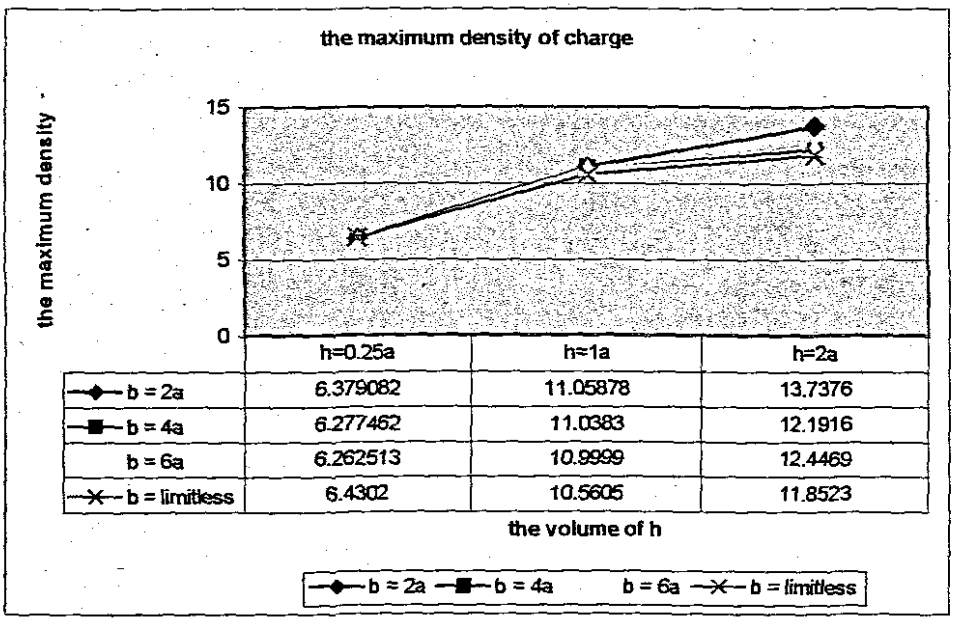

	h=0.25a	h=1a	h=2a
b = 2a	6.379082	11.05878	13.7376
b = 4a	6.277462	11.0383	12.1916
b = 6a	6.262513	10.9999	12.4469
b = limitless	6.4302	10.5605	11.8523

Figure 3.11: the trend of maximum charge density with different h/a and b/a and the data table in the first type DPA element

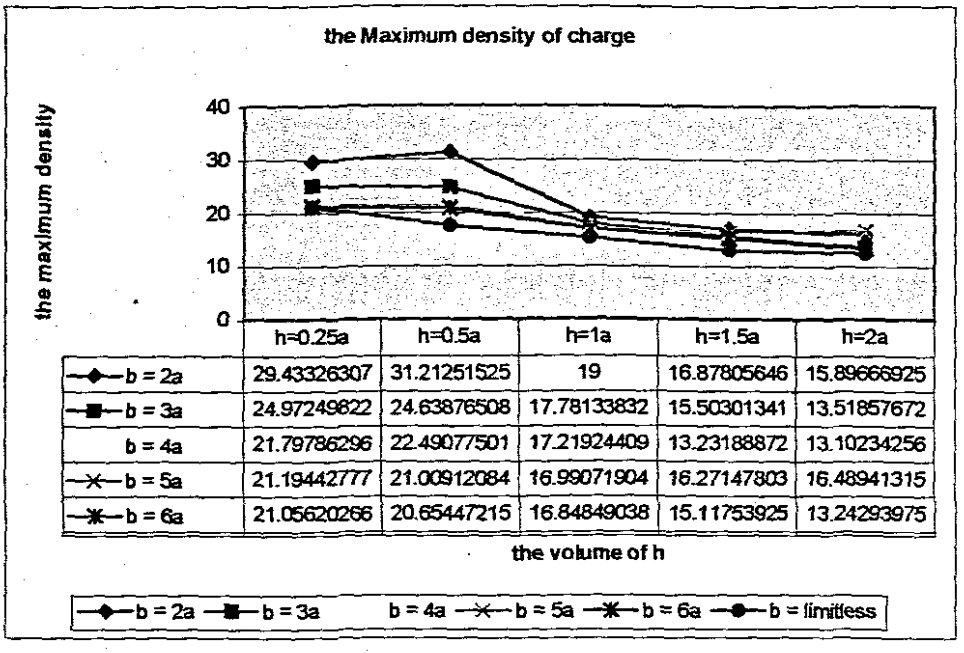

	h=0.25a	h=0.5a	h=1a	h=1.5a	h=2a
b = 2a	29.43326307	31.21251525	19	16.87805646	15.89666925
b = 3a	24.97249822	24.63876508	17.78133832	15.50301341	13.51857672
b = 4a	21.79786296	22.49077501	17.21924409	13.23188872	13.10234256
b = 5a	21.19442777	21.00912084	16.99071904	16.27147803	16.48941315
b = 6a	21.05620266	20.65447215	16.84849038	15.11753925	13.24293975

Figure 3.12: the trend of maximum charge density with different h/a and b/a and the data table in the second type DPA element

For the effective structure of IDE that have been used in the large volume applications, such as aerospace structure applications, the effect of surface charge density intensity and distribution difference between the center and edge of electrode can be ignored during

further mechanical properties analysis. But for the small volume or micro dimension in the applications such as MEMS, that kind of effect cannot be ignored.

Furthermore, this characteristic of charge density also is the key for explaining the non-uniform phenomenon of the electrical field that have been completed in this research project, and will give the important advise for the design and improvement of the PDA products. The concrete analyses have been completed in Appendix A.

Further accurate effects from the charge density on the IDE on the properties of DPA elements and products cannot be described only based on the above analysis results. As the first step for the analysis of electrical field in DPA elements, the non-uniform phenomenon of charge density on the electrodes will affect the Capacitance, Distribution and Intensity of electrical field analysis immediately. The intensity and distribution function of charge density – $\rho(s)$ will be applied for further analysis on electrical field. Furthermore, it is one important part in the non-uniform electrical field and mechanical properties analytical analysis that is the major objective in this chapter.

3.2.3 Capacitance analysis of DPA Elements

A capacitor is a device for storing electric charge and, hence, electric energy. It consists of two conductors separated by an insulating medium. We define its capacitance as the ratio of the charge on one of the conductors to the applied voltage (potential difference). Thus, the capacitance C of a capacitor is

$$C = \frac{|Q|}{|V|} \tag{3.7}$$

where C = capacitance in farads, F
Q = charge in coulombs, C
V = potential difference in volts, V

As a special electrical element, the capacitance of DPA is evidently different from the general capacitors that have been used at present. Up to now, due to the complex structures of DPA, the accurate analytical analysis for the capacitance of DPA element have never been discussed and studied. In this work, the capacitance of DPA element has been discussed by applying the basic electromagnetic principles and functions.

Formula (3.7) can be written in terms of the surface charge density $\rho(s)$, and $\mathbf{E}_s$ between the electrodes as

$$C = \frac{\left|\int_s \rho(s)ds\right|}{\left|-\int_b^a \mathbf{E}_s \bullet d\mathbf{l}\right|} \tag{3.8}$$

and

$$\rho(s) = \rho_X(l) \cdot \rho_Y(l)$$

Considering the two type of DPA elements that have been shown in the Figure 3.13, applying the electrical field intensity formula,

$$\mathbf{E}_s = \iint_s \frac{\rho(s) \cdot \mathbf{r} ds}{4\pi\varepsilon R^2} = \iint_s \frac{\rho_X(l) \cdot \rho_Y(l) \mathbf{r} ds}{4\pi\varepsilon R^2} \tag{3.9}$$

and

$$\mathbf{E}_s = \mathbf{E}_X + \mathbf{E}_Y + \mathbf{E}_Z \tag{3.10}$$

where ε - the compound dielectric constant of piezoelectric material

$\mathbf{E}_X$, $\mathbf{E}_Y$ and $\mathbf{E}_Z$ are the branches of $\mathbf{E}_s$ on the 'X', 'Y' and 'Z' axis.

Considering that the 'X' axis line charge density function $\rho_X(l)$ has depended on the voltage that has been applied in the DPA element, it can be supposed to be a constant during the following analysis processes.

$$\rho_X(l) = constant$$

Formula (3.8) can be written again as

$$C = \frac{\left| \int_s \rho_Y(l) ds \right|}{\left| -\int_b^a (\mathbf{E}_X + \mathbf{E}_Y + \mathbf{E}_Z) \bullet d\mathbf{l} \right|} \tag{3.11}$$

In the formula (3.11), the capacitance for the different types of DPA elements can be determined by the charge density function $\rho_Y(l)$ that has been discussed in section 3.2.2 and the integral path from point 'b' to point 'a', which has been shown in Figure 3.13. Furthermore, the charge density function and the integral path also are depended on the structure of the DPA element and the pattern of IDE. Moreover, the capacitance of DPA elements are not depended on the volt used on the IDE of DPA elements.

Comparing the formula (3.7) and formula (3.11), the integral following arbitrary path from point 'b' to point 'a' will get the same result due to the same potential difference between any point on electrode 'B' and any point on electrode 'A'. Considering the symmetry characters of DPA elements with the 'X' axis and the boundary conditions that the edge effects have been ignored, the best integral path is 'Path 1' that has been shown in Figure 3.13.

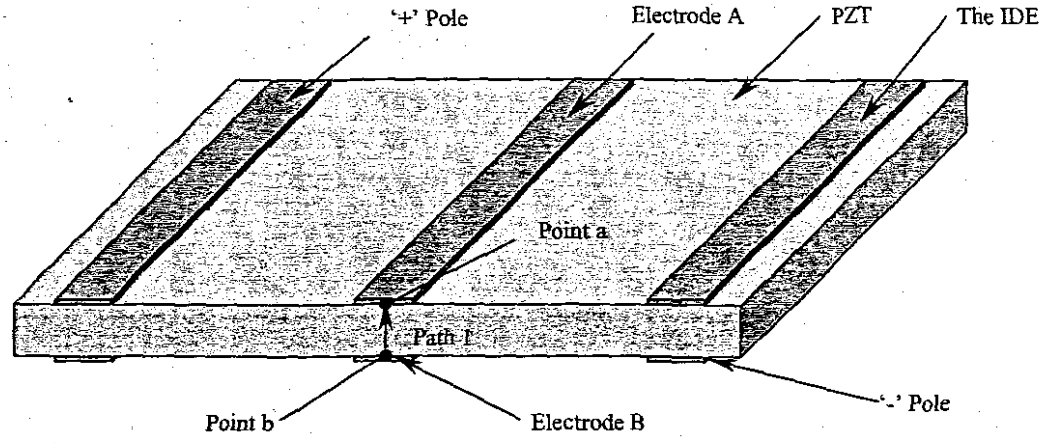

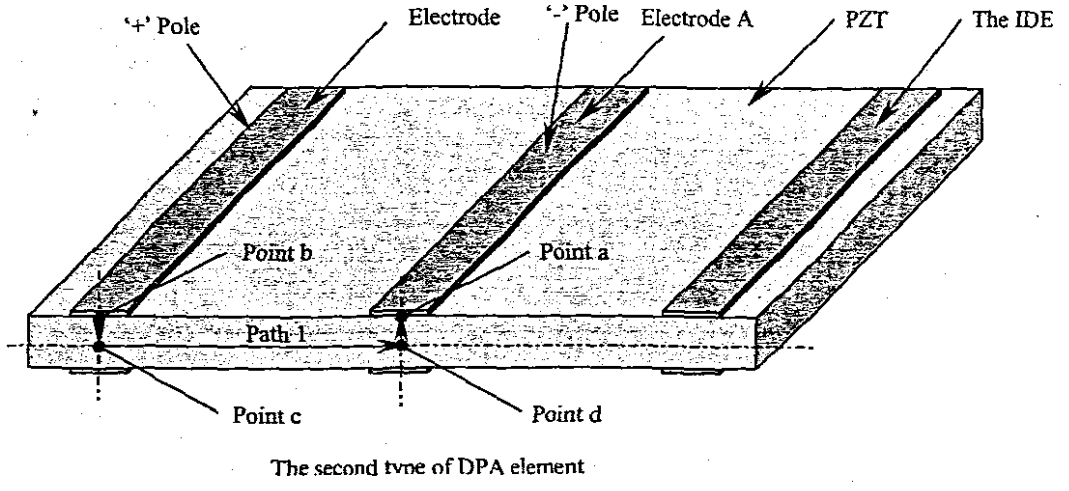

Figure 3.13: the best integral path in the two type of DPA elements

For the first type of DPA element, formula (3.11) can be rewritten as

$$C = \frac{\left| \int_s \rho_Y(l) ds \right|}{\left| -\int_c^a \mathbf{E}_Z dl \right|} \tag{3.11.1}$$

For the second type of DPA element,

$$C = \frac{\left| \int_s \rho_Y(l) ds \right|}{\left| -\left(\int_b^c \mathbf{E}_Z dl + \int_c^d \mathbf{E}_Y dl + \int_d^a \mathbf{E}_Z dl \right) \right|} \tag{3.11.2}$$

Due to the hypotheses that have been written down on the above,

$$\int_b^c \mathbf{E}_Z dl = \int_a^d \mathbf{E}_Z dl$$

So the formula 3.11.2 can be rewritten as

$$C = \frac{\left| \int_s \rho_Y(l) ds \right|}{\left| -\left(2\int_b^c \mathbf{E}_Z dl + \int_c^d \mathbf{E}_Y dl \right) \right|} \tag{3.11.3}$$

3.2.4 Analytical analysis of Electrical Field

DPA is one kind of actuator that has been driven by electrical signal. The properties of DPA are decided by the intensity and the distribution of electrical field in the actuator. At the same time, the actuator can be damaged by the defect of electrical field in the actuator, including the excessive intensity and gradient. So the accurate distribution and intensity analysis for the electrical filed in the actuator have to be completed for improving the DPA design and manufacture.

In the following analysis, the 'Y' axis line charge density $\rho_Y(l)$ has been considered as the uniform charge density. The effects on the distribution and intensity of electrical field have been discussed in Appendix B.

For the first type of DPA element that has been shown in the Figure 3.1, applying the electrical field intensity formula (3.9)

$$\mathbf{E}_s = \iint_s \frac{\rho(s) \cdot \mathbf{r} ds}{4\pi\varepsilon R^2} \tag{3.12}$$

where

$$\mathbf{r} = \frac{(x-\xi)\mathbf{i} + (y-\eta)\mathbf{j} + (z-\mu)\mathbf{k}}{R}$$

$$R = \sqrt{(x-\xi)^2 + (y-\eta)^2 + (z-\mu)^2}$$

the electrical field have been gotten during the integrate steps,

$$\mathbf{E} = E_x\mathbf{i} + E_y\mathbf{j} + E_z\mathbf{k} \tag{3.13}$$

and

$$E_x = 0$$

$$E_y = \frac{\bar{\rho}_S}{4\pi\varepsilon_{,}}\sum_n ln\left\{\frac{[(2nb+a)-\eta]^2+[\mu-h]^2}{[(2nb-a)-\eta]^2+[\mu-h]^2}\times\frac{[(2nb-a)-\eta]^2+[\mu+h]^2}{[(2nb+a)-\eta]^2+[\mu+h]^2}\right\}$$

$$E_z = \frac{\bar{\rho}_S}{4\pi\varepsilon}\sum_n 2i\cdot\left\{\frac{(2nb+a-\eta)\cdot a\tanh\left[\frac{(h-\mu)i}{|2nb+a-\eta|}\right]}{|2nb+a-\eta|}+\frac{(-2nb+a+\eta)\cdot a\tanh\left[\frac{(h-\mu)i}{|-2nb+a+\eta|}\right]}{|-2nb+a+\eta|}\right.$$

$$\left.+\frac{(-2nb+a+\eta)\cdot a\tanh\left[\frac{(\mu+h)i}{|-2nb+a+\eta|}\right]}{|-2nb+a+\eta|}+\frac{(2nb+a-\eta)\cdot a\tanh\left[\frac{(\mu+h)i}{|2nb+a-\eta|}\right]}{|2nb+a-\eta|}\right\}+C_z$$

$$C_z = \begin{cases} 4\pi, & \text{when } |\eta-2\text{nb}| < a \\ 2\pi, & \text{when } |\eta-2\text{nb}| = a \\ 0 & \text{when } |\eta-2\text{nb}| > a \end{cases}$$

$$\bar{\rho}_S = \frac{CV}{A}$$

where
- $2b$ -- the distance between two centre-line of electrodes;
- $2a$ -- the width of each electrode;
- $2h$ -- the thickness of actuator;
- $\bar{\rho}_S$ -- the surface charge density,
- ε -- the piezoelectric dielectric medium;
- n -- the number of pole in one side.
- C -- the capacitance of the DPA elements,
- V -- the volt of apply on the actuator,
- A -- the total area of poles in one element.

Here, consider the actual situation of DPA, then the 'X' direction electrical field effect can be decreased by improving the design. So, the 'X' direction non-uniform electrical field effect has been ignored.

Because there are three layers between both sides of IDE, which has been shown in Figure-1, the improvement on formula (3.13), in completed form, can be found to be

$$\mathbf{E}_{imp} = E_{impx}\mathbf{i} + E_{impy}\mathbf{j} + E_{impz}\mathbf{k} \qquad (3.13.1)$$

The differences of formula (3.13) and formula (3.13.1) are:

For the two cover layers:
$h_{imp} = h_1 + h_2$ and $\varepsilon = \varepsilon_{co}$

For the centre layer—PZT material layer:

$$h_{imp} = h_2 + \frac{\varepsilon_{co}}{\varepsilon_{PZT}} h_1 \text{ and } \varepsilon = \varepsilon_{PZT}$$

Applying formula (3.13), the Figure 3.14, 3.15, 3.16, 3.17 have shown the distribution and intensity of electrical field in one DPA element. Here the rate of 'b/a' is 4, and the rate of 'h/a' is 1.

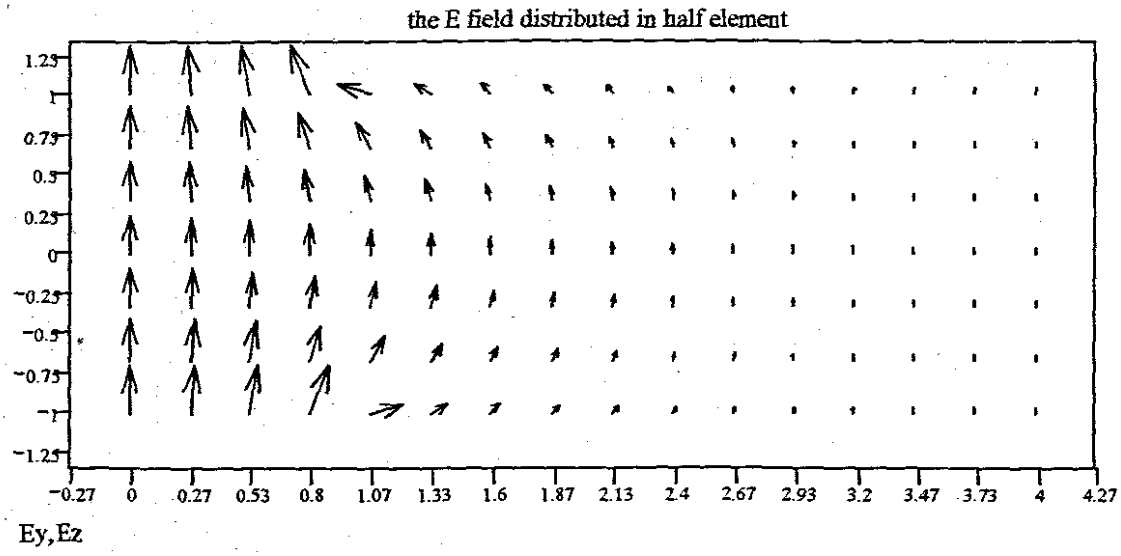

Figure 3.14: the electrical field distributed in half DPA element

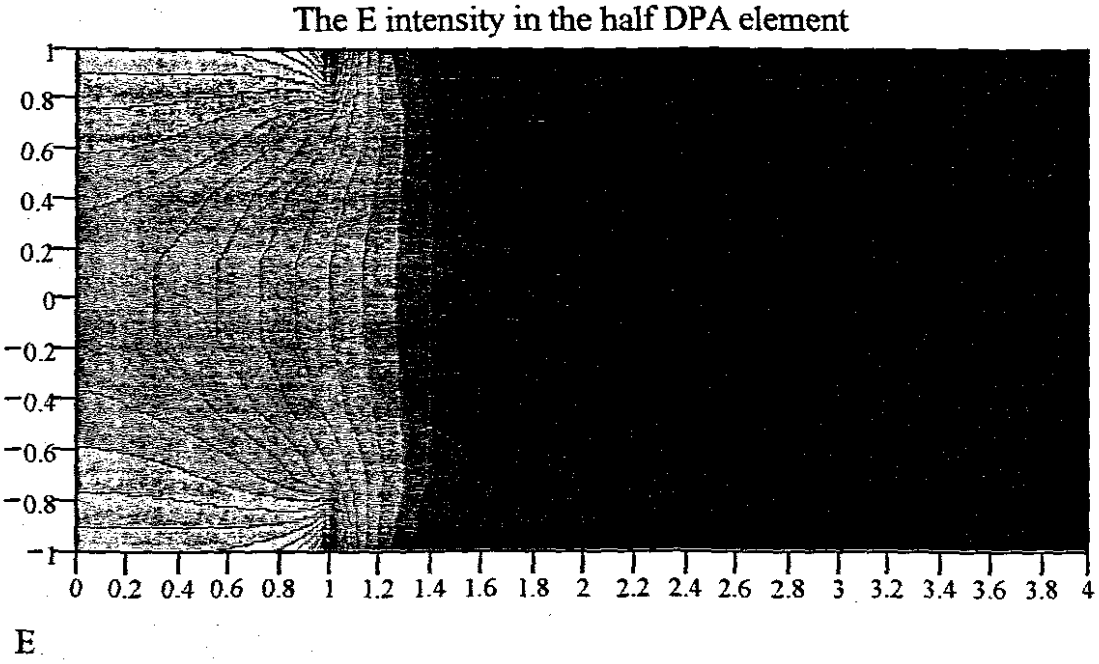

Figure 3.15: the E intensity distributed in the first type of DPA element

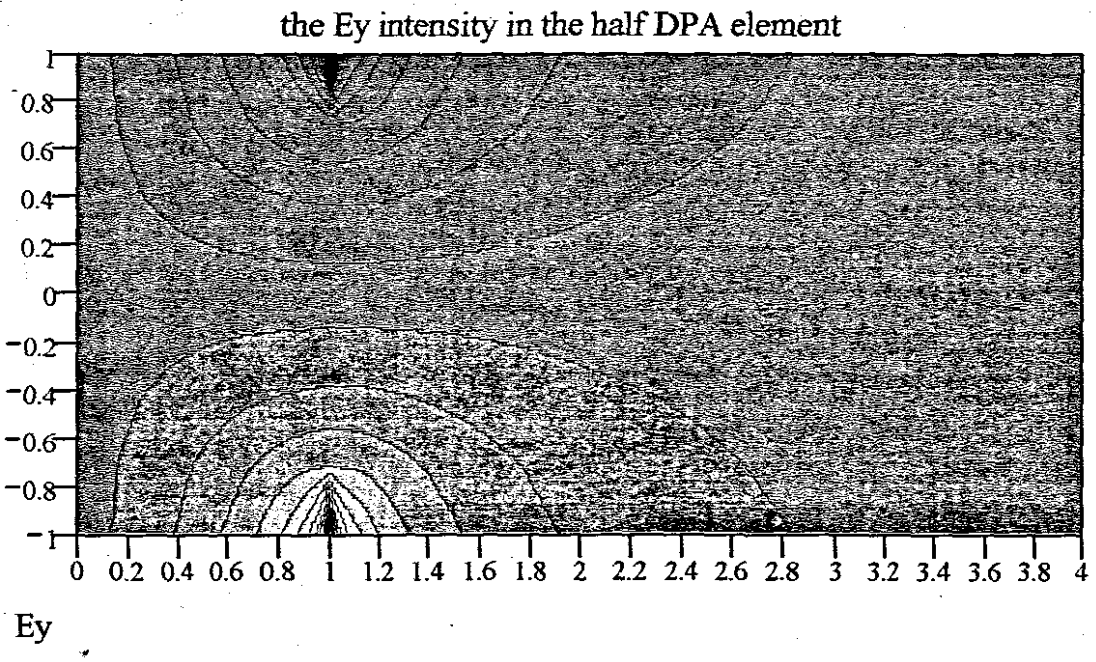

Figure 3.16: the Ey intensity in the first type of DPA element

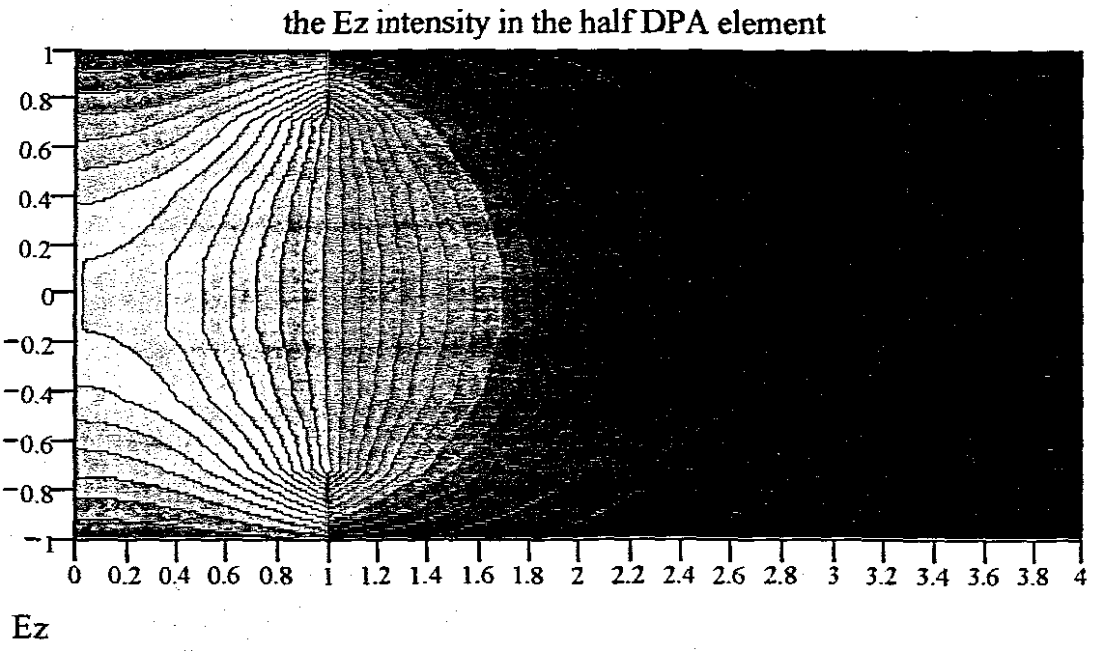

Figure 3.17: the Ez intensity in the first type of DPA element

For the second type of DPA element that have been shown in the Figure 3.2

$$\mathbf{E} = E_x\mathbf{i} + E_y\mathbf{j} + E_z\mathbf{k}$$

and

$$E_x = 0$$

$$E_y = \frac{\bar{\rho}_S}{4\pi\varepsilon}\sum_n ln\left\{\frac{[(4nb-a)-\eta]^2+(\mu-h)^2}{[(4nb+a)-\eta]^2+(\mu-h)^2}\times\frac{[(4nb-a)-\eta]^2+(\mu+h)^2}{[(4nb+a)-\eta]^2+(\mu+h)^2}\right.$$
$$\left.\times\frac{[((4n+2)b+a)-\eta]^2+(h-\mu)^2}{[((4n+2)b-a)-\eta]^2+(h-\mu)^2}\times\frac{[((4n+2)b+a)-\eta]^2+(h+\mu)^2}{[((4n+2)b-a)-\eta]^2+(h+\mu)^2}\right\}$$

$$E_z = \frac{\bar{\rho}_S}{4\pi\varepsilon}\sum_n 2i\cdot\left\{\frac{(4nb-a-\eta)\cdot a\tanh\left[\frac{|h-\mu|\cdot i}{|4nb-a-\eta|}\right]}{|4nb-a-\eta|}-\frac{(4nb+a-\eta)\cdot a\tanh\left[\frac{|h-\mu|\cdot i}{|4nb+a-\eta|}\right]}{|4nb+a-\eta|}\right.$$
$$+\frac{(4nb+a-\eta)\cdot a\tanh\left[\frac{|\mu+h|\cdot i}{|4nb+a-\eta|}\right]}{|4nb+a-\eta|}+\frac{(4nb-a-\eta)\cdot a\tanh\left[\frac{|\mu+h|\cdot i}{|4nb-a-\eta|}\right]}{|4nb-a-\eta|}$$
$$+\frac{((4n+2)b+a-\eta)\cdot a\tanh\left[\frac{|h-\mu|\cdot i}{|(4n+2)b+a-\eta|}\right]}{|(4n+2)b+a-\eta|}-\frac{((4n+2)b-a-\eta)\cdot a\tanh\left[\frac{|h-\mu|\cdot i}{|(4n+2)b-a-\eta|}\right]}{|(4n+2)b-a-\eta|}$$
$$\left.+\frac{((4n+2)b-a-\eta)\cdot a\tanh\left[\frac{|\mu+h|\cdot i}{|(4n+2)b-a-\eta|}\right]}{|(4n+2)b-a-\eta|}-\frac{((4n+2)b+a-\eta)\cdot a\tanh\left[\frac{|\mu+h|\cdot i}{|(4n+2)b+a-\eta|}\right]}{|(4n+2)b+a-\eta|}\right\}$$

where
- $2b$ -- the distance between two centre-line of electrodes;
- $2a$ -- the width of each electrode;
- $2h$ -- the thickness of actuator;
- $\bar{\rho}_S$ -- the surface charge density,
- ε -- the piezoelectric dielectric medium;
- n -- the number of pole in one side.

Consider the simple actual situation of DPA, there are three layers between the both sides of poles as in Figure 3.2, the improvement on formula (3.13), in completed form, can be found to be

$$\mathbf{E}_{imp} = E_{impx}\mathbf{i} + E_{impy}\mathbf{j} + E_{impz}\mathbf{k} \qquad (3.13.2)$$

The differences of formula (3.13) and formula (3.13.2) are,

For the two cover layers:
$h_{imp} = h_1 + h_2$ and $\varepsilon = \varepsilon_{co}$

For the centre layer—PZT material layer:

$$h_{imp} = h_2 + \frac{\varepsilon_{co}}{\varepsilon_{PZT}} h_1 \text{ and } \varepsilon = \varepsilon_{PZT}$$

and the Figure 3.18, 3.19, 3.20, and 3.21 have shown the distribution and intensity of electrical field in the one of second type of DPA element. Here the rate of 'b/a' is 4, and the rate of 'h/a' is 1.

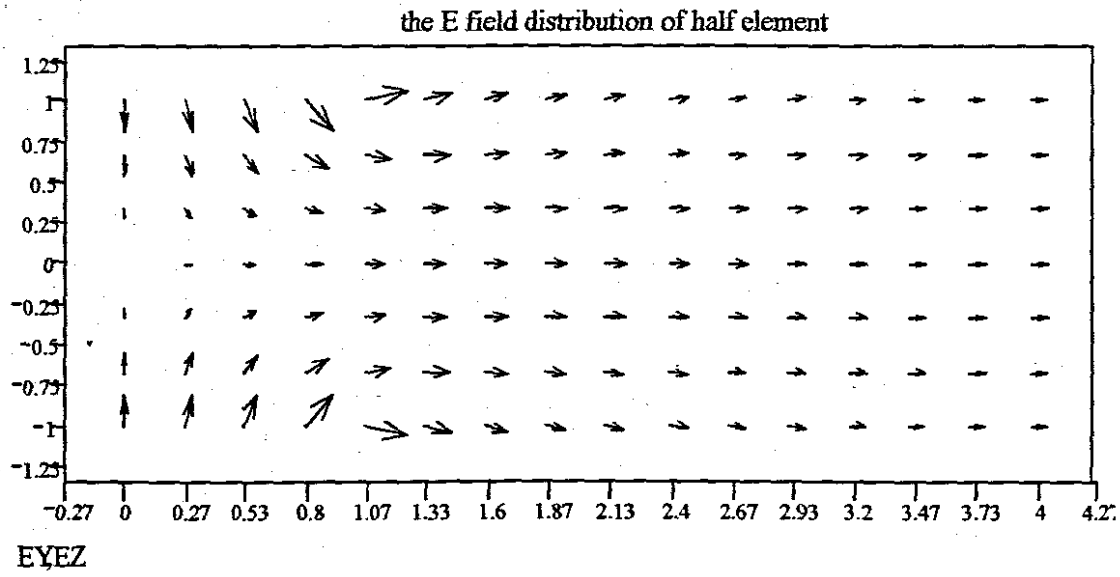

Figure 3.18: the electrical field distributed in half DPA element

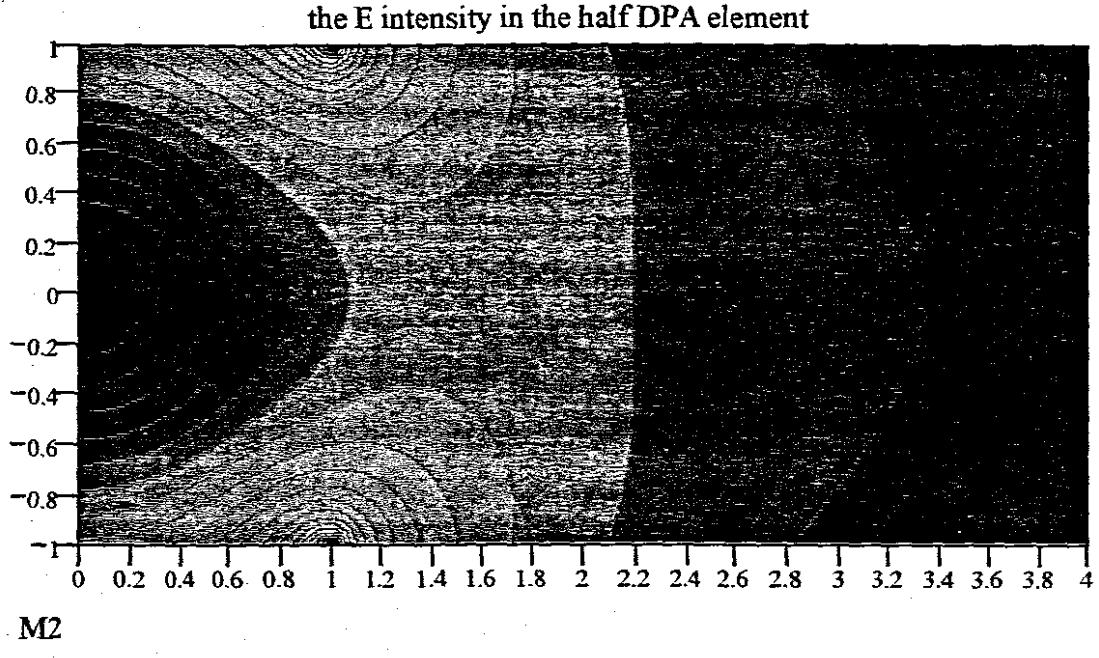

Figure 3.19: the E intensity distributed in the second type of DPA element

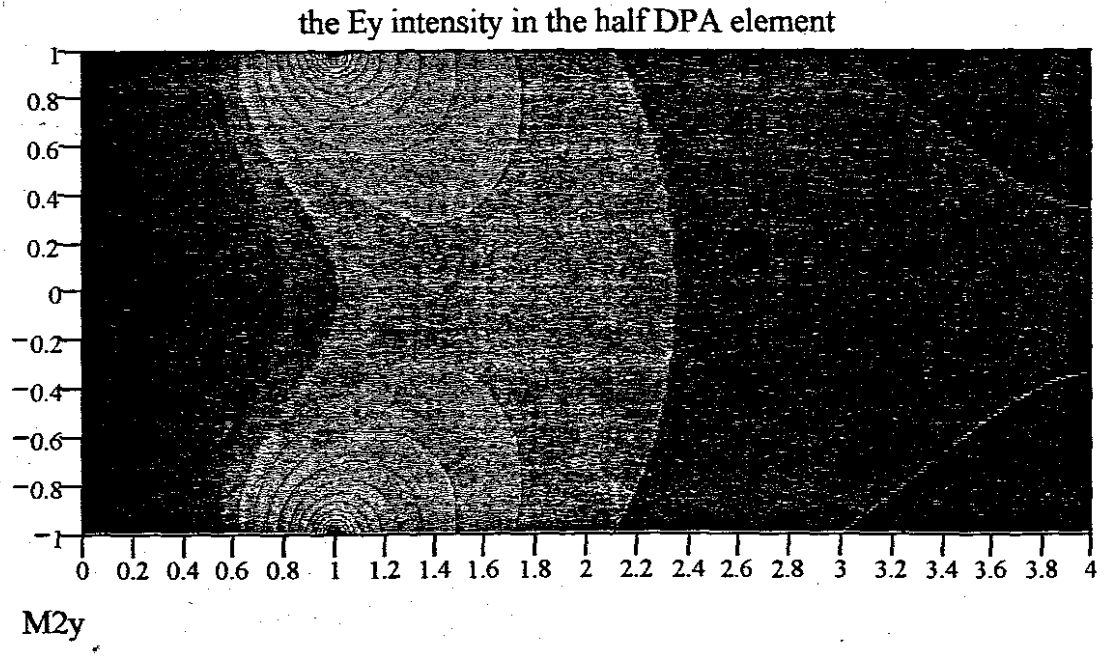

Figure 3.20: the Ey intensity in the second type of DPA element

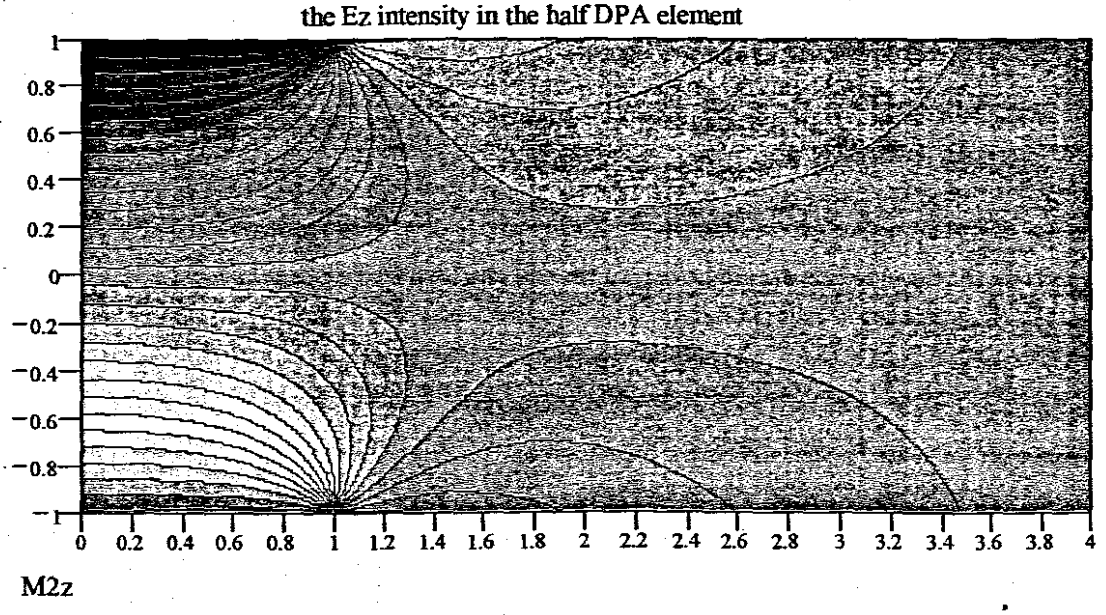

Figure 3.21: the Ez intensity in the second type of DPA element

Considering the intensity and distribution of electrical field on the different axis, which have been shown in the above figures, the non-uniform phenomenon of electrical field in the two types of DPA element are obvious and cannot be ignored during the models and properties analysis. As the example for the distribution of electrical field, the particular numerical values have not been recorded in the above figures. But the distribution characteristic and trend of electrical field, especially the excessive intensity and gradient

area near the edge of electrodes have been shown clearly. As a result, the damage of piezoelectric material always appears in this area.

3.2.5 Summary of the Electrical Field

Following the above analysis of Charge Density, Capacitance and the intensity and distribution of electrical field, the research of electrical field in the two type of DPA element have been completed. The intensity of electrical field can be found by the equations, and the distributions of electrical field on the different axis have been shown in the above figures. For more different structure of DPA element with different ratios of 'h/a' and 'b/a', the intensity and distribution analysis have been done in the Appendices.

Due to the work that have been done in the above sections, the non-uniform phenomenon of electrical field in the DPA element have been analyzed completely.

For the first type of DPA element, the electrical field has been concentrated in the piezoelectric material between the two sides electrodes. In this area, the intensity of electrical field is big enough to drive the piezoelectric material. And other parts of DPA element, the intensity of electrical field has been reduced quickly. Due to the fact that the DPA has been driven by the intensity of electrical field in the actuator, the intensity of electrical field should be as big as possible. So, for the first type of DPA element, the electrodes on both sides should be wide enough for improving the property of electrical field in the DPA element. For the second type of DPA element, the non-uniform phenomenon of electrical field is less than that in the first type of DPA element, especially on the 'Y' direction. In this type of element, the intensity of electrical field on the 'Y' axis is the major power source to drive the piezoelectric material and the actuator. So the properties of electrical field intensity on this direction are more important than on other directions.

Up to now, the numerical analysis for the electrical field in the two typical DPA elements has been completed. And the analytical function was also improved and discussed. Further work is about the mechanical properties analysis of DPA elements.

3.3 The Mechanical Properties Analysis of DPA Elements

3.3.1 Introduction

Micro mechanical modeling began at least a hundred years ago, when the technical advantages of multiphase materials became evident. Since that time, thousands of models for the prediction of mechanical electrical properties have been developed, using dozens of different approaches. A quick review of any book on composite mechanics will reveal methods such as elasticity continuum methods, variational principles, finite elements, averaging techniques, and mechanics of materials approaches, to name the most common. Generally, these models are divided into predicting two classes of properties – transport

properties (conduction, dielectric, permeability, thermal, etc.) and mechanical properties (stiffness and strength).

In order to define a complete micro mechanics problem, four main elements must be considered in the model

- The individual phases and their properties
- A method for governing field distributions
- The microstructure geometry
- The appropriate boundary conditions

After the analytical analysis models of electrical field in the DPA elements have been completed in the previous sections, the next step for developing the DPA technology in this work is the analysis for the mechanical performance of DPA elements applying the results that have been obtained. The four items are discussed in reference to the modeling methods that will be applied to the mechanical properties analysis of DPA element with the intensity and distribution result of electrical field.

3.3.2 The Analytical Models of DPA Applying the Analytical Result of Electrical Field

Using the piezoelectric constitutive relations that have been discussed in the last chapter:

$$\begin{Bmatrix} \mathbf{D} \\ \mathbf{S} \end{Bmatrix} = \begin{bmatrix} \epsilon^{\mathbf{T}} & \mathbf{d} \\ \mathbf{d}_t & \mathbf{s}^{\mathbf{E}} \end{bmatrix} \begin{Bmatrix} \mathbf{E} \\ \mathbf{T} \end{Bmatrix} \tag{3.14}$$

and

$$\begin{Bmatrix} \mathbf{D} \\ \mathbf{T} \end{Bmatrix} = \begin{bmatrix} \epsilon^{\mathbf{S}} & \mathbf{e} \\ -\mathbf{e}_t & \mathbf{c}^{\mathbf{E}} \end{bmatrix} \begin{Bmatrix} \mathbf{E} \\ \mathbf{S} \end{Bmatrix} \tag{3.14.1}$$

where

$$\mathbf{c}^{\mathbf{E}} = \left(\mathbf{s}^{\mathbf{E}}\right)^{-1} \qquad \mathbf{e} = \mathbf{d}\mathbf{c}^{\mathbf{E}} \qquad \epsilon^{\mathbf{S}} = \epsilon^{\mathbf{T}} - \mathbf{d}\mathbf{c}^{\mathbf{E}}\mathbf{d}_t$$

and the complete formula (3.14) to analyse the effect from the electrical field.

$$\begin{Bmatrix} D_1 \\ D_2 \\ D_3 \\ S_1 \\ S_2 \\ S_3 \\ S_4 \\ S_5 \\ S_6 \end{Bmatrix} = \begin{bmatrix} \varepsilon_{11}^T & 0 & 0 & 0 & 0 & 0 & 0 & d_{15} & 0 \\ 0 & \varepsilon_{11}^T & 0 & 0 & 0 & 0 & d_{15} & 0 & 0 \\ 0 & 0 & \varepsilon_{33}^T & d_{31} & d_{31} & d_{33} & 0 & 0 & 0 \\ 0 & 0 & d_{31} & s_{11}^E & s_{12}^E & s_{13}^E & 0 & 0 & 0 \\ 0 & 0 & d_{31} & s_{12}^E & s_{11}^E & s_{13}^E & 0 & 0 & 0 \\ 0 & 0 & d_{33} & s_{13}^E & s_{13}^E & s_{33}^E & 0 & 0 & 0 \\ 0 & d_{15} & 0 & 0 & 0 & 0 & s_{55}^E & 0 & 0 \\ d_{15} & 0 & 0 & 0 & 0 & 0 & 0 & s_{55}^E & 0 \\ 0 & 0 & 0 & 0 & 0 & 0 & 0 & 0 & s_{66}^E \end{bmatrix} \begin{Bmatrix} E_1 \\ E_2 \\ E_3 \\ T_1 \\ T_2 \\ T_3 \\ T_4 \\ T_5 \\ T_6 \end{Bmatrix} \tag{3.15}$$

So, consider the electrical field formulas (3.13) that have been obtained above,

$$\begin{Bmatrix} D_2 \\ D_3 \\ S_1 \\ S_2 \\ S_3 \\ S_4 \end{Bmatrix} = \begin{bmatrix} \varepsilon_{11}^T & 0 & 0 & 0 & 0 & d_{15} \\ 0 & \varepsilon_{33}^T & d_{31} & d_{31} & d_{33} & 0 \\ 0 & d_{31} & s_{11}^E & s_{12}^E & s_{13}^E & 0 \\ 0 & d_{31} & s_{12}^E & s_{11}^E & s_{13}^E & 0 \\ 0 & d_{33} & s_{13}^E & s_{13}^E & s_{33}^E & 0 \\ d_{15} & 0 & 0 & 0 & 0 & s_{55}^E \end{bmatrix} \begin{Bmatrix} E_2 \\ E_3 \\ T_1 \\ T_2 \\ T_3 \\ T_4 \end{Bmatrix} \tag{3.16}$$

where, **D** is the electrical displacement, **S** is the strain, **E** is the electric field, **T** is the stress. Subscript 't' denotes a matrix transpose. These complementary electrical and mechanical fields are related through the material properties: the dielectric 'ε^T', the induced strain constant '**d**', and the compliance 's^E'.

For the second type pole distributed of DPA in the Figure 3.2, because the pole direction is 'Y' direction, by rewriting the constitutive relations formula (3.15), we get:

$$\begin{Bmatrix} D_2 \\ D_3 \\ S_1 \\ S_2 \\ S_3 \\ S_4 \end{Bmatrix} = \begin{bmatrix} \varepsilon_{33}^T & 0 & d_{31} & d_{33} & d_{31} & 0 \\ 0 & \varepsilon_{11}^T & 0 & 0 & 0 & d_{15} \\ d_{31} & 0 & s_{11}^E & s_{13}^E & s_{12}^E & 0 \\ d_{33} & 0 & s_{13}^E & s_{33}^E & s_{13}^E & 0 \\ d_{31} & 0 & s_{12}^E & s_{13}^E & s_{11}^E & 0 \\ 0 & d_{15} & 0 & 0 & 0 & s_{55}^E \end{bmatrix} \begin{Bmatrix} E_2 \\ E_3 \\ T_1 \\ T_2 \\ T_3 \\ T_4 \end{Bmatrix} \tag{3.17}$$

The first step is to recognize those field variables that are equal in the two phases as independent variables, and reorganize the constitutive relations as functions of those variables.

For the first type pole distributed of DPA:

$$S_1 \quad S_2 \quad T_3 \quad T_4 \quad D_3 \quad E_2$$

Rewriting the constitutive relations (3.16) as a formula of these independent variables then gives (for the piezoceramic phase):

$$D_2 = \varepsilon_{11}^T E_2 + d_{15} T_4$$

$$E_3 = \frac{s_{11}^E + s_{12}^E}{\left(s_{11}^E + s_{12}^E\right)\varepsilon_{33}^T - 2d_{31}^2} D_3 - \frac{d_{31}}{\left(s_{11}^E + s_{12}^E\right)\varepsilon_{33}^T - 2d_{31}^2} S_1 - \frac{d_{31}}{\left(s_{11}^E + s_{12}^E\right)\varepsilon_{33}^T - 2d_{31}^2} S_2 - \frac{d_{33}\left(s_{11}^E + s_{12}^E\right) - 2d_{31}s_{13}^E}{\left(s_{11}^E + s_{12}^E\right)\varepsilon_{33}^T - 2d_{31}^2} T_3$$

$$T_1 = -\frac{d_{31}}{\left(s_{11}^E + s_{12}^E\right)\varepsilon_{33}^T - 2d_{31}^2} D_3 + \frac{s_{11}^E\varepsilon_{33}^T - d_{31}^2}{\left[\left(s_{11}^E + s_{12}^E\right)\varepsilon_{33}^T - 2d_{31}^2\right]\left(s_{11}^E - s_{12}^E\right)} S_1 - \frac{s_{12}^E\varepsilon_{33}^T - d_{31}^2}{\left[\left(s_{11}^E + s_{12}^E\right)\varepsilon_{33}^T - 2d_{31}^2\right]\left(s_{11}^E - s_{12}^E\right)} S_2 - \frac{s_{11}^E\varepsilon_{33}^T - d_{31}d_{33}}{\left(s_{11}^E + s_{12}^E\right)\varepsilon_{33}^T - 2d_{31}^2} T_3$$

$$T_2 = -\frac{d_{31}}{\left(s_{11}^E + s_{12}^E\right)\varepsilon_{33}^T - 2d_{31}^2} D_3 - \frac{s_{12}^E\varepsilon_{33}^T - d_{31}^2}{\left[\left(s_{11}^E + s_{12}^E\right)\varepsilon_{33}^T - 2d_{31}^2\right]\left(s_{11}^E - s_{12}^E\right)} S_1 + \frac{s_{11}^E\varepsilon_{33}^T - d_{31}^2}{\left[\left(s_{11}^E + s_{12}^E\right)\varepsilon_{33}^T - 2d_{31}^2\right]\left(s_{11}^E - s_{12}^E\right)} S_2 - \frac{s_{13}^E\left(s_{11}^E + s_{12}^E\right)\varepsilon_{33}^T - s_{11}^E s_{12}^E\varepsilon_{33}^T - d_{31}d_{33}s_{11}^E}{\left[\left(s_{11}^E + s_{12}^E\right)\varepsilon_{33}^T - 2d_{31}^2\right]s_{11}^E} T_3$$

$$S_3 = \frac{d_{33}\left(s_{11}^E + s_{12}^E\right) - 2d_{31}s_{13}^E}{\left(s_{11}^E + s_{12}^E\right)\varepsilon_{33}^T - 2d_{31}^2} D_3 + \frac{s_{11}^E\varepsilon_{33}^T - d_{31}d_{33}}{\left(s_{11}^E + s_{12}^E\right)\varepsilon_{33}^T - 2d_{31}^2} S_1 + \frac{s_{11}^E\varepsilon_{33}^T - d_{31}d_{33}}{\left(s_{11}^E + s_{12}^E\right)\varepsilon_{33}^T - 2d_{31}^2} S_2 + \frac{\left(s_{11}^E + s_{12}^E\right)\left(s_{11}^E s_{33}^E - s_{13}^E s_{13}^E\right)\varepsilon_{33}^T - \left(s_{11}^E - s_{12}^E\right)s_{13}^E s_{11}^E\varepsilon_{33}^T - d_{33}^2 s_{11}^E\left(s_{11}^E + s_{12}^E\right) - 2d_{31}s_{11}^E\left(d_{31}s_{33}^E - 2d_{33}s_{13}^E\right)}{\left[\left(s_{11}^E + s_{12}^E\right)\varepsilon_{33}^T - 2d_{31}^2\right]s_{11}^E} T_3$$

$$S_4 = d_{15}E_2 + s_{55}^E T_4$$

The above can be written for the epoxy-matrix phase by setting all d_{ij} to zero and enforcing elastic isotropy.

$$D_2 = \varepsilon_{11} E_2$$

$$E_3 = \frac{1}{\varepsilon_{11}} D_3$$

$$T_1 = \frac{s_{11}}{(s_{11}+s_{12})(s_{11}-s_{12})}S_1 - \frac{s_{12}}{(s_{11}+s_{12})(s_{11}-s_{12})}S_2 - \frac{s_{11}}{(s_{11}+s_{12})}T_3$$

$$T_2 = -\frac{s_{12}}{(s_{11}+s_{12})(s_{11}-s_{12})}S_1 + \frac{s_{11}}{(s_{11}+s_{12})(s_{11}-s_{12})}S_2 - \frac{s_{12}s_{12}}{(s_{11}+s_{12})s_{11}}T_3$$

$$S_3 = \frac{s_{11}}{(s_{11}+s_{12})}S_1 + \frac{s_{11}}{(s_{11}+s_{12})}S_2 + \frac{s_{11}^3 - s_{12}^3}{(s_{11}+s_{12})s_{11}}T_3$$

$$S_4 = (s_{11}-s_{12})T_4$$

This may also be written more compactly as.

$$\begin{Bmatrix} D_2 \\ E_3 \\ T_1 \\ T_2 \\ S_3 \\ S_4 \end{Bmatrix}_{p,m} = \mathbf{A}_{p,m} \begin{Bmatrix} E_2 \\ D_3 \\ S_1 \\ S_2 \\ T_3 \\ T_4 \end{Bmatrix}_{p,m} \tag{3.18}$$

$$\begin{Bmatrix} D_2 \\ E_3 \\ T_1 \\ T_2 \\ S_3 \\ S_4 \end{Bmatrix}_{p} = \begin{bmatrix} A_{11}^p & 0 & 0 & 0 & 0 & A_{16}^p \\ 0 & A_{22}^p & A_{23}^p & A_{24}^p & A_{25}^p & 0 \\ 0 & A_{32}^p & A_{33}^p & A_{34}^p & A_{35}^p & 0 \\ 0 & A_{42}^p & A_{43}^p & A_{44}^p & A_{45}^p & 0 \\ 0 & A_{52}^p & A_{53}^p & A_{54}^p & A_{55}^p & 0 \\ A_{61}^p & 0 & 0 & 0 & 0 & A_{66}^p \end{bmatrix}_p \begin{Bmatrix} E_2 \\ D_3 \\ S_1 \\ S_2 \\ T_3 \\ T_4 \end{Bmatrix}_p \tag{3.19}$$

$$\begin{Bmatrix} D_2 \\ E_3 \\ T_1 \\ T_2 \\ S_3 \\ S_4 \end{Bmatrix}_{m} = \begin{bmatrix} A_{11}^m & 0 & 0 & 0 & 0 & 0 \\ 0 & A_{22}^m & 0 & 0 & 0 & 0 \\ 0 & 0 & A_{33}^m & A_{34}^m & A_{35}^m & 0 \\ 0 & 0 & A_{43}^m & A_{44}^m & A_{45}^m & 0 \\ 0 & 0 & A_{53}^m & A_{54}^m & A_{55}^m & 0 \\ 0 & 0 & 0 & 0 & 0 & A_{66}^m \end{bmatrix}_m \begin{Bmatrix} E_2 \\ D_3 \\ S_1 \\ S_2 \\ T_3 \\ T_4 \end{Bmatrix}_m \tag{3.20}$$

where $\mathbf{A}_{p,m}$ is the matrix of constants from the above equations. The average stress, however, is some combination of stresses in the two phases, where the contribution for

each is in proportion to the fraction of each phase. This is easily proven through a simple free body diagram. For example, for the 'Y' direction.

$$\overline{T}_2 = v_2^p T_2^p + v_2^m T_2^m \tag{3.21}$$

where v_2^p is the fraction of piezoceramic (p) measured across the element in the '2(Y)' direction. Carrying out this combination for all directions simultaneously yields.

$$\begin{Bmatrix} \overline{D}_2 \\ \overline{E}_3 \\ \overline{T}_1 \\ \overline{T}_2 \\ \overline{S}_3 \\ \overline{S}_4 \end{Bmatrix} = v_2^p \begin{Bmatrix} D_2 \\ E_3 \\ T_1 \\ T_2 \\ S_3 \\ S_4 \end{Bmatrix}_p + v_2^m \begin{Bmatrix} D_2 \\ E_3 \\ T_1 \\ T_2 \\ S_3 \\ S_4 \end{Bmatrix}_m \tag{3.22}$$

and since the independent variables are equal in both phases,

$$\begin{Bmatrix} \overline{D}_2 \\ \overline{E}_3 \\ \overline{T}_1 \\ \overline{T}_2 \\ \overline{S}_3 \\ \overline{S}_4 \end{Bmatrix} = \left(v_2^p \mathbf{A}_p\right) \begin{Bmatrix} E_2 \\ D_3 \\ S_1 \\ S_2 \\ T_3 \\ T_4 \end{Bmatrix}_p + \left(v_2^m \mathbf{A}_m\right) \begin{Bmatrix} E_2 \\ D_3 \\ S_1 \\ S_2 \\ T_3 \\ T_4 \end{Bmatrix}_m \tag{3.23}$$

Rewriting the above to return to the original form yields

$$\begin{Bmatrix} \overline{D}_2 \\ \overline{D}_3 \\ \overline{S}_1 \\ \overline{S}_2 \\ \overline{S}_3 \\ \overline{S}_4 \end{Bmatrix} = \begin{bmatrix} \varepsilon_{11}^{eff} & 0 & 0 & 0 & 0 & d_{15}^{eff} \\ 0 & \varepsilon_{33}^{eff} & d_{31}^{eff} & d_{31}^{eff} & d_{33}^{eff} & 0 \\ 0 & d_{31}^{eff} & s_{11}^{eff} & s_{12}^{eff} & s_{13}^{eff} & 0 \\ 0 & d_{31}^{eff} & s_{12}^{eff} & s_{11}^{eff} & s_{13}^{eff} & 0 \\ 0 & d_{33}^{eff} & s_{13}^{eff} & s_{13}^{eff} & s_{33}^{eff} & 0 \\ d_{15}^{eff} & 0 & 0 & 0 & 0 & s_{55}^{eff} \end{bmatrix}_A \begin{Bmatrix} E_2 \\ E_3 \\ T_1 \\ T_2 \\ T_3 \\ T_4 \end{Bmatrix} \tag{3.24}$$

where

$$\varepsilon_{11}^{eff} = v_2^p A_{11}^p + v_2^m A_{11}^m$$

$$d_{15}^{eff} = v_2^p A_{16}^p$$

$$s_{55}^{eff} = v_2^p A_{66}^p + v_2^m A_{66}^m$$

$$\varepsilon_{33}^{eff} = \left\{ \frac{\left[\left(v_2^p A_{44}^p + v_2^m A_{44}^m\right)A_{23}^p v_2^p - \left(v_2^p A_{34}^p + v_2^m A_{34}^m\right)A_{24}^p v_2^p\right]^2}{-\left[\left(v_2^p A_{44}^p + v_2^m A_{44}^m\right)\left(v_2^p A_{33}^p + v_2^m A_{33}^m\right) - \left(v_2^p A_{34}^p + v_2^m A_{34}^m\right)^2\right]\left[\left(v_2^p A_{44}^p + v_2^m A_{44}^m\right)\right]} \right.$$
$$\left. + \frac{\left[\left(v_2^p A_{44}^p + v_2^m A_{44}^m\right)\left(v_2^p A_{33}^p + v_2^m A_{33}^m\right) - \left(v_2^p A_{34}^p + v_2^m A_{34}^m\right)^2\right]\left[\left(v_2^p A_{44}^p + v_2^m A_{44}^m\right)\left(v_2^p A_{22}^p + v_2^m A_{22}^m\right) - \left(A_{24}^p v_2^{p\,2}\right)\right]}{\left[\left(v_2^p A_{44}^p + v_2^m A_{44}^m\right)\left(v_2^p A_{33}^p + v_2^m A_{33}^m\right) - \left(v_2^p A_{34}^p + v_2^m A_{34}^m\right)^2\right]\left[\left(v_2^p A_{44}^p + v_2^m A_{44}^m\right)\right]} \right\}^{-1}$$

$$d_{31}^{eff} = \frac{\left[\left(v_2^p A_{44}^p + v_2^m A_{44}^m\right)\left(v_2^p A_{33}^p + v_2^m A_{33}^m\right) - \left(v_2^p A_{34}^p + v_2^m A_{34}^m\right)^2\right]A_{24}^p v_2^p + \left[\left(v_2^p A_{44}^p + v_2^m A_{44}^m\right)A_{23}^p v_2^p - \left(v_2^p A_{34}^p + v_2^m A_{34}^m\right)A_{24}^p v_2^p\right]\left(v_2^p A_{44}^p + v_2^m A_{44}^m\right)}{\left[\left(v_2^p A_{44}^p + v_2^m A_{44}^m\right)A_{23}^p v_2^p - \left(v_2^p A_{34}^p + v_2^m A_{34}^m\right)A_{24}^p v_2^p\right]^2 - \left[\left(v_2^p A_{44}^p + v_2^m A_{44}^m\right)\left(v_2^p A_{33}^p + v_2^m A_{33}^m\right) - \left(v_2^p A_{34}^p + v_2^m A_{34}^m\right)^2\right]\left[\left(v_2^p A_{44}^p + v_2^m A_{44}^m\right)\left(v_2^p A_{22}^p + v_2^m A_{22}^m\right) - \left(A_{24}^p v_2^{p\,2}\right)\right]}$$

$$d_{33}^{eff} = \left\{ \frac{\left[\left(v_2^p A_{44}^p + v_2^m A_{44}^m\right)\left(v_2^p A_{33}^p + v_2^m A_{33}^m\right) - \left(v_2^p A_{34}^p + v_2^m A_{34}^m\right)^2\right]\left[\left(v_2^p A_{44}^p + v_2^m A_{44}^m\right)A_{23}^p v_2^p - \left(v_2^p A_{45}^p + v_2^m A_{45}^m\right)A_{24}^p v_2^p\right]}{\left[\left(v_2^p A_{44}^p + v_2^m A_{44}^m\right)A_{23}^p v_2^p - \left(v_2^p A_{34}^p + v_2^m A_{34}^m\right)A_{24}^p v_2^p\right]^2 - \left[\left(v_2^p A_{44}^p + v_2^m A_{44}^m\right)\left(v_2^p A_{33}^p + v_2^m A_{33}^m\right) - \left(v_2^p A_{34}^p + v_2^m A_{34}^m\right)^2\right]\left[\left(v_2^p A_{44}^p + v_2^m A_{44}^m\right)\left(v_2^p A_{22}^p + v_2^m A_{22}^m\right) - \left(A_{24}^p v_2^{p\,2}\right)\right]} \right.$$
$$\left. - \frac{\left[\left(v_2^p A_{44}^p + v_2^m A_{44}^m\right)\left(v_2^p A_{35}^p + v_2^m A_{35}^m\right) - \left(v_2^p A_{34}^p + v_2^m A_{34}^m\right)\left(v_2^p A_{45}^p + v_2^m A_{45}^m\right)\right]\left[\left(v_2^p A_{44}^p + v_2^m A_{44}^m\right)A_{23}^p v_2^p - \left(v_2^p A_{34}^p + v_2^m A_{34}^m\right)A_{24}^p v_2^p\right]}{\left[\left(v_2^p A_{44}^p + v_2^m A_{44}^m\right)A_{23}^p v_2^p - \left(v_2^p A_{34}^p + v_2^m A_{34}^m\right)A_{24}^p v_2^p\right]^2 - \left[\left(v_2^p A_{44}^p + v_2^m A_{44}^m\right)\left(v_2^p A_{33}^p + v_2^m A_{33}^m\right) - \left(v_2^p A_{34}^p + v_2^m A_{34}^m\right)^2\right]\left[\left(v_2^p A_{44}^p + v_2^m A_{44}^m\right)\left(v_2^p A_{22}^p + v_2^m A_{22}^m\right) - \left(A_{24}^p v_2^{p\,2}\right)\right]} \right\}$$

$$s_{11}^{eff} = -\frac{\left[\left(v_2^p A_{44}^p + v_2^m A_{44}^m\right)\left(v_2^p A_{22}^p + v_2^m A_{22}^m\right) - \left(A_{24}^p v_2^p\right)^2\right]}{\left[\left(v_2^p A_{44}^p + v_2^m A_{44}^m\right)A_{23}^p v_2^p - \left(v_2^p A_{34}^p + v_2^m A_{34}^m\right)A_{24}^p v_2^p\right]} d_{31}^{eff}$$

$$s_{12}^{eff} = -\frac{\left[\left(v_2^p A_{44}^p + v_2^m A_{44}^m\right)\left(v_2^p A_{22}^p + v_2^m A_{22}^m\right) - \left(A_{24}^p v_2^p\right)^2\right]}{\left[\left(v_2^p A_{44}^p + v_2^m A_{44}^m\right)A_{23}^p v_2^p - \left(v_2^p A_{34}^p + v_2^m A_{34}^m\right)A_{24}^p v_2^p\right]} d_{31}^{eff} - \frac{A_{24}^p v_2^p}{\left[\left(v_2^p A_{44}^p + v_2^m A_{44}^m\right)A_{23}^p v_2^p - \left(v_2^p A_{34}^p + v_2^m A_{34}^m\right)A_{24}^p v_2^p\right]}$$

$$s_{13}^{eff} = -\frac{\left[\left(v_2^p A_{44}^p + v_2^m A_{44}^m\right)\left(v_2^p A_{22}^p + v_2^m A_{22}^m\right) - \left(A_{24}^p v_2^p\right)^2\right]}{\left[\left(v_2^p A_{44}^p + v_2^m A_{44}^m\right)A_{23}^p v_2^p - \left(v_2^p A_{34}^p + v_2^m A_{34}^m\right)A_{24}^p v_2^p\right]} d_{33}^{eff} - \frac{\left(v_2^p A_{44}^p + v_2^m A_{44}^m\right)A_{25}^p v_2^p - \left(v_2^p A_{45}^p + v_2^m A_{45}^m\right)A_{24}^p v_2^p}{\left[\left(v_2^p A_{44}^p + v_2^m A_{44}^m\right)A_{23}^p v_2^p - \left(v_2^p A_{34}^p + v_2^m A_{34}^m\right)A_{24}^p v_2^p\right]}$$

$$s_{33}^{eff} = A_{52}^p v_2^p d_{33}^{eff} + \left[\left(A_{53}^p v_2^p + A_{53}^m v_2^m\right) + \left(A_{54}^p v_2^p + A_{54}^m v_2^m\right)\right]s_{13}^{eff} + \left(A_{55}^p v_2^p + A_{55}^m v_2^m\right)$$

and applying the formulas (3.14.1),

$$\begin{Bmatrix} \overline{\mathbf{D}} \\ \overline{\mathbf{T}} \end{Bmatrix} = \begin{bmatrix} \epsilon^{Seff} & \mathbf{e}^{eff} \\ -\mathbf{e}_t^{eff} & \mathbf{c}^{eff} \end{bmatrix} \begin{Bmatrix} \mathbf{E} \\ \mathbf{S} \end{Bmatrix} \tag{3.25}$$

where

$$\mathbf{c}^{eff} = \left(\mathbf{s}^{eff}\right)^{-1} \qquad \mathbf{e}^{eff} = \mathbf{d}^{eff}\mathbf{c}^{eff} \qquad \epsilon^{Seff} = \epsilon^{eff} - \mathbf{d}^{eff}\mathbf{c}^{eff}\mathbf{d}_t^{eff}$$

Apply the free boundary conditions on the actuator.

$$\begin{bmatrix} \bar{S}_1 \\ \bar{S}_2 \\ \bar{S}_3 \\ \bar{S}_4 \end{bmatrix} = \begin{bmatrix} 0 & d_{31}^{eff} \\ 0 & d_{31}^{eff} \\ 0 & d_{33}^{eff} \\ d_{15}^{eff} & 0 \end{bmatrix} \begin{bmatrix} E_2 \\ E_3 \end{bmatrix} \tag{3.26}$$

If the effect of cover layer is ignored, we get

$$d_{31}^{eff} = d_{31}^{p} \qquad d_{33}^{eff} = d_{33}^{p} \qquad d_{15}^{eff} = d_{15}^{p} \tag{3.27}$$

Using the following formulas.

$$\bar{S}_1 = \frac{\partial u}{\partial x} \qquad \bar{S}_2 = \frac{\partial v}{\partial y} \qquad \bar{S}_3 = \frac{\partial w}{\partial z}$$
$$\bar{S}_4 = \frac{1}{2}\left(\frac{\partial u}{\partial z} + \frac{\partial w}{\partial x}\right) = \frac{1}{2}\left(\frac{\partial v}{\partial z} + \frac{\partial w}{\partial y}\right) \tag{3.28}$$

The following formulas can be gotten easily.

$$u = \int_X d_{31}^{p} E_Z dx$$
$$v = \int_Y d_{31}^{p} E_Z dy \tag{3.29}$$
$$w = \int_Z d_{33}^{p} E_Z dz$$

For the first type of DPA, the strain on the 'Y' direction is more important than those on the other direction. And apply the formulas (3.29), the DPA strain on the 'Y' direction can be obtained.

Using the formulas (3.25), we get the relationship of the DPA stress and the applied electrical field. Consider the fixing boundary conditions on the actuator.

$$\begin{bmatrix} \bar{T}_1 \\ \bar{T}_2 \\ \bar{T}_3 \\ \bar{T}_4 \end{bmatrix} = \begin{bmatrix} 0 & e_{31}^{eff} \\ 0 & e_{31}^{eff} \\ 0 & e_{33}^{eff} \\ e_{15}^{eff} & 0 \end{bmatrix} \begin{bmatrix} E_2 \\ E_3 \end{bmatrix} \tag{3.30}$$

where

$$\mathbf{e}^{eff} = \mathbf{d}^{eff}\mathbf{c}^{eff} = \mathbf{d}^{eff}\left(\mathbf{s}^{eff}\right)^{-1}$$

For the second type pole distributed of DPA element,

$$S_1 \quad S_2 \quad S_4 \quad T_3 \quad E_2 \quad D_3$$

Rewriting the constitutive relations (3.17) as a function of these independent variables then gives (for the piezoceramic phase):

$$D_2 = \frac{\left(s_{11}^E s_{33}^E - s_{13}^E s_{13}^E\right)\varepsilon_{33}^T - d_{31}^2 s_{33}^E - d_{33}^2 s_{11}^E + 2d_{31}d_{33}s_{13}^E}{s_{11}^E s_{33}^E - s_{13}^E s_{13}^E} E_2 + \frac{d_{31}s_{33}^E - d_{33}s_{13}^E}{s_{11}^E s_{33}^E - s_{13}^E s_{13}^E} S_1$$
$$+ \frac{d_{33}s_{11}^E - d_{31}s_{13}^E}{s_{11}^E s_{33}^E - s_{13}^E s_{13}^E} S_2 + \frac{\left(d_{31}s_{33}^E - d_{33}s_{13}^E\right)\left(s_{11}^E - s_{13}^E\right)}{s_{11}^E s_{33}^E - s_{13}^E s_{13}^E} T_3$$

$$E_3 = \frac{s_{55}^E}{\varepsilon_{11}^T s_{55}^E - d_{15}^2} D_3 - \frac{d_{15}}{\varepsilon_{11}^T s_{55}^E - d_{15}^2} S_4$$

$$T_1 = -\frac{d_{31}s_{33}^E - d_{33}s_{13}^E}{s_{11}^E s_{33}^E - s_{13}^E s_{13}^E} E_2 + \frac{s_{33}^E}{s_{11}^E s_{33}^E - s_{13}^E s_{13}^E} S_1 - \frac{s_{13}^E}{s_{11}^E s_{33}^E - s_{13}^E s_{13}^E} S_2 + \frac{s_{13}^E s_{13}^E - s_{12}^E s_{33}^E}{s_{11}^E s_{33}^E - s_{13}^E s_{13}^E} T_3$$

$$T_2 = \frac{d_{31}s_{13}^E - d_{33}s_{11}^E}{s_{11}^E s_{33}^E - s_{13}^E s_{13}^E} E_2 - \frac{s_{13}^E}{s_{11}^E s_{33}^E - s_{13}^E s_{13}^E} S_1 + \frac{s_{11}^E}{s_{11}^E s_{33}^E - s_{13}^E s_{13}^E} S_2 - \frac{s_{13}^E s_{11}^E - s_{12}^E s_{13}^E}{s_{11}^E s_{33}^E - s_{13}^E s_{13}^E} T_3$$

$$S_3 = \frac{\left(d_{31}s_{33}^E - d_{33}s_{13}^E\right)\left(s_{11}^E - s_{12}^E\right)}{s_{11}^E s_{33}^E - s_{13}^E s_{13}^E} E_2 + \frac{s_{12}^E s_{33}^E - s_{13}^E s_{13}^E}{s_{11}^E s_{33}^E - s_{13}^E s_{13}^E} S_1$$
$$+ \frac{s_{11}^E s_{13}^E - s_{13}^E s_{12}^E}{s_{11}^E s_{33}^E - s_{13}^E s_{13}^E} S_2 + \frac{\left(s_{11}^E - s_{12}^E\right)\left(s_{33}^E s_{11}^E + s_{33}^E s_{12}^E - 2s_{13}^E s_{13}^E\right)}{s_{11}^E s_{33}^E - s_{13}^E s_{13}^E} T_3$$

$$T_4 = -\frac{d_{15}}{\varepsilon_{11}^T s_{55}^E - d_{15}^2} D_3 + \frac{\varepsilon_{11}^T}{\varepsilon_{11}^T s_{55}^E - d_{15}^2} S_4$$

The above can be written for the matrix phase by setting all d_{ij} to zero and enforcing elastic isotropy.

$$D_2 = \varepsilon_{11} E_2$$

$$E_3 = \frac{1}{\varepsilon_{11}} D_3$$

$$T_1 = \frac{s_{11}}{s_{11}s_{11} - s_{12}s_{12}} S_1 - \frac{s_{12}}{s_{11}s_{11} - s_{12}s_{12}} S_2 - \frac{s_{12}}{s_{11} + s_{12}} T_3$$

$$T_2 = -\frac{s_{12}}{s_{11}s_{11} - s_{12}s_{12}} S_1 + \frac{s_{11}}{s_{11}s_{11} - s_{12}s_{12}} S_2 - \frac{s_{12}}{s_{11} + s_{12}} T_3$$

$$S_3 = \frac{s_{12}}{s_{11} + s_{12}} S_1 + \frac{s_{12}}{s_{11} + s_{12}} S_2 + \frac{(s_{11} - s_{12})(s_{11} + 2s_{12})}{s_{11} + s_{12}} T_3$$

$$T_4 = \frac{1}{s_{11} - s_{12}} S_4$$

This may also be written more compactly as.

$$\begin{Bmatrix} D_2 \\ E_3 \\ T_1 \\ T_2 \\ S_3 \\ T_4 \end{Bmatrix}_{p,m} = \mathbf{A}_{p,m} \begin{Bmatrix} E_2 \\ D_3 \\ S_1 \\ S_2 \\ T_3 \\ S_4 \end{Bmatrix}_{p,m} \tag{3.31}$$

$$\begin{Bmatrix} D_2 \\ E_3 \\ T_1 \\ T_2 \\ S_3 \\ T_4 \end{Bmatrix}_{p} = \begin{bmatrix} A_{11}^p & 0 & A_{13}^p & A_{14}^p & A_{15}^p & 0 \\ 0 & A_{22}^p & 0 & 0 & 0 & A_{26}^p \\ A_{31}^p & 0 & A_{33}^p & A_{34}^p & A_{35}^p & 0 \\ A_{41}^p & 0 & A_{43}^p & A_{44}^p & A_{45}^p & 0 \\ A_{51}^p & 0 & A_{53}^p & A_{54}^p & A_{55}^p & 0 \\ 0 & A_{62}^p & 0 & 0 & 0 & A_{66}^p \end{bmatrix}_{p} \begin{Bmatrix} E_2 \\ D_3 \\ S_1 \\ S_2 \\ T_3 \\ S_4 \end{Bmatrix}_{p} \tag{3.32}$$

$$\begin{Bmatrix} D_2 \\ E_3 \\ T_1 \\ T_2 \\ S_3 \\ T_4 \end{Bmatrix}_{m} = \begin{bmatrix} A_{11}^m & 0 & 0 & 0 & 0 & 0 \\ 0 & A_{22}^m & 0 & 0 & 0 & 0 \\ 0 & 0 & A_{33}^m & A_{34}^m & A_{35}^m & 0 \\ 0 & 0 & A_{43}^m & A_{44}^m & A_{45}^m & 0 \\ 0 & 0 & A_{53}^m & A_{54}^m & A_{55}^m & 0 \\ 0 & 0 & 0 & 0 & 0 & A_{66}^m \end{bmatrix}_{m} \begin{Bmatrix} E_2 \\ D_3 \\ S_1 \\ S_2 \\ T_3 \\ S_4 \end{Bmatrix}_{m} \tag{3.33}$$

where $\mathbf{A}_{p,m}$ is the matrix of constants from the above equations. The average stress, however, is some combination of stresses in the two phases, where the contribution for

each is in proportion to the fraction of each phase. This is easily proven through a simple free body diagram. For example, for the 'Y' direction.

$$\overline{T}_2 = v_2^p T_2^p + v_2^m T_2^m \tag{3.34}$$

where v_2^p is the fraction of piezoceramic (p) measured across the element in the 'Y' direction. Carrying out this combination for all directions simultaneously yields.

$$\begin{Bmatrix} \overline{D}_2 \\ \overline{E}_3 \\ \overline{T}_1 \\ \overline{T}_2 \\ \overline{S}_3 \\ \overline{T}_4 \end{Bmatrix} = v_2^p \begin{Bmatrix} D_2 \\ E_3 \\ T_1 \\ T_2 \\ S_3 \\ T_4 \end{Bmatrix}_p + v_2^m \begin{Bmatrix} D_2 \\ E_3 \\ T_1 \\ T_2 \\ S_3 \\ T_4 \end{Bmatrix}_m \tag{3.35}$$

and since the independent variables are equal in both phases,

$$\begin{Bmatrix} \overline{D}_2 \\ \overline{E}_3 \\ \overline{T}_1 \\ \overline{T}_2 \\ \overline{S}_3 \\ \overline{T}_4 \end{Bmatrix} = \left(v_2^p \mathbf{A}_p\right) \begin{Bmatrix} E_2 \\ D_3 \\ S_1 \\ S_2 \\ T_3 \\ S_4 \end{Bmatrix}_p + \left(v_2^m \mathbf{A}_m\right) \begin{Bmatrix} E_2 \\ D_3 \\ S_1 \\ S_2 \\ T_3 \\ S_4 \end{Bmatrix}_m \tag{3.36}$$

Rewriting the above to return to the original form yields

$$\begin{Bmatrix} \overline{D}_2 \\ \overline{D}_3 \\ \overline{S}_1 \\ \overline{S}_2 \\ \overline{S}_3 \\ \overline{S}_4 \end{Bmatrix} = \begin{bmatrix} \varepsilon_{33}^{eff} & 0 & d_{31}^{eff} & d_{33}^{eff} & d_{31}^{eff} & 0 \\ 0 & \varepsilon_{11}^{eff} & 0 & 0 & 0 & d_{15}^{eff} \\ d_{31}^{eff} & 0 & s_{11}^{eff} & s_{13}^{eff} & s_{12}^{eff} & 0 \\ d_{33}^{eff} & 0 & s_{13}^{eff} & s_{33}^{eff} & s_{13}^{eff} & 0 \\ d_{31}^{eff} & 0 & s_{12}^{eff} & s_{13}^{eff} & s_{11}^{eff} & 0 \\ 0 & d_{15}^{eff} & 0 & 0 & 0 & s_{55}^{eff} \end{bmatrix}_{\mathbf{A}} \begin{Bmatrix} E_2 \\ E_3 \\ T_1 \\ T_2 \\ T_3 \\ T_4 \end{Bmatrix} \tag{3.37}$$

where

$$\varepsilon_{33}^{eff} = \frac{\left(A_{11}^p v_2^p + A_{11}^m v_2^m\right)\left(A_{34}^p v_2^p + A_{34}^m v_2^m\right) + \left(A_{14}^p v_2^p\right)^2}{\left(A_{34}^p v_2^p + A_{34}^m v_2^m\right)} + \left(A_{13}^p v_2^p - A_{14}^p v_2^p\right) d_{31}^{eff}$$

$$d_{31}^{eff}=\frac{A_{41}^{p}v_2^{p}\left(A_{34}^{p}v_2^{p}+A_{34}^{m}v_2^{m}\right)-A_{31}^{p}v_2^{p}\left(A_{44}^{p}v_2^{p}+A_{44}^{m}v_2^{m}\right)}{\left(A_{33}^{p}v_2^{p}+A_{33}^{m}v_2^{m}\right)\left(A_{44}^{p}v_2^{p}+A_{44}^{m}v_2^{m}\right)-\left(A_{34}^{p}v_2^{p}+A_{34}^{m}v_2^{m}\right)\left(A_{43}^{p}v_2^{p}+A_{43}^{m}v_2^{m}\right)}$$

$$d_{33}^{eff}=-\left[\frac{A_{41}^{p}v_2^{p}}{\left(A_{34}^{p}v_2^{p}+A_{34}^{m}v_2^{m}\right)}+d_{31}^{eff}\right]$$

$$\varepsilon_{11}^{eff}=\frac{A_{66}^{p}v_2^{p}+A_{66}^{m}v_2^{m}}{\left(A_{22}^{p}v_2^{p}+A_{22}^{m}v_2^{m}\right)\left(A_{66}^{p}v_2^{p}+A_{66}^{m}v_2^{m}\right)-\left(A_{26}^{p}v_2^{p}\right)^2}$$

$$d_{15}^{eff}=\frac{-A_{26}^{p}v_2^{p}}{\left(A_{22}^{p}v_2^{p}+A_{22}^{m}v_2^{m}\right)\left(A_{66}^{p}v_2^{p}+A_{66}^{m}v_2^{m}\right)-\left(A_{26}^{p}v_2^{p}\right)^2}$$

$$s_{11}^{eff}=\frac{A_{44}^{p}v_2^{p}+A_{44}^{m}v_2^{m}}{\left(A_{33}^{p}v_2^{p}+A_{33}^{m}v_2^{m}\right)\left(A_{44}^{p}v_2^{p}+A_{44}^{m}v_2^{m}\right)-\left(A_{34}^{p}v_2^{p}+A_{34}^{m}v_2^{m}\right)\left(A_{43}^{p}v_2^{p}+A_{43}^{m}v_2^{m}\right)}$$

$$s_{13}^{eff}=\frac{-\left(A_{34}^{p}v_2^{p}+A_{34}^{m}v_2^{m}\right)}{\left(A_{33}^{p}v_2^{p}+A_{33}^{m}v_2^{m}\right)\left(A_{44}^{p}v_2^{p}+A_{44}^{m}v_2^{m}\right)-\left(A_{34}^{p}v_2^{p}+A_{34}^{m}v_2^{m}\right)\left(A_{43}^{p}v_2^{p}+A_{43}^{m}v_2^{m}\right)}$$

$$s_{12}^{eff}=\frac{\left(A_{34}^{p}v_2^{p}+A_{34}^{m}v_2^{m}\right)\left(A_{45}^{p}v_2^{p}+A_{45}^{m}v_2^{m}\right)-\left(A_{35}^{p}v_2^{p}+A_{35}^{m}v_2^{m}\right)\left(A_{44}^{p}v_2^{p}+A_{44}^{m}v_2^{m}\right)}{\left(A_{33}^{p}v_2^{p}+A_{33}^{m}v_2^{m}\right)\left(A_{44}^{p}v_2^{p}+A_{44}^{m}v_2^{m}\right)-\left(A_{34}^{p}v_2^{p}+A_{34}^{m}v_2^{m}\right)\left(A_{43}^{p}v_2^{p}+A_{43}^{m}v_2^{m}\right)}$$

$$s_{33}^{eff}=\frac{1}{A_{34}^{p}v_2^{p}+A_{34}^{m}v_2^{m}}-s_{13}^{eff}$$

$$s_{55}^{eff}=\frac{A_{22}^{p}v_2^{p}+A_{22}^{m}v_2^{m}}{\left(A_{22}^{p}v_2^{p}+A_{22}^{m}v_2^{m}\right)\left(A_{66}^{p}v_2^{p}+A_{66}^{m}v_2^{m}\right)-\left(A_{26}^{p}v_2^{p}\right)^2}$$

At the same time, apply the free boundary conditions on the actuator.

$$\begin{bmatrix}\overline{S}_1\\ \overline{S}_2\\ \overline{S}_3\\ \overline{S}_4\end{bmatrix}=\begin{bmatrix}d_{31}^{eff} & 0\\ d_{33}^{eff} & 0\\ d_{31}^{eff} & 0\\ 0 & d_{15}^{eff}\end{bmatrix}\begin{bmatrix}E_2\\ E_3\end{bmatrix} \tag{3.38}$$

Ignoring the effect of cover layer, we get

$$d_{31}^{eff}=d_{31}^{p} \qquad d_{33}^{eff}=d_{33}^{p} \qquad d_{15}^{eff}=d_{15}^{p} \tag{3.39}$$

Using the following formulas,

$$\overline{S}_1 = \frac{\partial u}{\partial x} \qquad \overline{S}_2 = \frac{\partial v}{\partial y} \qquad \overline{S}_3 = \frac{\partial w}{\partial z}$$
$$\overline{S}_4 = \frac{1}{2}\left(\frac{\partial u}{\partial z} + \frac{\partial w}{\partial x}\right) = \frac{1}{2}\left(\frac{\partial v}{\partial z} + \frac{\partial w}{\partial y}\right) \tag{3.40}$$

the following formulas can be gotten easily.

$$u = \int_X d_{31}^p E_Y dx$$
$$v = \int_Y d_{33}^p E_Y dy \tag{3.41}$$
$$w = \int_Z d_{31}^p E_Y dz$$

For the first type of DPA, the strain on the 'Y' direction is more important than those on the other direction. And apply the formulas (3.41), the DPA strain on the 'Y' direction can be found to be

$$\begin{bmatrix} \overline{T}_1 \\ \overline{T}_2 \\ \overline{T}_3 \\ \overline{T}_4 \end{bmatrix} = \begin{bmatrix} e_{31}^{eff} & 0 \\ e_{33}^{eff} & 0 \\ e_{31}^{eff} & 0 \\ 0 & e_{15}^{eff} \end{bmatrix} \begin{bmatrix} E_2 \\ E_3 \end{bmatrix} \tag{3.42}$$

where

$$\mathbf{e}^{eff} = \mathbf{d}^{eff}\mathbf{c}^{eff} = \mathbf{d}^{eff}\left(\mathbf{s}^{eff}\right)^{-1}$$

Here, consider the formulas (3.26), (3.30), (3.38) and (3.42), the distribution of stress and strain in the DPA will depend on the distributed electrical field being used in the DPA. So, it is known that the electrical field distribution in the DPA is the most important effective factor for the performance of actuator. It will be more obvious in the complex shapes actuator.

3.4 The Finite Element Method for DPA Elements

The Finite Element Method (FEM) is a type of elasticity solution because it approximately satisfies the coupled electrical-mechanical governing equations. The problem is formulated in terms of displacement and voltage degrees of freedom, so that the compatibility and potential distribution equations are exactly satisfied. The energy formulation, however, only approximately satisfies the equilibrium and charge

distribution filed equations through a minimization of the total potential energy. The Finite Element, although an implicit approach to modeling effective material properties, is a convenient method for verifying the assumptions utilized in the simpler model (Uniform Fields approach).

In this section, the finite element approach has been used successfully for the analysis of two types of DPA element. The results will be compared with the analytical analysis result, which can be gotten by the equations in the above section, and the product testing data from the companies (ACX, etc.,) in the next section.

A commercially available FEM program (ABAQUS) with coupled, multi-field elements was used to model the two type of DPA element. In order to compare the result from the analytical analysis and the product testing data, one DPA product using the second type of DPA element with the special structure that have the same dimension with the product from the company have been analysed completely, including the character of electrical field and the mechanical properties. Some analysis results have been shown in the following figures.

Figure 3.22 is about the finite element analysis model in ABAQUS. Figure 3.23 and Figure 3.24 have shown the intensity and the distribution of electrical field analysis by the Finite Element Method (FEM). In these figures, the trend of electrical field in the figures is similar with the analytical analysis results that have been shown in the above figures. The Figure 3.25 and Figure 3.26 have shown the piezoelectric phenomenon of two types DPA elements. The Figure 3.27 and Figure 3.28 have given the numerical example analysis of FEM for the two types of DPA elements.

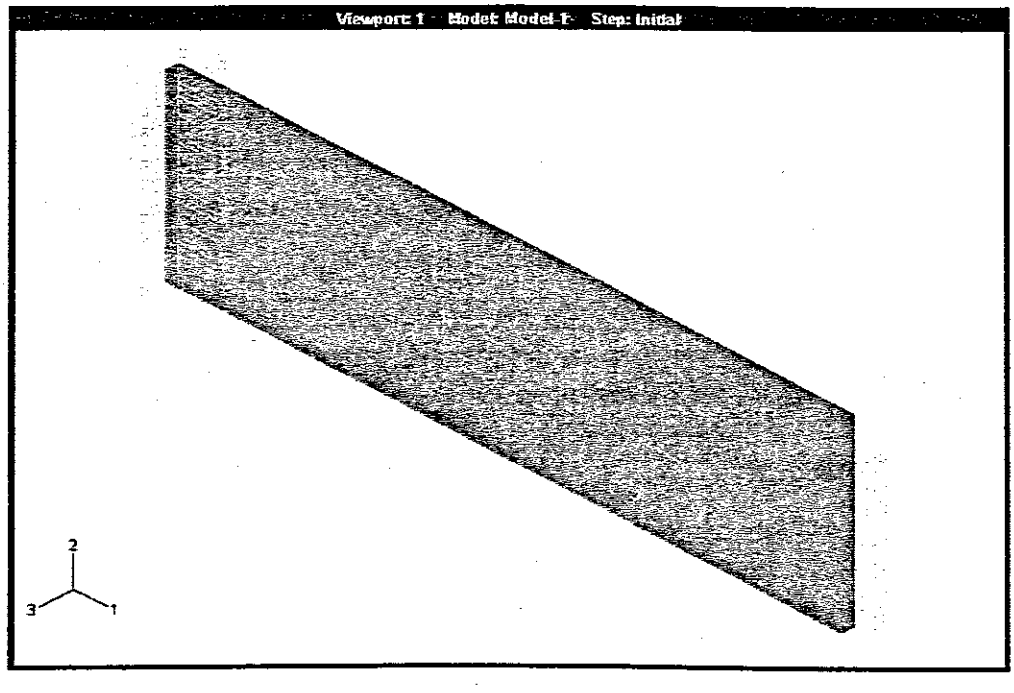

Figure 3.22: the ABAQUS analysis model.

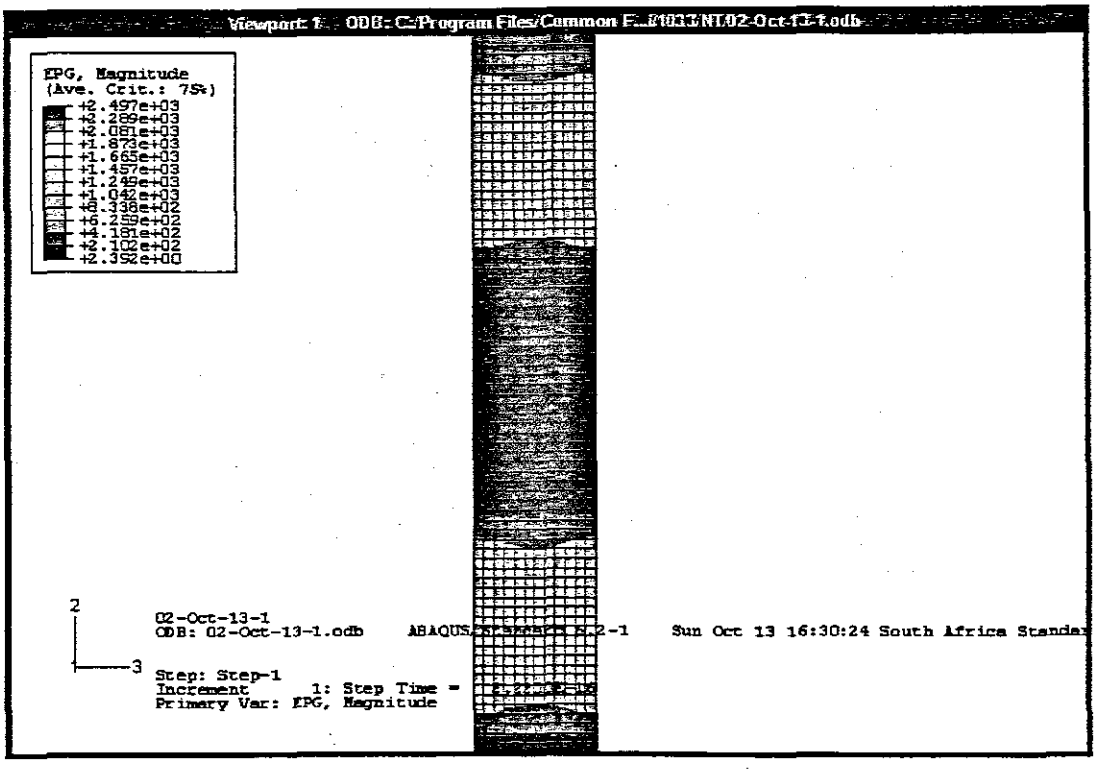

Figure 3.23: The electrical field analysis of the first type of DPA element by the FEM

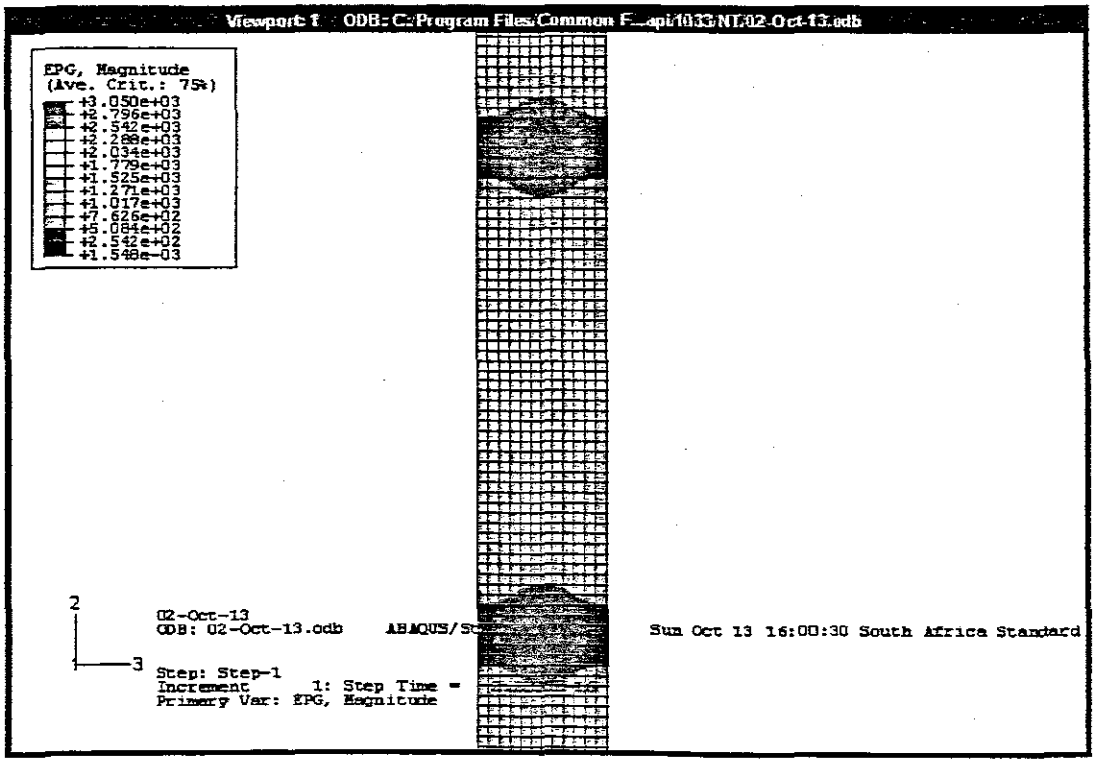

Figure 3.24: The electrical field analysis of the second type of DPA element by the FEM

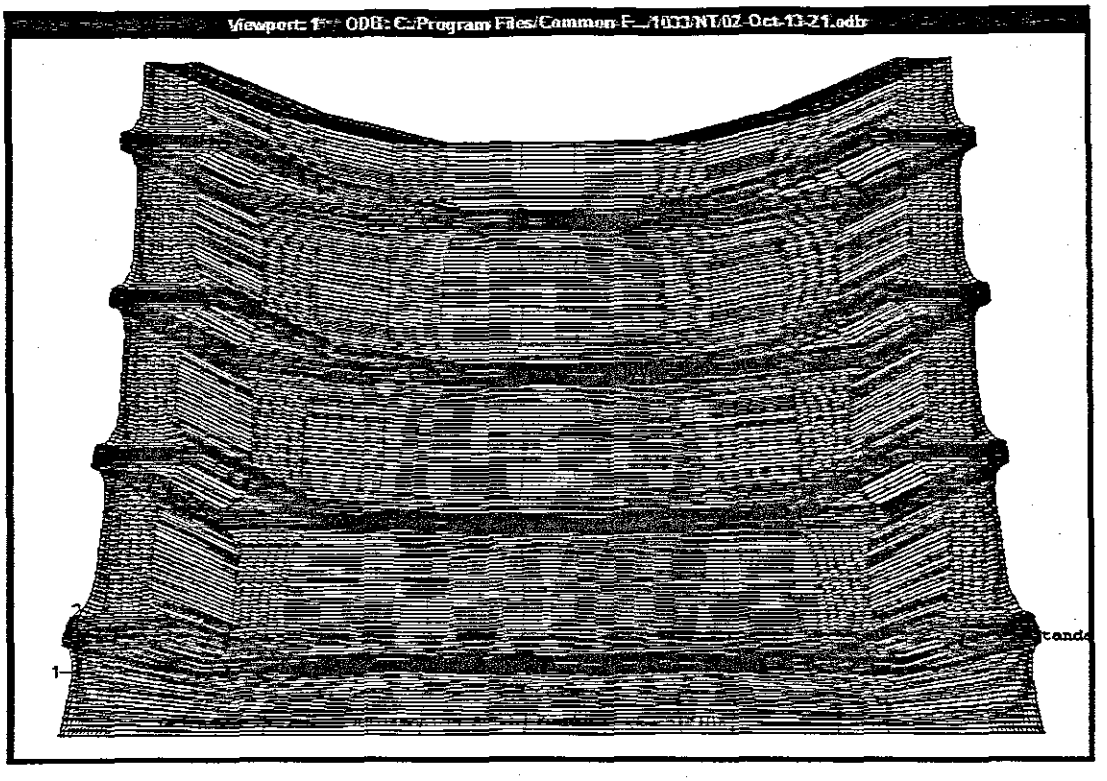

Figure 3.25: The piezoelectric phenomenon of the first type of DPA (contract)

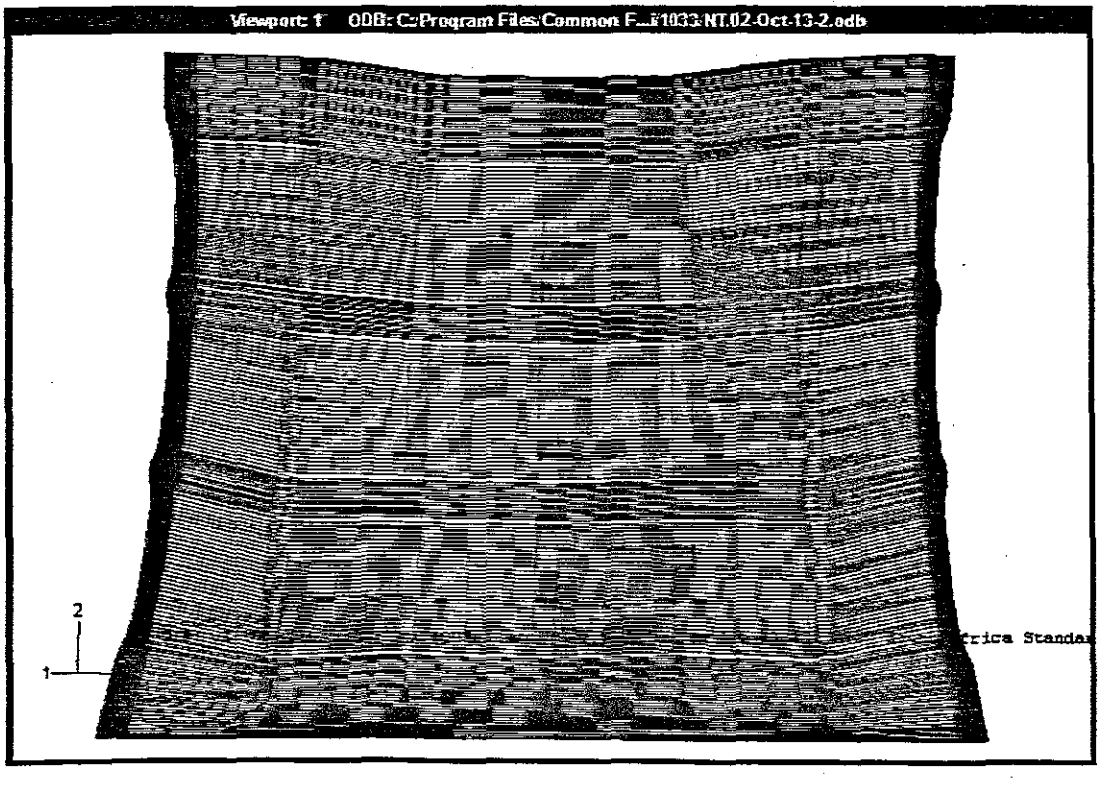

Figure 3.26: The piezoelectric phenomenon of the second type of DPA (expand)

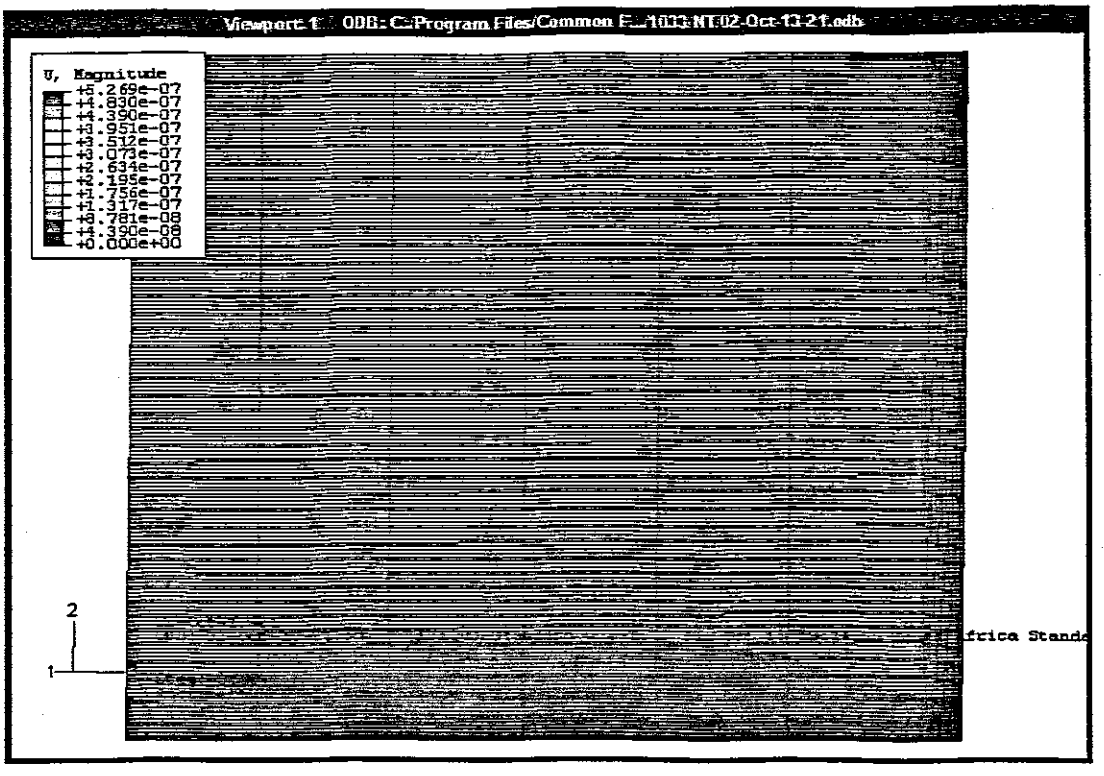

Figure 3.27: The strain analysis of the first type of DPA element by the FEM

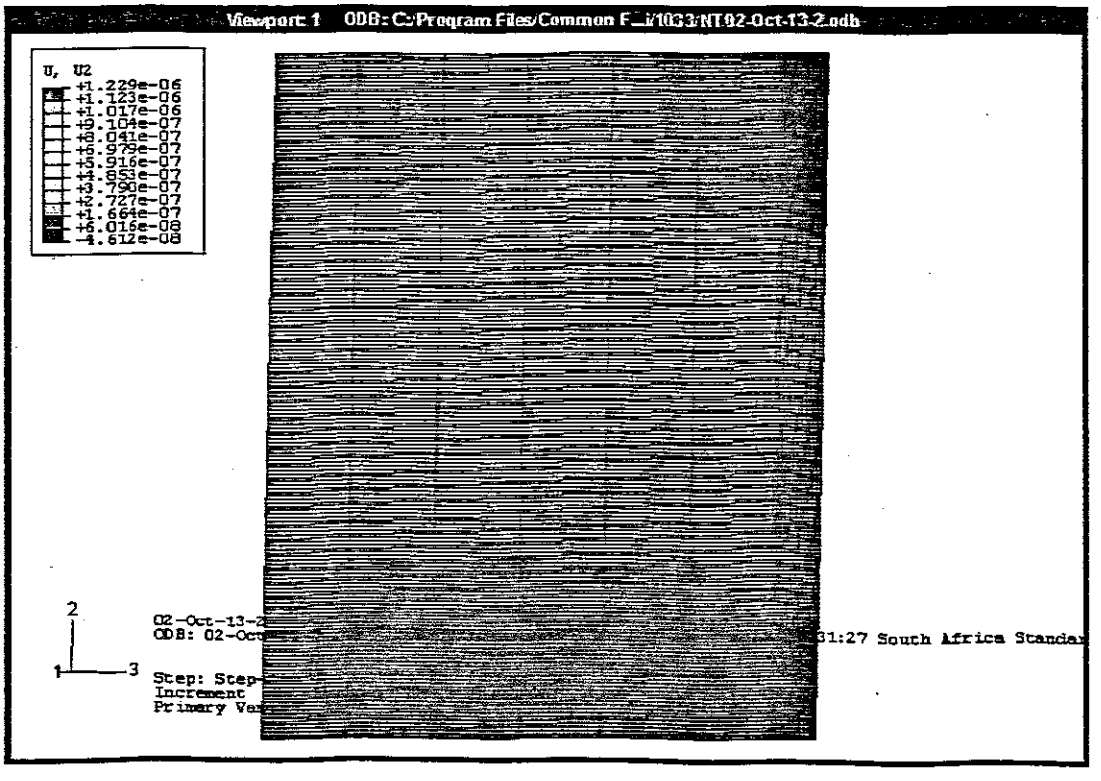

Figure 3.28: The strain analysis of the first type of DPA element by the FEM

3.5 Model Comparison between the Analytical Model and FEM

Applying the analytical model that have been obtained in the above section and the FEM by the finite element analysis program (ABAQUS), the model results have been compared in this research project. Some of the comparison results for the second type of DPA element have been shown in the following figures.

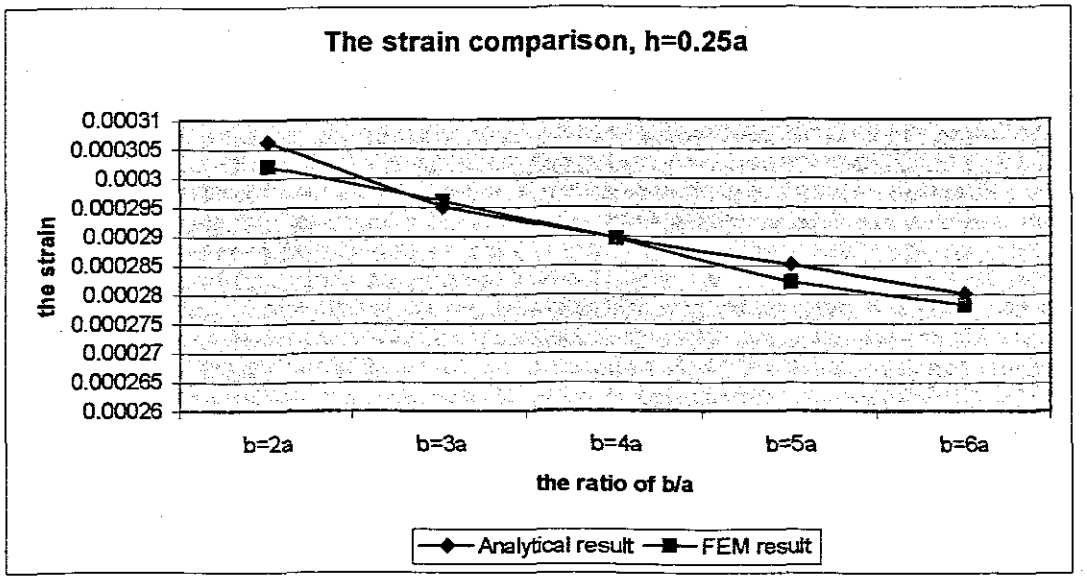

Figure 3.29: The strain result comparison between the analytical model and the FEM, h=0.25a

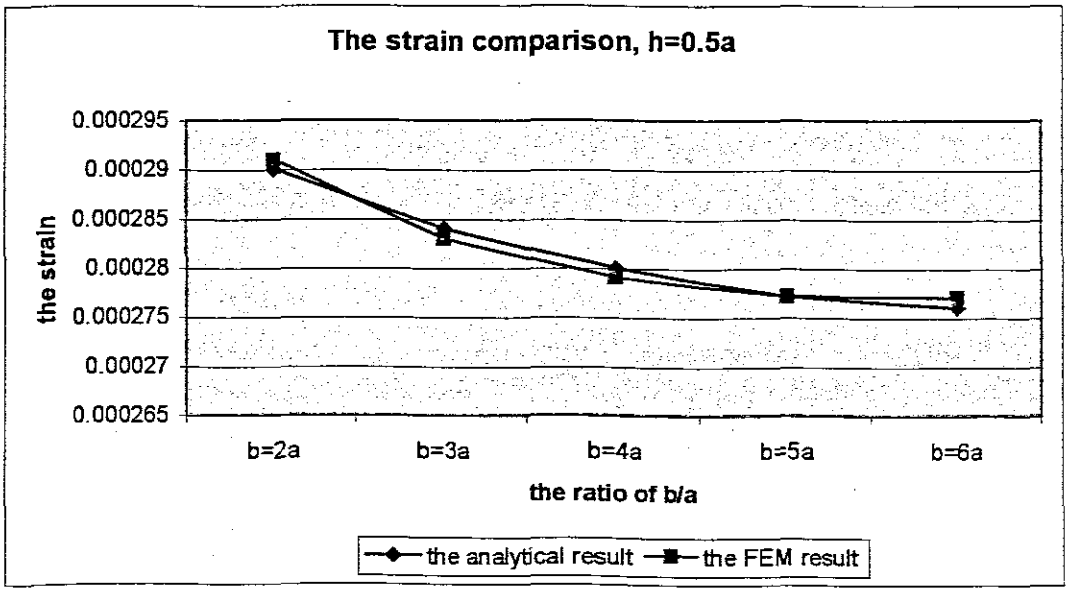

Figure 3.30: The strain result comparison between the analytical model and the FEM, h=0.5a

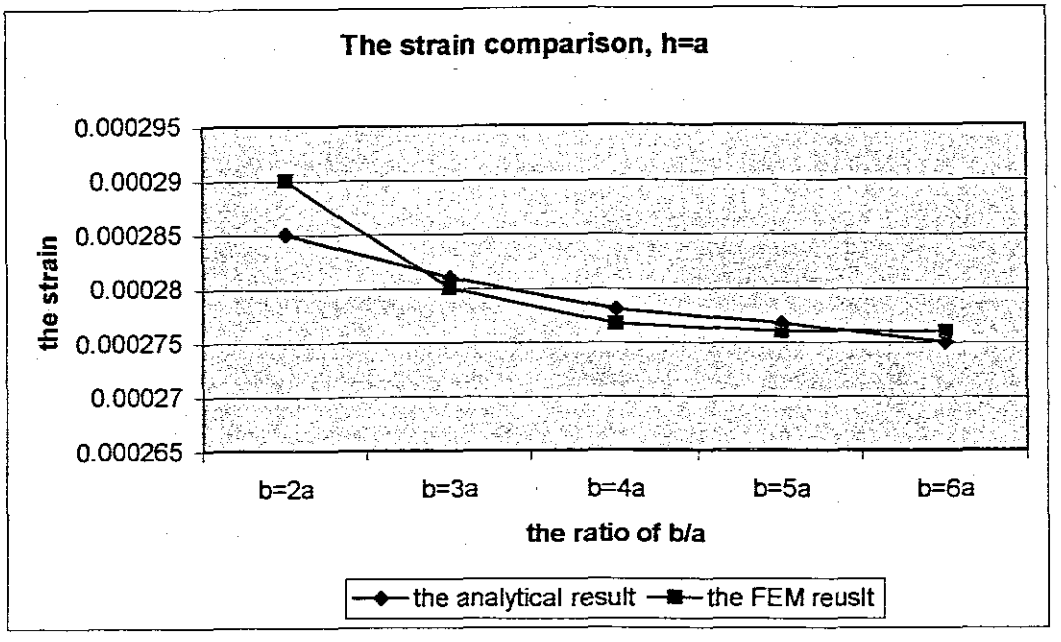

Figure 3.31: The strain result comparison between the analytical model and the FEM, h=a

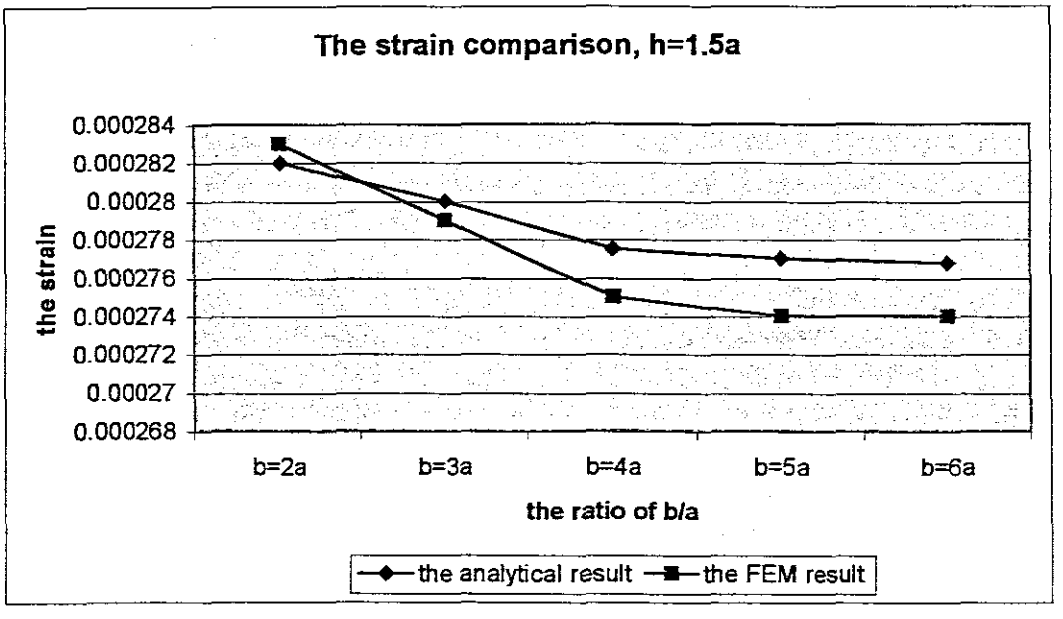

Figure 3.32: The strain result comparison between the analytical model and the FEM, h=1.5a

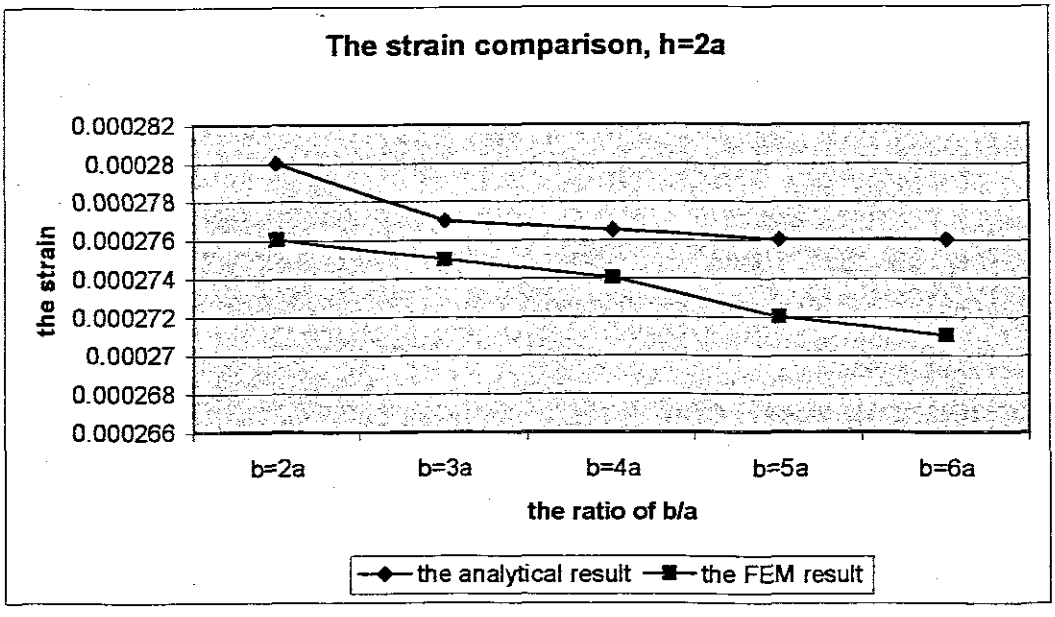

Figure 3.33: The strain result comparison between the analytical model and the FEM, h=2a

In the above figures, the structure of DPA in the 'Y' direction has been considered as long enough to ignore the effect from the edge of DPA. And the numerical values of strain that have been shown in the figures is the strain of DPA element centerline. Figure 3.34 shows another non-uniform phenomenon of the two types of DPA elements strain. In this figure, the strain between the center and the edge are not the same. For the general two type of DPA element, the strains of the element edge are always bigger than the strains of the element center. So, for the effective DPA product, the strain and stress will be bigger than the result of analytical analysis models.

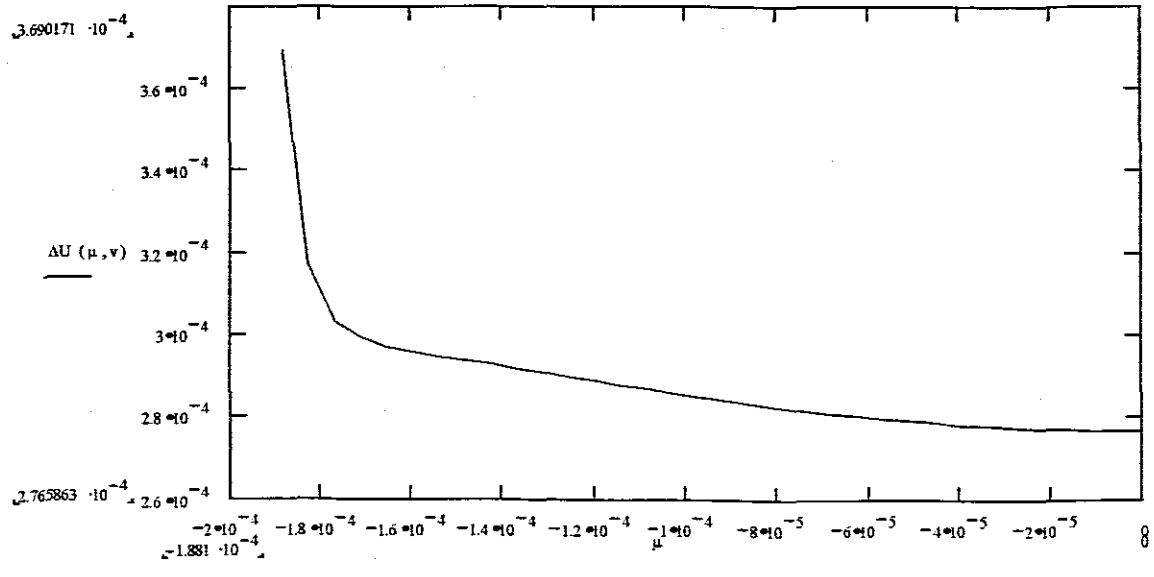

Figure 3.34: the trend of DPA element strain on the 'Y' direction.

The following figures (Figure 3.35 and Figure 3.36) are about the comparison between the analytical model result and the product testing data from the company. In these figures, the strain and stress of DPA product have been compared. Notice in this situation, the DPA elements have been analyzed with the special structure dimensions, which have the same volume with the DPA products.

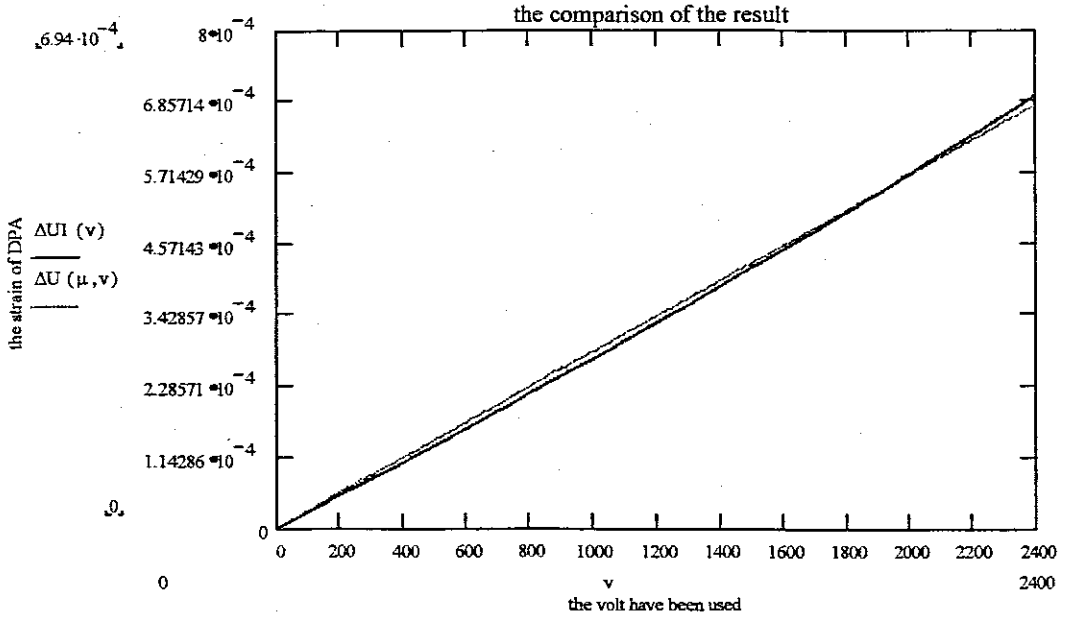

Figure 3.35: The strain comparison between the analytical result and the testing data

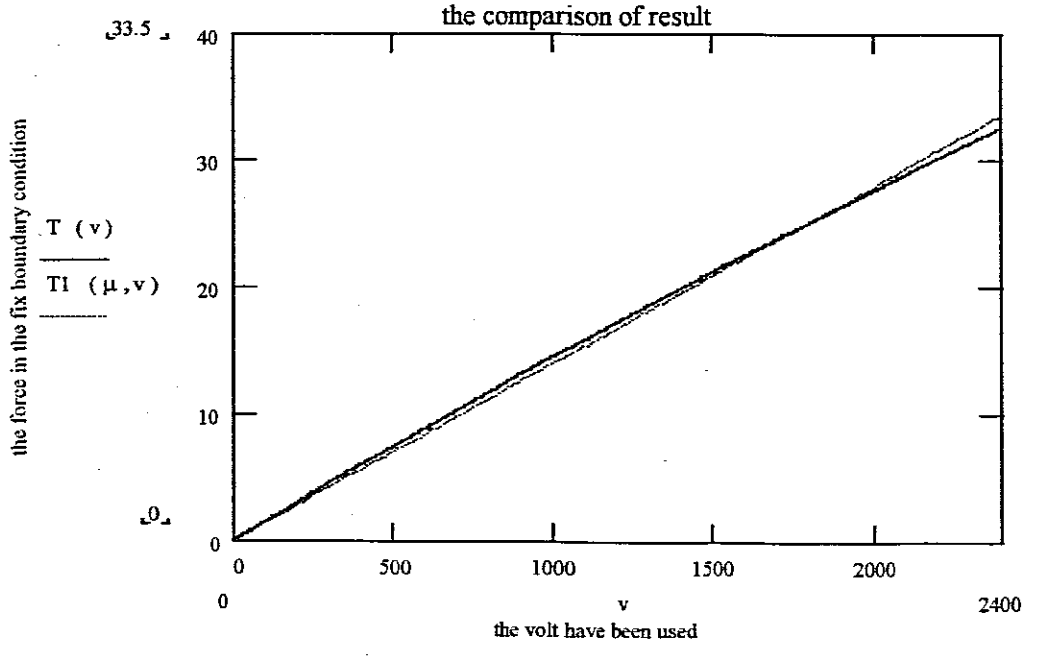

Figure 3.36: The stress comparison between the analytical result and the testing data

3.6 Summary

In this chapter, the analytical analysis models for two type of Distribution Piezoelectric Actuator (DPA) element have been developed. The first of this, the accurate distribution and intensity of electrical field in the DPA elements have been developed for the further mechanical properties analysis. The second, the mechanical property model, used a closed form approach based on simply combining the rules that allowed insight to the mechanisms that govern the composite response. These models have been analyzed and proven by the comparisons with the FEM analysis result (ABAQUS program) and the product testing data, which have been shown in the figures. Now these models can be used for the next chapter – the analysis of DPA with part circular shapes. Furthermore, the model in this chapter also can be used for the design and the improvement of the DPA product.

Chapter 4

Property Model of Part-Circular DPA

4.1 Introduction

Distributed Piezoelectric Actuator (DPA) is one kind of the most important and useful actuator in the smart technology. It can be used in different kinds of applications on the shape and vibrations active control. Up to now, all of the DPA theories investigations and the product designs are based on applying the approximate electrical field. And only the rectangular shape DPA has been studied. At present, more and more applications require a complex actuator that can be used in limited spaces and accomplish multi-motion especially in the high-tech industry and science field, which cannot be accomplished by the general DPA product at present. So, the DPA product with the complex shapes and structures are needed for solving the requirement from the high-tech industry and science field, such as aerospace structure and micro electro-mechanical systems (MEMS).

In the chapter 3, the analytical analysis models for the two types of DPA elements have been developed. These models were based on the electromagnetic principle and the composite structure theory are accurate enough for the numerical design and improvement of the DPA product. In this chapter, these models, especially the model for the second type of DPA element will be applied for developing the part circular DPA element that can be used for composite and more complex shapes for the required of application.

4.2 Analytical Model of Part-Circular DPA

4.2.1 Electrical Field Model of Part-Circular DPA

Following the same analysis steps that have been developed in Chapter 3, the analytical model for intensity and distribution of electrical field in the DPA with a quarter circular shape have been developed, which is the key for determining the mechanical properties of DPA product in further work.

The part-circular shape DPA is one kind of simple shape, which can be used to compose the complex shape, such as L-Shape, S-Shape, T-Shape and soon. Figure 4.1 shows the two types of part circular shape DPA with different distribution IDE.

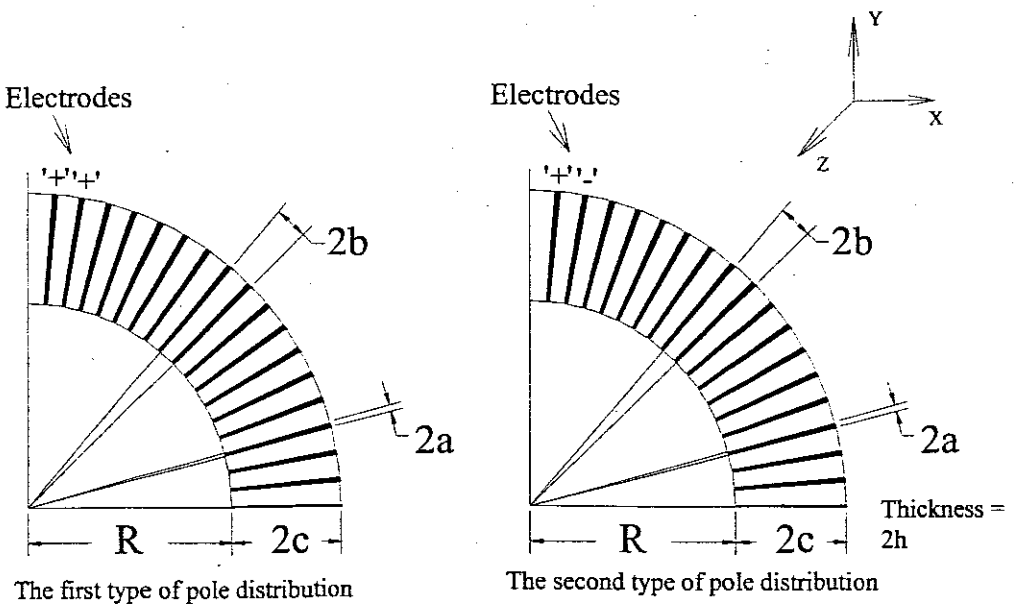

Figure 4.1: two type of part circular DPA with different pole distributions

For developing the analytical analysis models of part circular shape DPA, there are two methods that can be used. The first methods, applying the basic formula of electromagnetic,

$$\mathbf{E} = \int_S \frac{\rho_S \mathbf{a}_R}{4\pi\varepsilon R^2} dS \tag{4.1}$$

The differences between the rectangular and part circular shapes DPA element, here are

$$\mathbf{a}_R = \frac{(r\cos(\theta-\gamma)-\xi)\mathbf{r} + (r\sin(\theta-\gamma))\boldsymbol{\theta} + (z-\mu)\mathbf{z}}{R}$$

$$R = \sqrt{\xi^2 + r^2 - 2\xi \cdot r\cos(\theta-\gamma) + (z-\mu)^2}$$

$$dS = rd\theta dr$$

the intensity and distribution of electrical field in the part circular shape DPA have been gotten following the integration:

$$\mathbf{E} = E_r\mathbf{r} + E_\theta\boldsymbol{\theta} + E_z\mathbf{z} \tag{4.2}$$

Due to the miscelaneity of E_r, E_θ and E_z, only the E_θ, which is the most important component of **E**, has been shown in the Appendix C as an example. Figure 4.2 and Figure 4.3 just show the electrical field intensity on the θ direction in the second type of part circular DPA when the 'μ' is constant. In Figure 4.2, it is easy to be found that the trend of electrical field intensity and distribution have been changed with the different 'r'. As $R \approx 2c$ or $R < 2c$, this change are apparent, but as $R >> 2c$, the changes can be ignored.

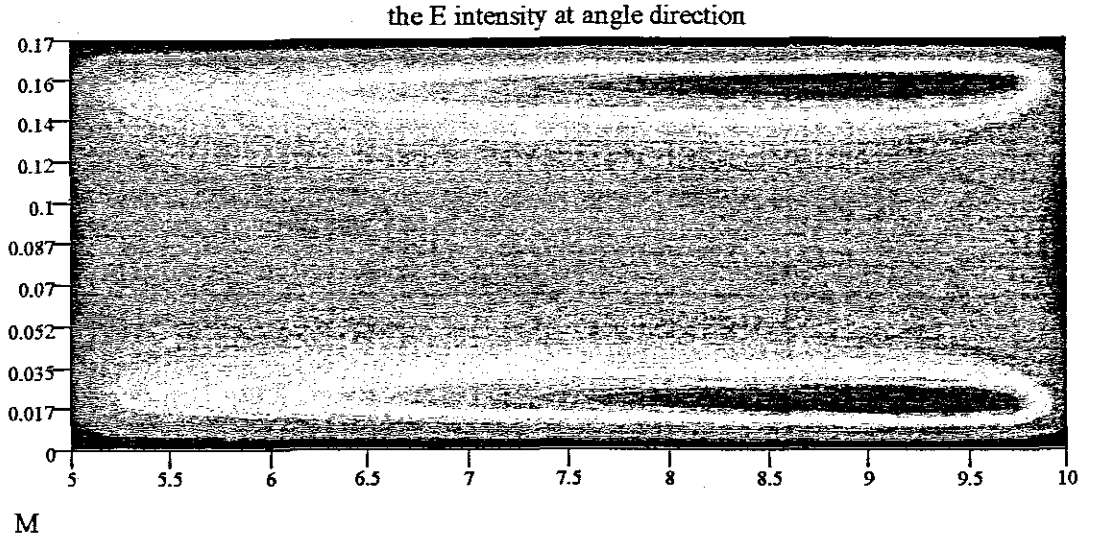

Figure 4.2: the E intensity on the θ direction in the second type of part circular DPA when the 'μ' is constant, $\frac{2c}{R} = 1$

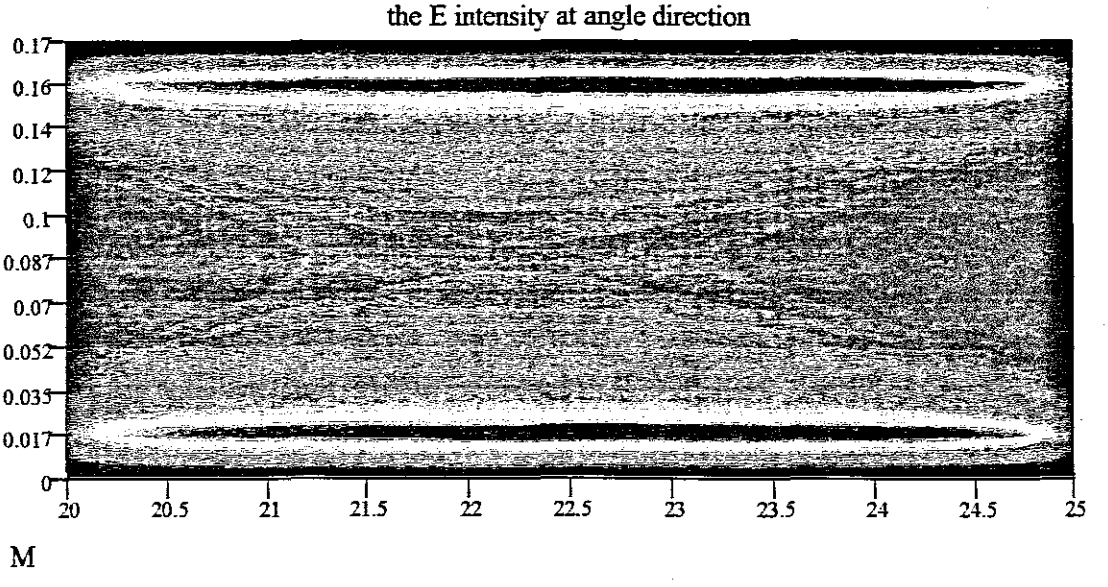

Figure 4.3: the E intensity on the θ direction in the second type of part circular DPA when the 'μ' is constant, $\frac{2c}{R} = 0.25$

The second method for developing the analytical analysis model of part circular DPA is the assembly of the analytical models for the two types of DPA elements that have been completed in Chapter 3.

Applying the formulas that have been developed in Chapter 3, and considering the structure ratio – 'h/a' and 'b/a', the intensity and distribution of electrical field in the part circular DPA element can be written approximately by the linear composition of the formulas about the intensity and distribution of electrical field in the two type of DPA element.

For the first type of DPA element,

$$\mathbf{E} = E_r\mathbf{r} + E_\theta\boldsymbol{\theta} + E_z\mathbf{z} \tag{4.2.1}$$

where

$$E_r = 0$$

$$E_\theta = \frac{\bar{\rho}_R(s)}{4\pi\varepsilon}\sum_n ln\left\{\frac{\{[(2nb+a)-\theta]R\}^2+[z-h]^2}{\{[(2nb-a)-\theta]R\}^2+[z-h]^2}\times\frac{\{[(2nb-a)-\theta]R\}^2+[z+h]^2}{\{[(2nb+a)-\theta]R\}^2+[z+h]^2}\right\}$$
$$+\frac{r}{R+2c}\frac{\bar{\rho}_{R+2c}(S)}{4\pi\varepsilon}\left[\sum_n ln\left\{\frac{\{[(2nb+a)-\theta](R+2c)\}^2+[z-h]^2}{\{[(2nb-a)-\theta](R+2c)\}^2+[z-h]^2}\times\frac{\{[(2nb-a)-\theta](R+2c)\}^2+[z+h]^2}{\{[(2nb+a)-\theta](R+2c)\}^2+[z+h]^2}\right\}\right.$$
$$\left.-\sum_n ln\left\{\frac{\{[(2nb+a)-\theta]R\}^2+[z-h]^2}{\{[(2nb-a)-\theta]R\}^2+[z-h]^2}\times\frac{\{[(2nb-a)-\theta]R\}^2+[z+h]^2}{\{[(2nb+a)-\theta]R\}^2+[z+h]^2}\right\}\right]$$

$$E_z = \frac{\bar{\rho}(s)}{4\pi\varepsilon}\sum_n 2i\cdot\left\{\frac{(2nb+a-\theta)r\cdot a\tanh\left[\frac{(h-z)i}{|(2nb+a-\theta)r|}\right]}{|(2nb+a-\theta)r|}+\frac{(-2nb+a+\theta)r\cdot a\tanh\left[\frac{(h-z)i}{|(-2nb+a+\theta)r|}\right]}{|(-2nb+a+\theta)r|}\right.$$
$$\left.+\frac{((-2nb+a+\theta)r)\cdot a\tanh\left[\frac{(z+h)i}{|(-2nb+a+\theta)r|}\right]}{|(-2nb+a+\theta)r|}+\frac{(2nb+a-\theta)r\cdot a\tanh\left[\frac{(\mu+h)i}{|(2nb+a-\theta)r|}\right]}{|(2nb+a-\theta)r|}\right\}+C_z$$

where

$$C_z = \begin{cases} 4\pi, & \text{when } |\eta - 2\text{nb}| < a \\ 2\pi, & \text{when } |\eta - 2\text{nb}| = a \\ 0 & \text{when } |\eta - 2\text{nb}| > a \end{cases}$$

For the second type of DPA element,

$$E_x = 0$$

$$E_y = \frac{\overline{\rho}_R(s)}{4\pi\varepsilon}\sum_n ln\left\{\frac{\{[(4nb-a)-\theta]R\}^2+(z-h)^2}{\{[(4nb+a)-\theta]R\}^2+(z-h)^2}\times\frac{\{[(4nb-a)-\theta]R\}^2+(z+h)^2}{\{[(4nb+a)-\theta]R\}^2+(z+h)^2}\right.$$
$$\left.\times\frac{\{[((4n+2)b+a)-\theta]R\}^2+(h-z)^2}{\{[((4n+2)b-a)-\theta]R\}^2+(h-z)^2}\times\frac{\{[((4n+2)b+a)-\theta]R\}^2+(h+z)^2}{\{[((4n+2)b-a)-\theta]R\}^2+(h+z)^2}\right\}$$
$$+\frac{r}{R+2c}\frac{\overline{\rho}_{R+2c}(s)}{4\pi\varepsilon}\left[\sum_n ln\left\{\frac{\{[(4nb-a)-\theta](R+2c)\}^2+(z-h)^2}{\{[(4nb+a)-\theta](R+2c)\}^2+(z-h)^2}\times\frac{\{[(4nb-a)-\theta](R+2c)\}^2+(z+h)^2}{\{[(4nb+a)-\theta](R+2c)\}^2+(z+h)^2}\right.\right.$$
$$\left.\times\frac{\{[((4n+2)b+a)-\theta](R+2c)\}^2+(h-z)^2}{\{[((4n+2)b-a)-\theta](R+2c)\}^2+(h-z)^2}\times\frac{\{[((4n+2)b+a)-\theta](R+2c)\}^2+(h+z)^2}{\{[((4n+2)b-a)-\theta](R+2c)\}^2+(h+z)^2}\right\}$$
$$-\sum_n ln\left\{\frac{\{[(4nb-a)-\theta]R\}^2+(z-h)^2}{\{[(4nb+a)-\theta]R\}^2+(z-h)^2}\times\frac{\{[(4nb-a)-\theta]R\}^2+(z+h)^2}{\{[(4nb+a)-\theta]R\}^2+(z+h)^2}\right.$$
$$\left.\left.\times\frac{\{[((4n+2)b+a)-\theta]R\}^2+(h-z)^2}{\{[((4n+2)b-a)-\theta]R\}^2+(h-z)^2}\times\frac{\{[((4n+2)b+a)-\theta]R\}^2+(h+z)^2}{\{[((4n+2)b-a)-\theta]R\}^2+(h+z)^2}\right\}\right]$$

$$E_z = \frac{\overline{\rho}(s)}{4\pi\varepsilon}\sum_n 2i\cdot\left\{\frac{(4nb-a-\theta)r\cdot a\tanh\left[\frac{|h-z|\cdot i}{|(4nb-a-\theta)r|}\right]}{|(4nb-a-\theta)r|}-\frac{(4nb+a-\theta)r\cdot a\tanh\left[\frac{|h-z|\cdot i}{|(4nb+a-\theta)r|}\right]}{|(4nb+a-\theta)r|}\right.$$
$$+\frac{(4nb+a-\theta)r\cdot a\tanh\left[\frac{|z+h|\cdot i}{|(4nb+a-\theta)r|}\right]}{|(4nb+a-\theta)r|}+\frac{(4nb-a-\theta)r\cdot a\tanh\left[\frac{|z+h|\cdot i}{|(4nb-a-\theta)r|}\right]}{|(4nb-a-\theta)r|}$$
$$+\frac{((4n+2)b+a-\theta)r\cdot a\tanh\left[\frac{|h-z|\cdot i}{|((4n+2)b+a-\theta)r|}\right]}{|((4n+2)b+a-\theta)r|}-\frac{((4n+2)b-a-\theta)r\cdot a\tanh\left[\frac{|h-z|\cdot i}{|((4n+2)b-a-\theta)r|}\right]}{|((4n+2)b-a-\theta)r|}$$
$$\left.+\frac{((4n+2)b-a-\theta)r\cdot a\tanh\left[\frac{|z+h|\cdot i}{|((4n+2)b-a-\theta)r|}\right]}{|((4n+2)b-a-\theta)r|}-\frac{((4n+2)b+a-\theta)r\cdot a\tanh\left[\frac{|z+h|\cdot i}{|((4n+2)b+a-\theta)r|}\right]}{|((4n+2)b+a-\theta)r|}\right\}$$

where
- $2b$ – the radian between two centre-line of electrodes;
- $2a$ – the radian of each electrode;
- $2c$ – the width of actuator in 'r' direction;
- $2h$ – the thickness of actuator;

$\overline{\rho}_S$ -- the surface charge density,
ε -- the piezoelectric dielectric medium;
n -- the number of pole in one side;
R -- the internal diameter of actuator;

4.2.2 Mechanical Property Model of Part-Circular DPA

Applying the formulas that have been developed in Chapter 3, the following formulas have been found as the actuator had been poled by two types of electrodes.

$$\begin{Bmatrix} \overline{D}_2 \\ \overline{D}_3 \\ \overline{S}_1 \\ \overline{S}_2 \\ \overline{S}_3 \\ \overline{S}_4 \end{Bmatrix} = \begin{bmatrix} \varepsilon_{11}^{eff} & 0 & 0 & 0 & 0 & d_{15}^{eff} \\ 0 & \varepsilon_{33}^{eff} & d_{31}^{eff} & d_{31}^{eff} & d_{33}^{eff} & 0 \\ 0 & d_{31}^{eff} & s_{11}^{eff} & s_{12}^{eff} & s_{13}^{eff} & 0 \\ 0 & d_{31}^{eff} & s_{12}^{eff} & s_{11}^{eff} & s_{13}^{eff} & 0 \\ 0 & d_{33}^{eff} & s_{13}^{eff} & s_{13}^{eff} & s_{33}^{eff} & 0 \\ d_{15}^{eff} & 0 & 0 & 0 & 0 & s_{55}^{eff} \end{bmatrix}_A \begin{Bmatrix} E_2 \\ E_3 \\ T_1 \\ T_2 \\ T_3 \\ T_4 \end{Bmatrix} \tag{4.3}$$

$$\begin{Bmatrix} \overline{D}_2 \\ \overline{D}_3 \\ \overline{S}_1 \\ \overline{S}_2 \\ \overline{S}_3 \\ \overline{S}_4 \end{Bmatrix} = \begin{bmatrix} \varepsilon_{33}^{eff} & 0 & d_{31}^{eff} & d_{33}^{eff} & d_{31}^{eff} & 0 \\ 0 & \varepsilon_{11}^{eff} & 0 & 0 & 0 & d_{15}^{eff} \\ d_{31}^{eff} & 0 & s_{11}^{eff} & s_{13}^{eff} & s_{12}^{eff} & 0 \\ d_{33}^{eff} & 0 & s_{13}^{eff} & s_{33}^{eff} & s_{13}^{eff} & 0 \\ d_{31}^{eff} & 0 & s_{12}^{eff} & s_{13}^{eff} & s_{11}^{eff} & 0 \\ 0 & d_{15}^{eff} & 0 & 0 & 0 & s_{55}^{eff} \end{bmatrix}_A \begin{Bmatrix} E_2 \\ E_3 \\ T_1 \\ T_2 \\ T_3 \\ T_4 \end{Bmatrix} \tag{4.4}$$

The differences in the formulas are the different coordinates having been applied. The same steps will be used for the following analysis. Using the translator between the cylindrical-coordinates and the perpendicular-coordinates, and ignoring the effect from the two cover layers of actuator, for the first type of part-circular DPA, we have

$$\begin{bmatrix} \overline{S}_x \\ \overline{S}_y \\ \overline{S}_z \end{bmatrix} = \begin{bmatrix} \cos(\eta) & \sin(\eta) & 0 \\ -\sin(\eta) & \cos(\eta) & 0 \\ 0 & 0 & 1 \end{bmatrix} \begin{bmatrix} \overline{S}_r \\ \overline{S}_\theta \\ \overline{S}_z \end{bmatrix} = \begin{bmatrix} \cos(\eta) & \sin(\eta) & 0 \\ -\sin(\eta) & \cos(\eta) & 0 \\ 0 & 0 & 1 \end{bmatrix} \begin{bmatrix} 0 & d_{31}^{eff} \\ 0 & d_{31}^{eff} \\ 0 & d_{33}^{eff} \end{bmatrix} \begin{bmatrix} E_\theta \\ E_z \end{bmatrix} \tag{4.5}$$

and for the second type of part-circular DPA, we get

$$\begin{bmatrix} \overline{S}_x \\ \overline{S}_y \\ \overline{S}_z \end{bmatrix} = \begin{bmatrix} \cos(\eta) & \sin(\eta) & 0 \\ -\sin(\eta) & \cos(\eta) & 0 \\ 0 & 0 & 1 \end{bmatrix} \begin{bmatrix} \overline{S}_r \\ \overline{S}_\theta \\ \overline{S}_z \end{bmatrix} = \begin{bmatrix} \cos(\eta) & \sin(\eta) & 0 \\ -\sin(\eta) & \cos(\eta) & 0 \\ 0 & 0 & 1 \end{bmatrix} \begin{bmatrix} d_{31}^{eff} & 0 \\ d_{33}^{eff} & 0 \\ d_{31}^{eff} & 0 \end{bmatrix} \begin{bmatrix} E_\theta \\ E_z \end{bmatrix} \tag{4.6}$$

and

$$\Delta R = \int_L \bar{S}_r dl$$
$$\Delta\theta = \int_L \bar{S}_\theta dl \qquad (4.7)$$
$$\Delta z = \int_Z \bar{S}_z dz$$

and the total displacements of part circular DPA on the different directions with the free boundary condition situation can be gotten using formulas (4.8)

$$\begin{aligned} u &= R\cos\theta(\cos\Delta\theta - 1) - R\sin\theta\sin\Delta\theta + \Delta R\cos(\theta + \Delta\theta) \\ v &= R\sin\theta(\cos\Delta\theta - 1) + R\cos\theta\sin\Delta\theta + \Delta R\sin(\theta + \Delta\theta) \\ w &= \Delta z \end{aligned} \qquad (4.8)$$

where R -- the distance between the point and the centre of the circular.
θ -- the angle between the 'X'-axis and the radius through the point

As in Chapter 3, the stress of part circular DPA with the fixed boundary condition situation can be obtained by applying the formula (4.9) and formula (4.10),

$$\begin{bmatrix} \bar{T}_r \\ \bar{T}_\theta \\ \bar{T}_z \\ \bar{T}_4 \end{bmatrix} = \begin{bmatrix} 0 & e_{31}^{eff} \\ 0 & e_{31}^{eff} \\ 0 & e_{33}^{eff} \\ e_{15}^{eff} & 0 \end{bmatrix} \begin{bmatrix} E_\theta \\ E_z \end{bmatrix} \qquad (4.9)$$

$$\begin{bmatrix} \bar{T}_r \\ \bar{T}_\theta \\ \bar{T}_z \\ \bar{T}_4 \end{bmatrix} = \begin{bmatrix} e_{31}^{eff} & 0 \\ e_{33}^{eff} & 0 \\ e_{31}^{eff} & 0 \\ 0 & e_{15}^{eff} \end{bmatrix} \begin{bmatrix} E_\theta \\ E_z \end{bmatrix} \qquad (4.10)$$

where

$$\mathbf{e}^{eff} = \mathbf{d}^{eff}\mathbf{c}^{eff} = \mathbf{d}^{eff}\left(\mathbf{s}^{eff}\right)^{-1}$$

The analytical analysis models of part circular shape DPA element have been developed as the formulas (4.8), (4.9) and (4.10), which applied the electrical field functions (4.2) and (4.2.1). In those formulas, the multi-motion properties of part circular shape DPA are evident. It is the biggest difference in mechanical properties field between the rectangular and part circular shape DPA. The special benefits of part circular DPA that have been used in the applications will be discovered based on the multi-motion properties.

4.3 Finite Element Method of Part-Circular DPA

The Finite Element Method (FEM) for two types of part-circular DPA elements (Figure 4.4) has been analyzed by the commercial program (ABAQUS). The strain and displacements of two types part-circular DPA element on the different directions have been shown in the following figures (from Figure 4.5 to Figure 4.10). In those figures, the multi-motion properties difference between the first type and the second type of part circular shape DPA can be found. The second type of part circular DPA has more 'smooth' displacement on the different point with the same angle 'θ'. The edge of second type DPA can keep the same center with circular. Due to those mechanical properties that it has, the second type of part circular DPA can be used in more applications than the first type of part circular DPA.

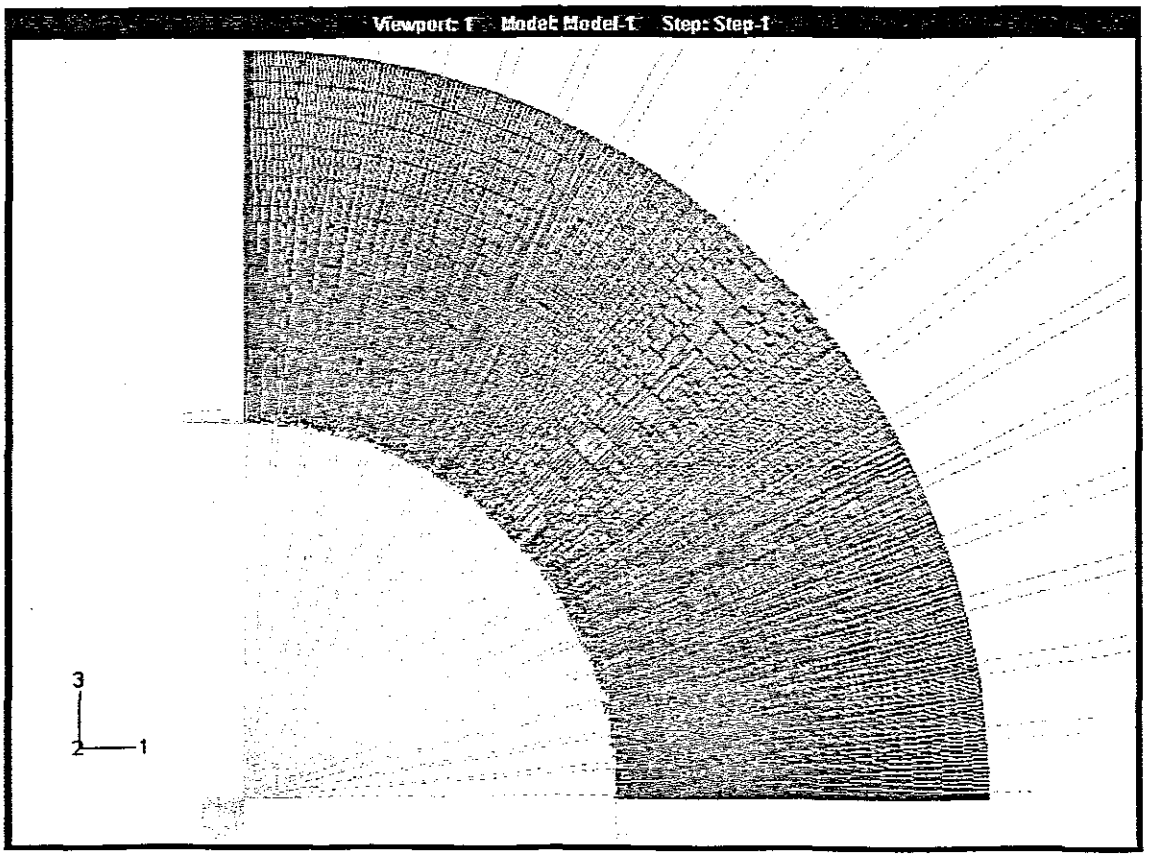

Figure 4.4: The DPA element analysis model for the ABAQUS program

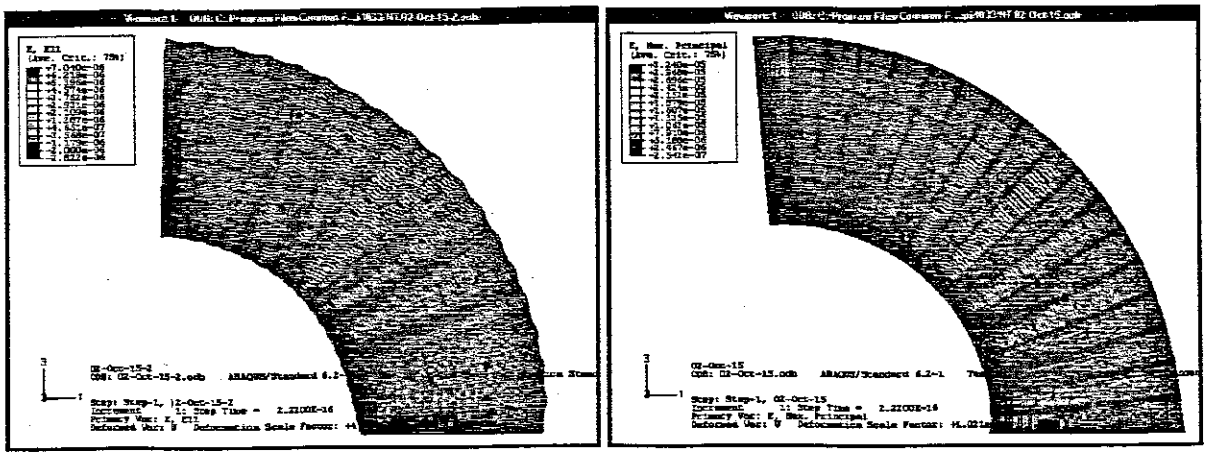

Figure 4.5: The two types of DPA element strain on the '1' axis (expansion)

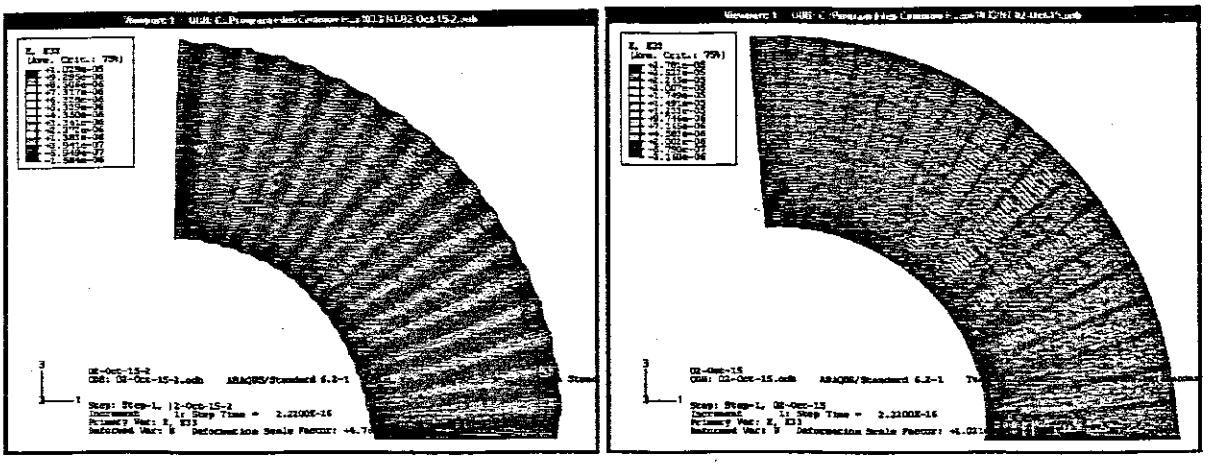

Figure 4.6: The two types of DPA element strain on the '3' axis (expansion)

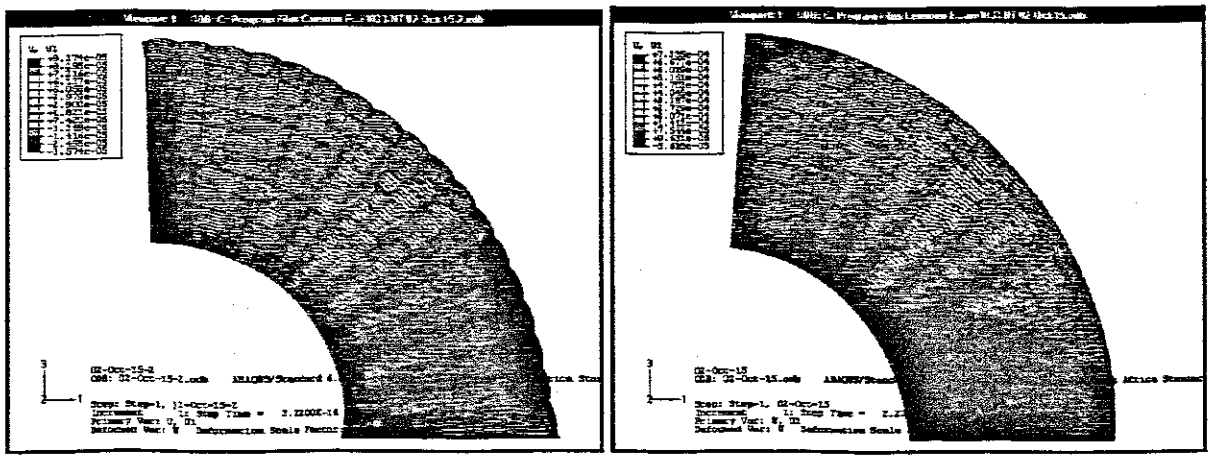

Figure 4.7: The two types of DPA element displacements on the '1' axis (contract)

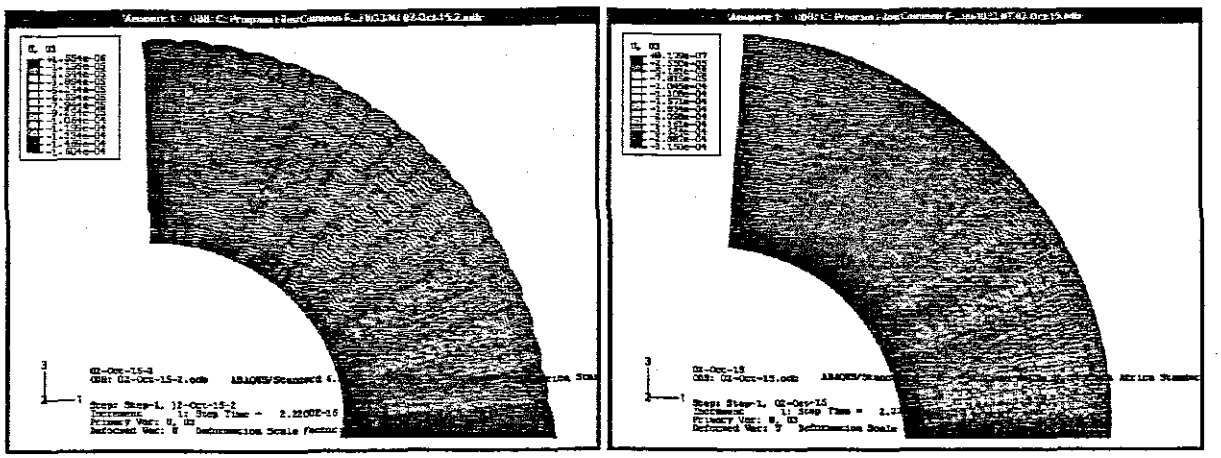

Figure 4.8: The two types of DPA element displacements on the '3' axis (contract)

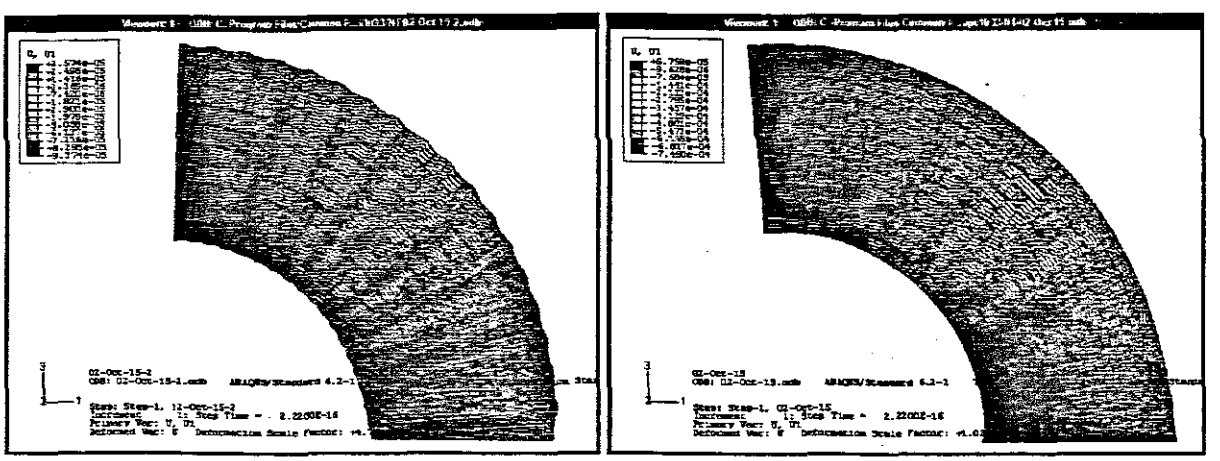

Figure 4.9: The two types of DPA element displacements on the '1' axis (expansion)

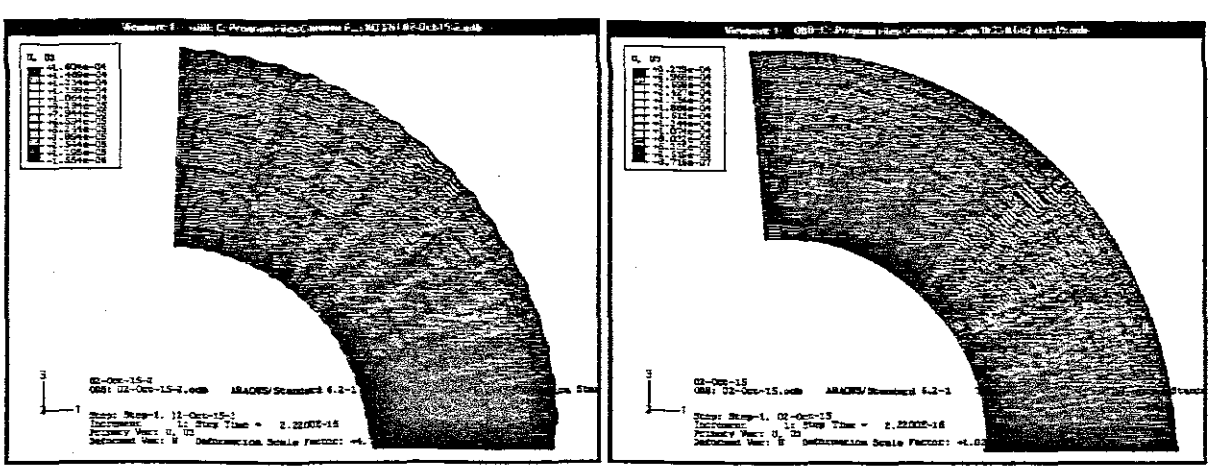

Figure 4.10: The two types of DPA element displacement on the '3' axis (expansion)

4.4 Model Comparison between Analytical Model and FEM Comparison

The analytical models of two types of part circular DPA element and the FEM analysis have been developed in the above sections. In this section, the major objective is the models result comparison between the analytical and FEM. In the following figures, the two type analytical models and FEM have been compared. The comparison results have been shown in those figures.

Due to the discussions that have been done in the last section, only the analytical models for second type of part circular DPA element have been compared in this section. Figure 4.11 is the comparison results for element center strains in 'θ' axis. Other figures (from Figure 4.12 to Figure 4.15) are about the comparison results for DPA displacement in '1' and '3' direction.

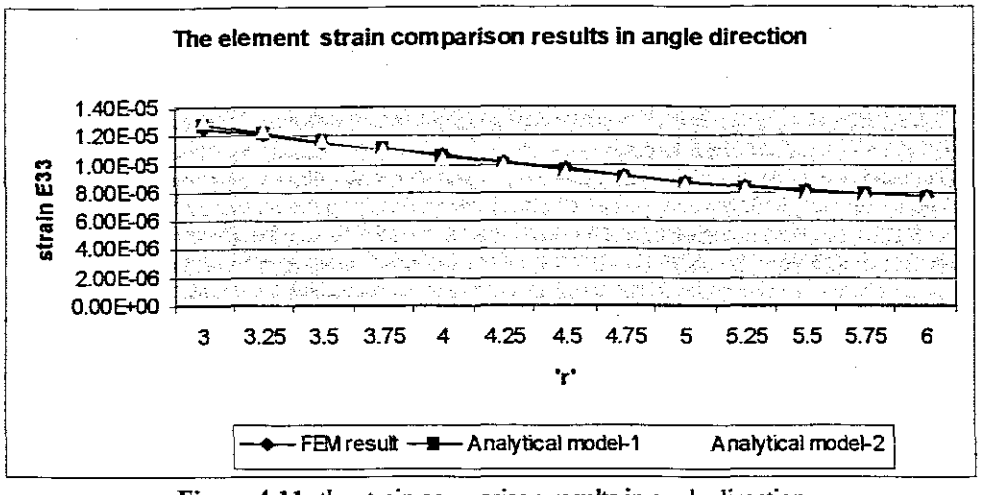

Figure 4.11: the strain comparison results in angle direction

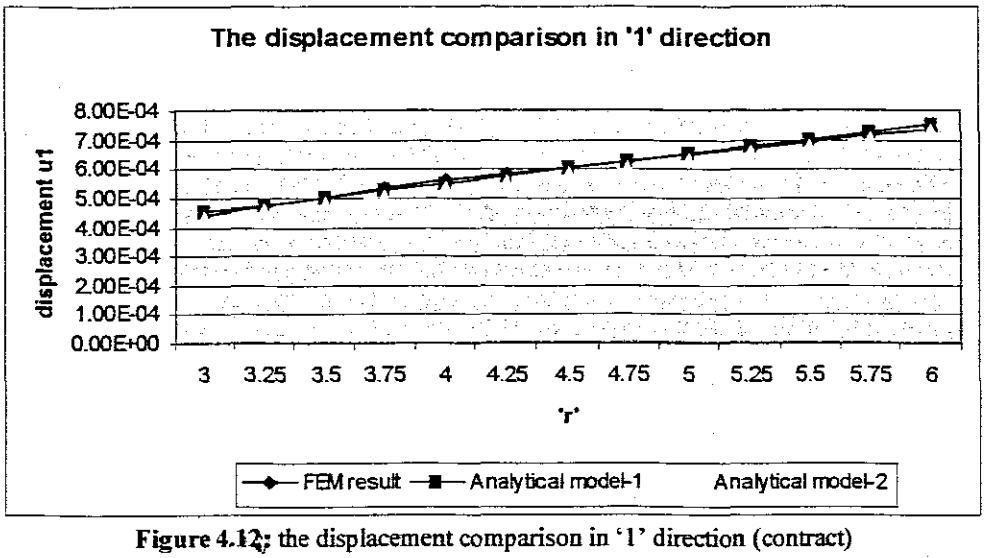

Figure 4.12: the displacement comparison in '1' direction (contract)

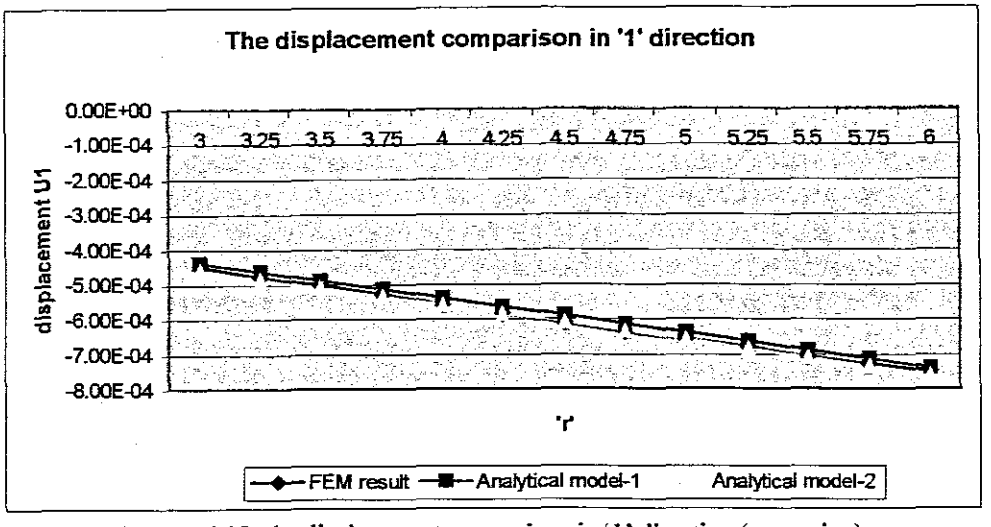

Figure 4.13: the displacement comparison in '1' direction (expansion)

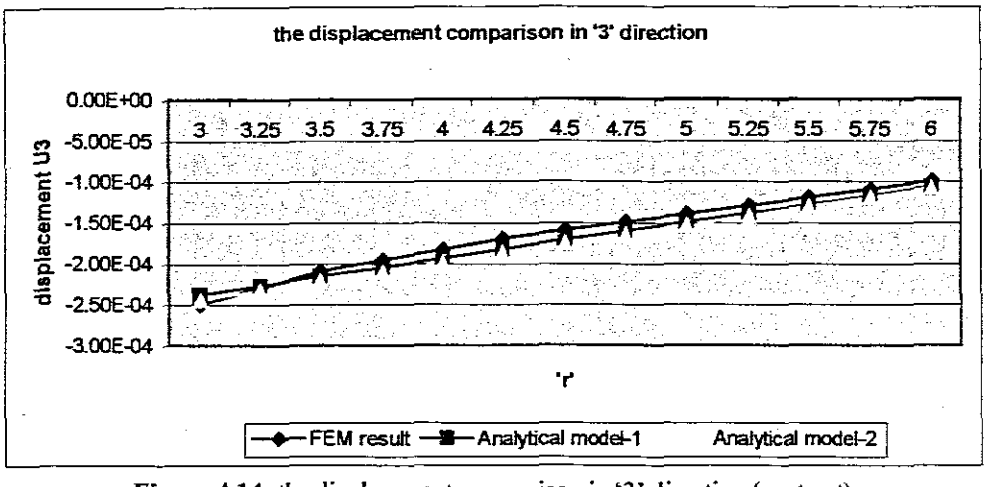

Figure 4.14: the displacement comparison in '3' direction (contract)

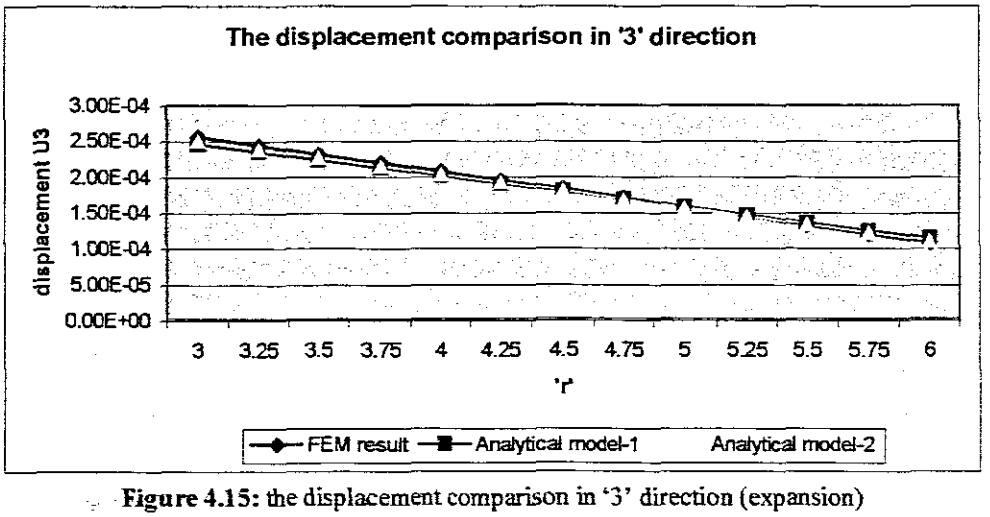

Figure 4.15: the displacement comparison in '3' direction (expansion)

In the above figures, the results from the two types analytical model and FEM are closed to each other. The accuracy and reliability of analytical models that have been developed in the above section have been proved here. Because this kind of DPA element with part circular shape have never been manufactured, the comparison between the analytical models result and product testing data cannot be completed.

4.5 Summary

In this chapter, the analytical models for one kind of improved distributed piezoelectric actuator (DPA) with the part circular shape have been developed. The mechanical properties of this shape DPA have also been discussed using the analysis result comparisons between the analytical models and FEM.

In the first half of this chapter, the analytical models for part circular shape DPA element have been developed by applying the models that have been developed in Chapter 3. The complex formulas for the electrical field in the DPA elements have been completed and improved. The mechanical properties models also been developed in this chapter. In the second half of this chapter, the multi-motion mechanical properties of this kind of shape DPA have been analyzed and discussed by the analysis result comparisons between the analytical models and FEM. Due to the different mechanical properties between the part circular shape DPA and the rectangular DPA, more applications in the aerospace and MEMS field that need the multi-motion in the limited space will be developed by using the new shape DPA in the future.

Chapter 5

Conclusions and Recommendations

5.1 Summary

This thesis was directed at the development of Distributed Piezoelectric Actuator (DPA) analytical analysis models for structural actuation. Active control of structures and system is a rapidly growing field that incorporates actuators and sensors into an otherwise 'passive' structure for the purpose of improving performance. Performance can take a number of forms, depending on the particular application, but usually focuses on the attenuation of structural vibrations. A reduction in vibration levels can result in longer structural lifetimes for structure.

The general piezoelectric actuators that have been manufactured previously with the host structure can only provide the strain and stress in one point in the structure. Continuous strain and stress on the structure surface or in the structure have never been realized until the Distributed Piezoelectric Actuator (DPA) have been studied and manufactured. Up to now, this kind of actuator has been used in many applications on different fields, such as aerospace structures, MEMS and other high-tech industry. In line with the improvement of applications, the distributed piezoelectric actuator with different shapes and structures has been requested for completing the complex functions in the applications. Because the current analysis models are not the accurate models, the improved accurate analytical analysis models have to be developed and used in the further design and manufacture of the DPA with complex shapes. This thesis was motivated by this challenge.

Due to the different situation between the uniform electrode and inter digitated electrode (IDE) that have been used in the distributed piezoelectric actuator, the major goal of this work was to develop the analytical analysis models for the two type of DPA element at first. Secondly, the analytical models for the part circular shape DPA have been developed by applying the models that have been developed in this work. The following objective have been done in this work:

- Develop methods for characterizing constituent materials for use in structural actuation and active composites systems
- Develop the analytical analysis models for DPA with two type distribution inter digitated electrode
- Develop the analysis models for DPA with part circular shapes

The first objective was investigated in chapter 2. This chapter dealt with fundamental issues of the bulk materials, and understanding how the choice of these materials affected the overall composite behavior and ease of manufacturing. The first part of the chapter characterized the ceramic material. A family of bulk ceramics, ranging from piezoelectrically soft to very hard, were characterized and compared using new metrics particular to the needs of structural actuation. The soft ceramics, such as PZT 5H and 5A, exhibited better actuation capability at low and high field regimes of operation, while the hard ceramics were better suited for the high stress environments that might be encountered in structural applications. PZT 5H was chosen for further characterization at this point for its high electro-mechanical coupling, and ease of poling. Poling studies of PZT 5H determined the necessary conditions for full poling, as a function of poling temperature, electric field, and time. The required electric field could be related to the composite through a common metric known as the coercive field. An aging study identified the aging trend for PZT 5H, showing it to be linear with decades in time, and substantiated the use of a 24 hour aging time found in most references. Finally, a method was developed for characterization of individual PZT, allowing measurement of the maximum strain and coercive field. This information was used as inputs to the models of Chapter 3.

The second objective was developed in Chapter 3. This chapter has developed the accurate analytical analysis models for the two type of DPA element, which will be used for the Chapter 4. Firstly, applying the fundamentals of electromagnetic theory, the formulas about the distribution and intensity of charge density in inter digitated electrode branch with different structure ratios have been developed. Secondly, as a capacitor, the formulas for calculating the capacitance of different DPA elements have been achieved based on the charge density analysis that have been done before. After the charge density and capacitance analysis, the analytical analysis models of electrical field in the DPA elements have been completed. These models for electrical field have never been simplified during the above process.

The second half of Chapter 3 characterized the mechanical models for DPA elements with the different electrodes. This technique was a generalization of the mechanics of materials approach, but extended to three dimensions and to incorporate electromechanical coupling. This model predicted the composite effective properties by assuming non-uniform electrical and uniform mechanical fields within each material. Due to its closed form nature, this model could provide physical insight into the governing material and geometrical terms that dominated the composite response. At the end of this chapter, through the comparison between the result from the analytical analysis models, FEM and the product testing data have been shown in those figures, the reliability of analytical analysis model have been proved. And those analytical models will be used in the Chapter 4 for the DPA with part circular shapes.

The third objective has been completed in Chapter 4. In this chapter, the analytical models for electrical field and mechanical properties of part circular shape DPA have been developed based on the results in the Chapter 3. The characteristics on electrical field and mechanical properties of DPA have been discussed by the analytical and

numerical results. Through the analysis of the results from the analytical model and FEM, the different complex strain and motion characteristics in the part circular shape DPA with two types of element have been discovered. The numerical results also have been discussed at the end of this chapter.

5.2 Conclusions

As one kind of smart actuator, Distributed Piezoelectric Actuator (DPA) has some special mechanical properties based on the piezoelectric phenomenon. In this work, the analytical analysis models for the two types of DPA elements and the part circular shape DPA have been developed. And the multi mechanical properties of part circular shape DPA have been discussed for the further applications in the aerospace structure and MEMS.

- *The Analytical Analysis Models for DPA elements*

The analytical analysis models for the two types of DPA elements have been developed in the Chapter 3. For those models, the key points about how to apply the analytical analysis models that have been developed in the Chapter 3 have been shown in Table 5.1. The analytical models are simpler when used in large and normal volume applications. For the small and micro volume applications, the analytical models have to be considered more carefully.

	Large & Normal Volume Applications	Small & Micro Volume Applications
Applications field	Aerospace structure	Micro Electro-Mechanical System
The effect of charge density	Ignored	Considered
The effect of edge	Ignored	Considered
The effect of epoxy material	Ignored	Considered

Table 5.1: The key points of DPA analytical model applications

- *The Analytical Analysis Models for Part Circular shape DPA*

In this research project, one of the special developments is about the analytical analysis models for part circular shape DPA, which have been developed for discussing the special mechanical properties of DPA that can be applied in some applications that need the multi-motion and complex control. In Chapter 4, the multi-motion mechanical properties of part circular DPA element have been proved by the analytical analysis models and the FEM using the Finite Element program (ABAQUS). Due to the different type of IDE that have been applied in the DPA element, the mechanical properties of two

type of part circular DPA are different. The second type of part circular DPA is better than the first type of DPA when used in the applications.

- *The FEM for the different type of DPA analysis*

As one kind of supplementary analysis, the FEM have been used in this research project to prove the accuracy and reliability of analytical analysis models. By comparing the analytical model analysis results, FEM results and product testing data, it has been proved that the analytical models are better than FEMs. Unfortunately, due to the complex formulas that have been applied in the analytical models, for the more complex structure DPA element analysis, the FEMs will be more easy to be used than analytical analysis models.

5.3 Recommendations for Future Work

Up to now, the analytical analysis models for two types of DPA elements and part circular shape DPA element have been developed completely. Through calculating applying the analytical models, the mechanical properties can be forecasted before building the prototypes.

The future work will be focused on some directions to develop the manufacture of DPA and the applications in the MEMS field. First research direction is about the composite materials properties model improvement. Due to the micro volume of applications in the MEMS field, the DPA mechanical properties will depend on the multi materials that have been included in the actuator. The effect from other material to actuator cannot be ignored in this situation. The development and improvement of the composite model will be important for the DPA design. The second direction is about the dynamic respond and mechanical properties of complex shape DPA element with host structure when it has been used in the applications.

Bibliography

Abramorich H 1998 "Deflection control of laminated composite beams with piezoceramic layers-closed form solution", *Composite Struct.* 43, pp. 217-31.

Aburatani, H., Harada, S., Uchino, K., and A. Furuta, 1994, "Destruction Mechanisms in Ceramic Multilayer Actuators", *Japan J. Appl. Phys*, Vol. 33, 1, No. 5B, pp. 3091-3094.

Aldraihem O J, wetherhold R C and Singh T 1997 "Distributed control of laminated beams: Timoshenko vs. Euler-Bernoulli theory", *J. Intell. Master. Syst. Struct.* 8, pp. 149-57.

Berlincourt, D., 1964, *J. Acoust. Soc Am.*, No. 36, pp. 515-20.

Chandrashekhara k and Varadarajan s 1997 "Adaptive shape control of composite beams with piezoelectric actuators", *J. Intell. Mater. Syst. Struct.* 8, pp. 112-24.

Crawely E F and Anderson E H 1990 "Detailed models of piezoelectric actuation of beams", *J. Intell. Mater. Syst. Struct.* 1, pp. 4-25.

Crawley, E.F., 1994, "Intelligent Structures for Aerospace: A Technology Overview and Assessment", *AIAA Journal*, Vol. 32, No. 8, pp 1689-1699.

Feuillard, G., Lethiecq, Amazit, Y., Certon, D., Millar, C., and Patat, F., 1993, "Experimental Determination of the Surface Acoustic Wave Properties of New Fine Grain Piezoelectric Ceramics", *J. Appl. Phys.*, Vol. 74, No. 11, pp. 6523-29.

Gentilman R L, Fiore D, Torri R and Glynn J 1998 "Piezoelectric smart pands for active control of underwater vibration and noise", *Industrial and Commercial Applications of smart structures technologies vol 3326* (Bellingham, WA: SPIE), pp. 252-8.

Hagood, N.W., Kindel, R., Ghandi, K., and P. Gaudenzi, 1993, "Improving Transverse Actuation of Piezoceramics using Interdigitated Surface Electrodes", SPIE Paper, pp. 1917-25, *Proceedings of the 1993 North American Conference on Smart Structures and Materials*, Albuquerque, NM.

Heyliger P and Brooks S 1996 "Exact solutions for laminated piezoelectric plates in cylindrical bending", *J. Appl. Mech.*63, pp. 903-10.

Heyliger P 1994 "Static behavior of laminated elastic/piezoelectric plates", *AIAA* J 32, pp. 2481-4.

Hopleins M A, Henderson D A, Moses R W, Ryall T, Zimcik D G and Spangler R L 1998 "Active vibration-suppression system applied to twin-tail buffeting", *Industrial and Commercial Applications of Smart Structures Technologies vol 3326* (Bellingham, WA: SPIE), pp. 27-33.

Huang j H and wu T L 1996 "Analysis of hybrid multilayered piezoelectric plates", *Int. J. Eng. Sci* 34, pp. 171-81.

http://www.mide.com/lab/quickpack.html 2002.

http://www.piezo.com/bendedu.html 2002.

Jaffe, B., Cook Jr., W.R., and H. Jaffe, 1971, "Piezoelectric Ceramics", Academic Pres.

Lee C K 1990 "Theory of laminated piezoelectric plates for the design of distributed sensors/actuators. Part 1: governing equations and reciprocal relationships", *J. Acoust. Soc. Am.* 87, pp. 1144-58.

Lee J S and Jiang L Z 1996 "Exact electroelastic analysis of piezoelectric laminae via state space approach", *Int. J. Solids Struct.* 33, pp. 977-90.

Mitchell J A and Reddy J N 1995 "A refined hybrid plate theory for composite laminates with piezoelectric laminate", *Int. J. Solides struct.* 32, pp. 2345-67.

Newnham R E and Gregory R R 1991 "Smart electroceramics", *J. Am. Ceram. Soc.* 74, pp. 463-80.

Ray M C, Rao K M and samanta B 1993 "Exact Solution for static analysis of intelligent structures under cylindrical bending", *Comput. Struct.* 47, pp. 1031-42.

Ray M, Chen t and Baz a 1997 "Vibration control of cylindrical shells using active constrained layer damping Proc", *Smart Structures and Materials Conf.* Vol 3045, pp. 293-314.

Rongong J and Tomlinson G 1997 "Passive and active constrained layer damping of ring-type structures Proc", *Smart structures and Materials Conf. on Passive Damping* vol 3045, pp. 282-92.

Shields W H, Ro J and Baz A M 1997 "Control of sound radiation from a plate into an acoustic cavity using active piezoelectric-damping composites", *Math. Contr. Smart Struct. vol 3039* (Bellingham, WA: SPIE), pp. 70-9.

Strub F K 1996 "A feasibility study of using smart materials for rotor control", *Smart Mater. Struct.* 5, pp. 1-10.

Suleman A and Goncalves M A 1997 "Optimisation issues in applications of piezoelectric actuators in panel flutter control", *Mathematics and Control in Smart Structure vol 3039* (Bellingham, WA: SPIE), pp. 335-47.

Sun B H and Huang D 2001 "Vibration suppression of laminated composite beams with a piezo-electric damping layer", *Composite Struct.* 53, pp. 437-447.

Vel S S and Batra R C 2000 "Three-dimensional analytical solution for hybrid multilayered piezoelectric plates", *J. Appl. Mech.* 67, pp. 558-67.

Yoshikawa, S., and T. Shrout, 1993, "Multilayer Piezoelectric Actuators – Structures and Reliability", *AIAA Paper No 93-1711-CP*, pp. 3581-3586.

Appendix A

The mechanical properties effects from the charge density.

The mechanical properties effects from the non-uniform surface charge density on the DPA element have been shown in the following figures.

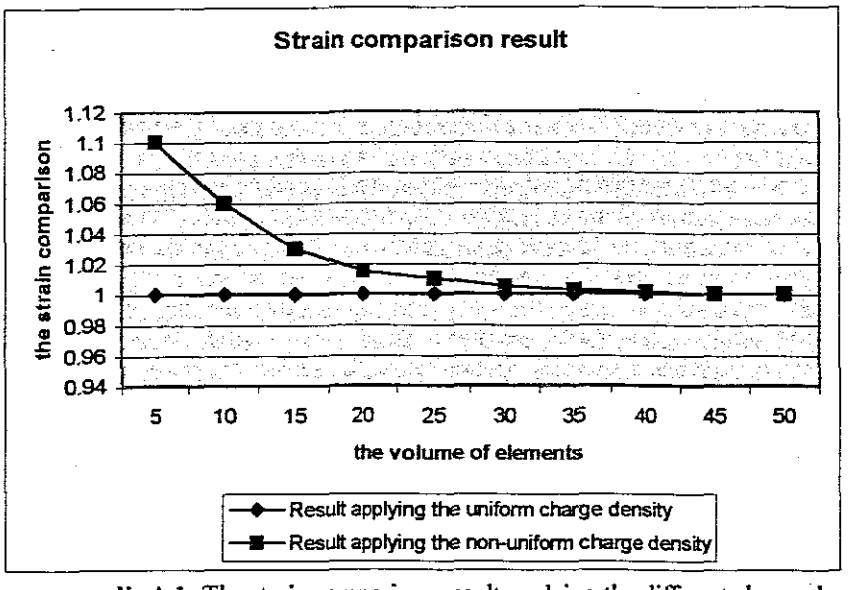

Figure appendix A 1: The strain comparison result applying the different charge density.

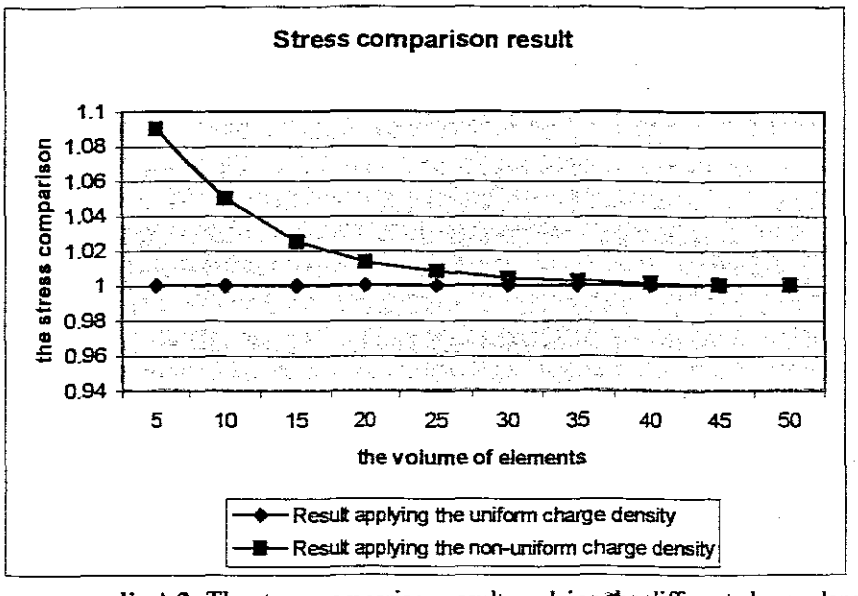

Figure appendix A 2: The stress comparison result applying the different charge density.

Appendix B

The electrical field effects from the charge density

The difference distribution and intensity of electrical field, which have been applied the non-uniform charge density, have been shown in the following figures.

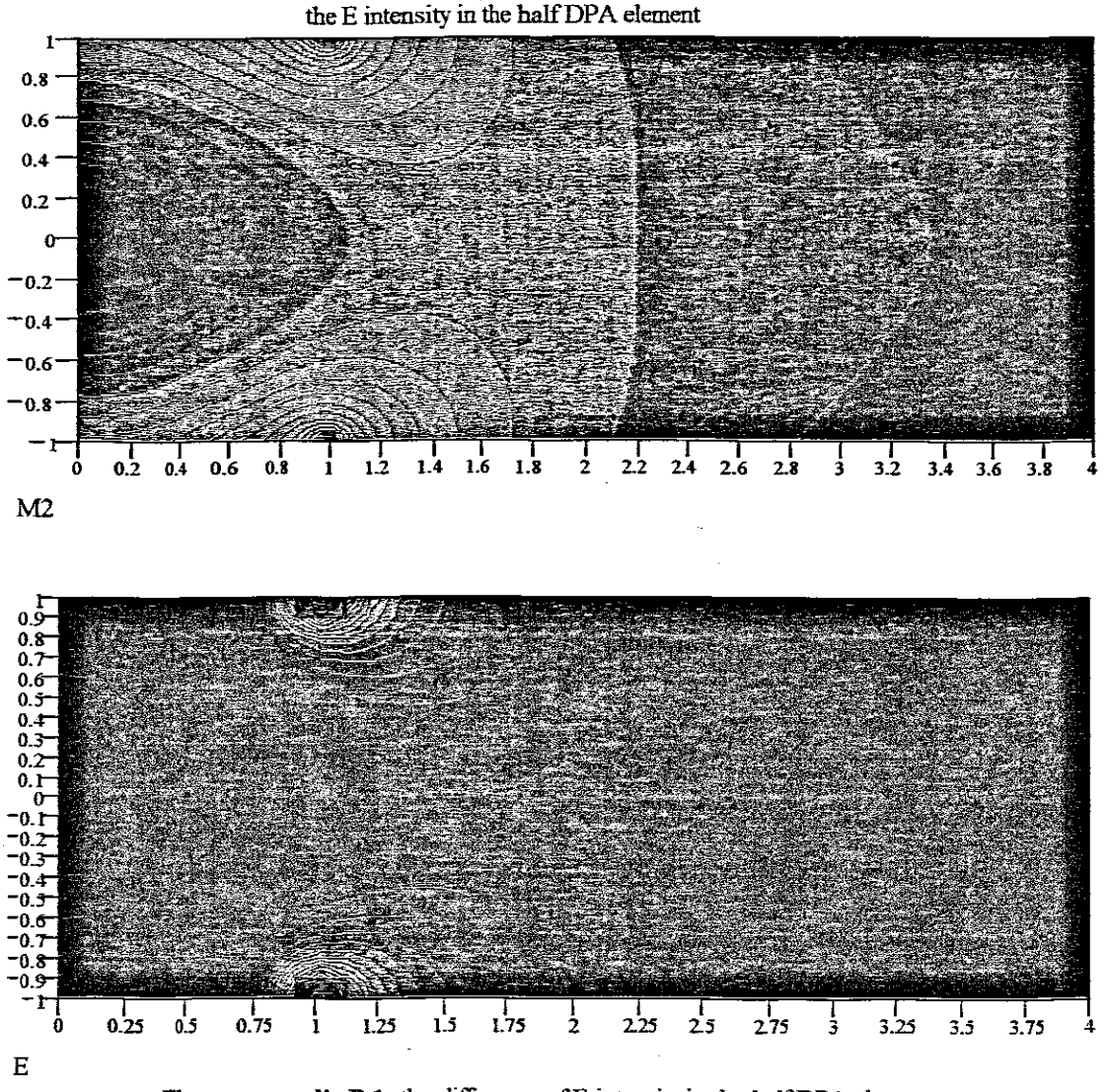

Figure appendix B 1: the difference of E intensity in the half DPA elements.

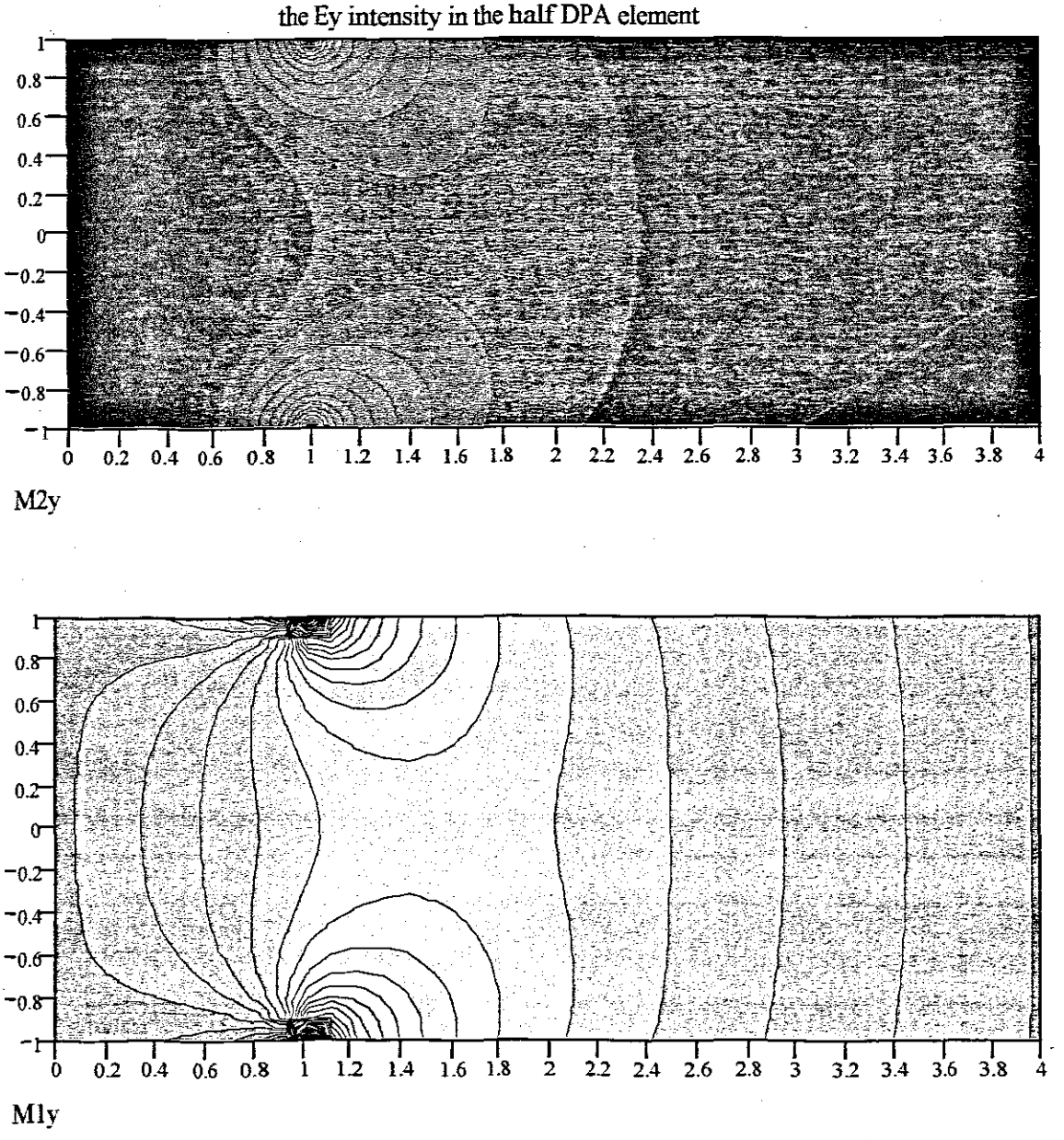

Figure appendix B 2: the difference of Ey intensity in the half DPA elements.

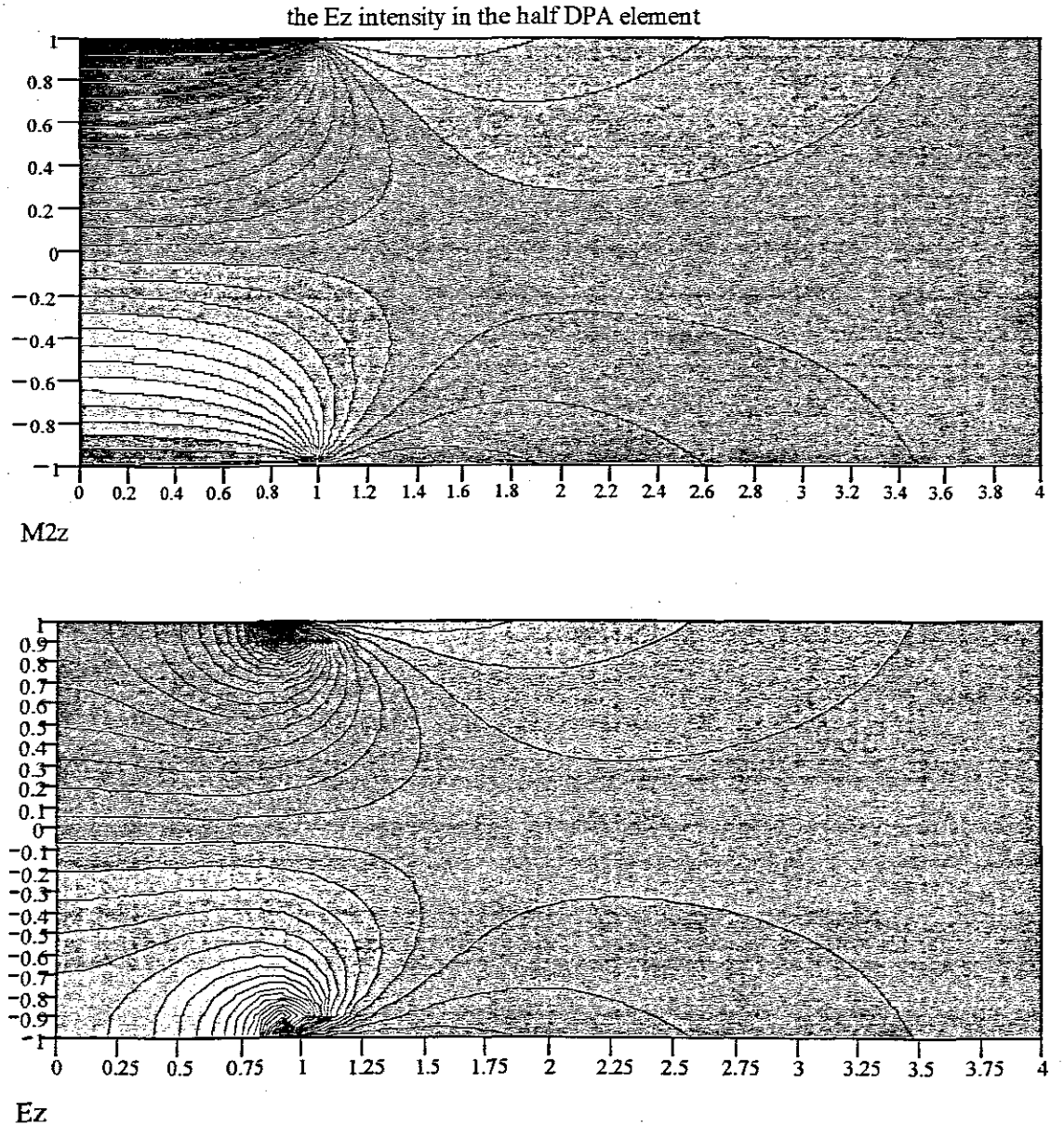

Figure appendix B 3: the difference of Ez intensity in the half DPA elements.

Appendix C

The analytical result of E_θ in the part circular DPA element

The formula for E_θ in the second type of part circular DPA element can be gotten by the MathCAD program.

E_θ =

mcad_simplify(mcad_add(mcad_add(subs(0_r='0_r',int((subs(0_q='0_q',int(mcad_divide
(mcad_multiply((mcad_multiply(0_r,sin(mcad_biminus(0_`Mu`,0_q)))),0_r),mcad_powe
r((mcad_sqrt(mcad_add(mcad_biminus(mcad_add(mcad_power(0_x,2),mcad_power(0_r
,2)),mcad_multiply(mcad_multiply(mcad_multiply(2,0_x),0_r),cos(mcad_biminus(0_`M
u`,0_q)))),mcad_power((mcad_biminus(0_`Mu`,0_z)),2)))),3)),0_`mu`=mcad_biminus(m
cad_multiply(mcad_multiply(4,0_n),0_b),0_a)..mcad_add(mcad_multiply(mcad_multipl
y(4,0_n),0_b),0_a)))),0_r=0_R..mcad_add(0_R,mcad_multiply(2,0_c)))),subs(0_r='0_r',i
nt((subs(0_q='0_q',int(mcad_divide(mcad_multiply((mcad_multiply(0_r,sin(mcad_bimin
us(0_`Mu`,0_q)))),0_r),mcad_power((mcad_sqrt(mcad_add(mcad_biminus(mcad_add(m
cad_power(0_x,2),mcad_power(0_r,2)),mcad_multiply(mcad_multiply(mcad_multiply(2,
0_x),0_r),cos(mcad_biminus(0_`Mu`,0_q)))),mcad_power((mcad_add(0_`Mu`,0_z)),2)))
),3)),0_`mu`=mcad_biminus(mcad_multiply(mcad_multiply(4,0_n),0_b),0_a)..mcad_add
(mcad_multiply(mcad_multiply(4,0_n),0_b),0_a)))),0_r=0_R..mcad_add(0_R,mcad_mult
iply(2,0_c))))),(mcad_add(subs(0_r='0_r',int((subs(0_q='0_q',int(mcad_divide(mcad_mul
tiply((mcad_multiply(0_r,sin(mcad_biminus(0_`Mu`,0_h)))),0_r),mcad_power((mcad_sq
rt(mcad_add(mcad_biminus(mcad_add(mcad_power(0_x,2),mcad_power(0_r,2)),mcad_
multiply(mcad_multiply(mcad_multiply(2,0_x),0_r),cos(mcad_biminus(0_`Mu`,0_q)))),
mcad_power((mcad_biminus(0_`Mu`,0_z)),2)))),3)),0_`mu`=mcad_biminus(mcad_add(
mcad_multiply(mcad_multiply(4,0_n),0_b),mcad_multiply(2,0_b)),0_a)..mcad_add(mca
d_add(mcad_multiply(mcad_multiply(4,0_n),0_b),mcad_multiply(2,0_b)),0_a)))),0_r=0_
R..mcad_add(0_R,mcad_multiply(2,0_c)))),subs(0_r='0_r',int((subs(0_q='0_q',int(mcad_
divide(mcad_multiply((mcad_multiply(0_r,sin(mcad_biminus(0_`Mu`,0_h)))),0_r),mcad
_power((mcad_sqrt(mcad_add(mcad_biminus(mcad_add(mcad_power(0_x,2),mcad_pow
er(0_r,2)),mcad_multiply(mcad_multiply(mcad_multiply(2,0_x),0_r),cos(mcad_biminus(
0_`Mu`,0_q)))),mcad_power((mcad_add(0_`Mu`,0_z)),2)))),3)),0_`mu`=mcad_biminus(
mcad_add(mcad_multiply(mcad_multiply(4,0_n),0_b),mcad_multiply(2,0_b)),0_a)..mca
d_add(mcad_add(mcad_multiply(mcad_multiply(4,0_n),0_b),mcad_multiply(2,0_b)),0_a
)))),0_r=0_R..mcad_add(0_R,mcad_multiply(2,0_c)))))));

Appendix D

FEM Input File Example (ABAQUS)

```
*Heading
 02-Oct-15-1
** Job name: 02-Oct-15-1 Model name: Model-1
**
** PARTS
**
*Part, name=Part-1
*End Part
**
** ASSEMBLY
**
*Assembly, name=Assembly
**
*Instance, name=Part-1-1, part=Part-1
*Node
     1,    38.2166,         1.,         0.
     2,    38.2166,        0.8,         0.
     ..........................................
     ..........................................
     16925,         0.,        0.2,     76.4331
     16926,         0.,         0.,     76.4331
*Element, type=C3D8E
   1,  547,  548,  554,  553,    1,    2,    8,    7
   2,  548,  549,  555,  554,    2,    3,    9,    8
   ..................................................
   ..................................................
   13499, 16918, 16919, 16925, 16924, 16372, 16373, 16379, 16378
   13500, 16919, 16920, 16926, 16925, 16373, 16374, 16380, 16379
*Orientation, name=Ori-110, system=CYLINDRICAL
    38.2166,         0.,         0.,     38.2166,         0.,         1.
1, 0.
** Region: (Section-1:Picked), (Material Orientation:Picked)
*Elset, elset=_I1, internal, generate
    1,  13500,     1
** Section: Section-1
*Solid Section, elset=_I1, orientation=Ori-110, material=PZT-5A
1.,
*End Instance
*Nset, nset=_G4, internal, instance=Part-1-1
```

```
   1,   2,   3,   4,   5,   6, 547, 548, 549, 550, 551, 552, 1093, 1094, 1095,
   ..........................................................................
   ..........................................................................
   15837, 15838, 15839, 15840, 16381, 16382, 16383, 16384, 16385, 16386
*Elset, elset=_G4, internal, instance=Part-1-1
   1,   2,   3,   4,   5, 451, 452, 453, 454, 455, 901, 902, 903, 904, 905,
   ..........................................................................
   ..........................................................................
   12605, 13051, 13052, 13053, 13054, 13055
*Nset, nset=_G5, internal, instance=Part-1-1, generate
   6, 16926,    6
*Elset, elset=_G5, internal, instance=Part-1-1, generate
   5, 13500,    5
*Nset, nset=_G70, internal, instance=Part-1-1, generate
   6, 16926,    6
*Elset, elset=_G70, internal, instance=Part-1-1, generate
   5, 13500,    5
*Nset, nset=_G71, internal, instance=Part-1-1, generate
   1, 16921,    6
*Elset, elset=_G71, internal, instance=Part-1-1, generate
   1, 13496,    5
*End Assembly
**
** MATERIALS
**
*Material, name=PZT-5A
*Density
7800.,
*Dielectric
1800.,
*Elastic, type=ENGINEERING CONSTANTS
 6.5e+10, 5.5e+10, 6.5e+10,    0.3,    0.3,    0.3, 1.5e+10, 1.5e+10
 1.5e+10,
*Piezoelectric, type=E
0.,      0.,      0.,      0.,      0.,      0., -1.79e-10,  3.5e-10
 -1.79e-10,      0.,      0.,      0.,      0.,      0.,      0.
      0.,      0.
** ----------------------------------------------------------------
**
** STEP: Step-1
**
*Step, name=Step-1
02-Oct-15-1
*Static
1., 1., 1e-05, 1.
**
```

```
** BOUNDARY CONDITIONS
**
** Name: BC-1 Type: Symmetry/Antisymmetry/Encastre
*Boundary
_G4, ENCASTRE
** Name: EF-0 Type: Electric potential
*Boundary
_G71, 9, 9, 30987.
** Name: EF-30987 Type: Electric potential
*Boundary
_G70, 9, 9
**
** OUTPUT REQUESTS
**
*Restart, write, frequency=1
**
** FIELD OUTPUT: F-Output-1
**
*Output, field
*Node Output
U, EPOT, RCHG, CECHG
*Element Output
S, E, PE, PEEQ, PEMAG, LE, EPG, CHRGS
**
** HISTORY OUTPUT: H-Output-1
**
*Output, history, variable=PRESELECT
*El Print, freq=999999
*Node Print, freq=999999
*End Step
```